Title
Investigating the Role of Metabolism in Tissue Homeostasis and Tumor Initiation by Hair Follicle Stem Cells

Author
Flores, Aimee Alyssa

Publication Date
2018

Peer reviewed|Thesis/dissertation

UNIVERSITY OF CALIFORNIA

Los Angeles

Investigating the Role of Metabolism in Tissue Homeostasis and Tumor Initiation by Hair Follicle Stem Cells

A dissertation submitted in partial satisfaction of the

requirements for the degree Doctor of Philosophy

in Molecular Biology

by

Aimee Alyssa Flores

2018

ABSTRACT OF THE DISSERTATION

Investigating the Role of Metabolism in Tissue Homeostasis and Tumor Initiation by Hair Follicle Stem Cells

by

Aimee Alyssa Flores

Doctor of Philosophy in Molecular Biology

University of California, Los Angeles, 2018

Professor William Edward Lowry, Chair

For an increasing number of cancers, the cell of origin has been demonstrated to be the resident adult stem cell. One such cancer is squamous cell carcinoma, for which recent studies in our lab traced its origin to the hair follicle stem cells. Malignant transformation is thought to coincide with a dramatic shift towards the use of glycolysis and establishment of a 'Warburg' state – increased metabolism of glucose to lactate. How the Warburg Effect is established during tumor initiation and progression *in vivo* remains unclear. The current consensus is that the bulk of the energy generated in most adult tissue cells is created by oxidative phosphorylation, while more highly proliferative cells, such as activated immune cells and cells transformed to make a tumor, mainly use glycolysis. Little is known about how individual cell types generate energy *in vivo*, however, and how their metabolism influences basic cell fate decisions such as cell division, migration or differentiation.

Using genetically engineered mouse models that allow the study of both tissue homeostasis and the Warburg Effect *in vivo*, I have made important observations that provide the basis for new investigations into the role of metabolism in key cell fate decisions by adult stem cells. In this dissertation I present data indicating that hair follicle stem cells possess a unique metabolic profile that may be critical for their maintenance and for their response to oncogenic insults. Importantly, they suggest the possibility that the "Warburg Effect" is the result of the expansion of an already glycolytic subpopulation, namely the hair follicle stem cells.

The dissertation of Aimee Alyssa Flores is approved.

I ŜI·ǘKŜǊ wΦ /ĸǊǎǘƨŦ˨

I ʎƭI·Ǌè Ann /ƨƭƭŜǊ

5I·ƴI· [ŜI·ƴƴŜ ʬƨƴŜă

Michael Alan Teitell

William Edward Lowry, Committee Chair

University of California, Los Angeles

201y

This dissertation is dedicated to

My beloved grandmother, Ester Manuela Santos

Table of Contents

List of Figures

Chapter 1: Introduction

Chapter 2: Lactate dehydrogenase activity drives hair follicle stem cell activation

Chapter 3: Hmga2 is dispensable for cutaneous squamous cell carcinoma

Chapter 4: Tumor suppressor identity can contribute to heterogeneity of phenotype in hair follicle stem cell-induced squamous cell carcinoma

Chapter 5: Increased lactate dehydrogenase activity is dispensable in squamous carcinoma cells of origin

Acknowledgements

Pursuing my career in research has been the most fulfilling experience, and I have many people to thank for their help and encouragement along the way.

I would like to thank my thesis advisor and mentor, Dr. Bill Lowry, for his endless support and guidance over the past five years. Bill provided the perfect research environment for me to grow as a scientist and as a person. With just the right combination of hypothesis-driven inquiry, independent thought, creativity, and teamwork, I could not have asked for a better lab and mentor. I would also like to thank my thesis committee, Dr. Heather Christofk, Dr. Hilary Coller, Dr. Leanne Jones, and Dr. Michael Teitell for their continued guidance and advice.

Thanks to all the members of the Lowry Lab both past and present for the support, encouragement, and friendship they have shared with me throughout my time at UCLA. Thanks to Dr. Andrew White, Anqi Liu, Matilde Miranda, Jessica Cinkornpumin, Dr. Yuan Xie, Dr. Xavier Gaeta, Dr. Minori Ohashi, Dr. Igal Germanguz, Dr. Rie Takahashi, Dr. Jim Rheinwald, Dr. Tom Allison, Elena Korsakova and Ivy Pham. I extend special thanks to my talented undergraduate students Saitiel Sandoval-Gonzalez, Laila Sathe, Mallory Neebe and Jeanny Hu. Thanks to my collaborators and friends outside the Lowry Lab including Dr. Peter Mullen, Dr. Abby Krall, Dr. David Jelinek, Dr. Daniel Braas, Min Zhao, Roy Doumani and Samantha Le. I am also grateful for the constant support from administration and staff within the UCLA MBIDP including Dr. Luisa Iruela-Arispe, Helen Houldsworth, Jennifer Miller, Dr. Pamela Hurley, Stephanie Cuellar and Ashley TerHorst.

Finally, I would like to extend my sincerest gratitude to my family, without whose love and support I would not be here. My most heartfelt thanks to my parents, Misael and Ester Flores, for being my greatest inspiration. All that I am I owe to you. Thank you for always believing in me.

Chapter 2 was originally published in Nature Cell Biology. Aimee Flores, John Schell, Abigail S. Krall, David Jelinek, Matilde Miranda, Melina Grigorian, Daniel Braas, Andrew C. White, Jessica L. Zhou, Nicholas A. Graham, Thomas Graeber, Pankaj Seth, Denis Evseenko, Hilary A. Coller, Jared Rutter, Heather R. Christofk & William E. Lowry. 2017. Lactate dehydrogenase activity drives hair follicle stem cell activation. Nature Cell Biology volume 19, pages 1017–1026 (2017). It is accessible with the DOI:10.1038/ncb3575. It is reprinted here with permission by Springer Nature. A.F. and A.C.W. were supported by a fellowship from the Eli and Edythe Broad Center for Regenerative Medicine at UCLA. A.C.W. and M.G. were supported by a fellowship from the Tumor Cell Biology program at UCLA (NIH). A.C.W. was also supported by a training grant from CIRM. D.J. was supported by awards from a New Idea Award from the Leukemia Lymphoma Society, the Jonsson Comprehensive Cancer Center, the UCLA Clinical Translational Science Institute UL1TR000124, the Prostate Cancer SPORE at UCLA P50 CA092131, and the Eli & Edythe Broad Center for Regenerative Medicine & Stem Cell Research. N.A.G. is a postdoctoral trainee supported by the UCLA Scholars in Oncologic Molecular Imagining program (NCI/NIH grant R25T CA098010). A.S.K. was supported by a UCLA Dissertation Year Fellowship. H.A.C. was supported by National Institute of General Medical Sciences R01-GM081686 and R01-GM0866465. J.R. was supported by NIH (RO1GM094232). H.R.C. was supported by a Research Scholar Grant, RSG-16-111-01-MPC, from the American Cancer Society and the Eli & Edythe Broad Center of Regenerative Medicine and Stem Cell Research at UCLA and Rose Hills Foundation Research Award. W.E.L. was supported by NIH-NIAMS (5R01AR57409), an Impact award from CTSI and the Jonsson Comprehensive Cancer Foundation, and The Gaba Fund through the Eli & Edythe Broad Center of Regenerative Medicine at UCLA.

Chapter 3 was originally published in Experimental Dermatology. Andrew White*, Aimee Flores*, Jessica Ong and William E. Lowry. 2016. Hmga2 is dispensable for cutaneous squamous cell

carcinoma. Experimental Dermatology. Volume25, Issue 5 May 2016 Pages 409-412. It is accessible with the DOI: https://doi.org/10.1111/exd.12978. It is reprinted here with permission under the Creative Commons License CC BY-NC. ACW was supported by a CIRM training grant. This work was supported by NIH R01 from NIAMS, and the Jonsson Cancer Center Foundation.

Chapter 4 was originally published in Experimental Dermatology. Aimee Flores, William Grant, Andrew C. White, Phillip Scumpia, Rie Takahashi and William E. Lowry. 2016. Tumor suppressor identity can contribute to heterogeneity of phenotype in hair follicle stem cell-induced squamous cell carcinoma. Experimental Dermatology. Volume25, Issue 9 September 2016 Pages 733-735. It is accessible with the DOI: https://doi.org/10.1111/exd.13037. It is reprinted here with permission under the Creative Commons License CC BY-NC. This work was supported by NIH (5R01AR057409-05 and TCBT32CA09056), a CIRM Training Grant (TG2-01169), a fellowship from the Broad Center for Regenerative Medicine (UCLA, AF), MARC program (UCLA, WG).

Chapter 5 is unpublished work currently under peer review at Nature Communications. It reflects work performed by Aimee Flores, Saitiel Sandoval-Gonzalez, Rie Takahashi, Laila Sathe, Lu Wei, Caius Radu, J Jolly, Nick Graham, Heather Christofk, and William E. Lowry.

Vita

2010	Bachelor of Science in Biological Sciences with Honors, University of Southern California; Los Angeles, CA
2010	Phi Sigma Theta National Honor Society Order of Merit Award; University of Southern California; Los Angeles, CA
2013	Master of Science, Molecular and Experimental Pathology, University of Southern California; Los Angeles, CA
2013	Pathology Conference Keck School of Medicine Outstanding Presentation Award; University of Southern California; Los Angeles, CA
2013	Student of the Year, Department of Pathology at Keck School of Medicine; University of Southern California; Los Angeles, CA
2013-Present	Molecular Biology Interdepartmental Doctoral Program; University of California Los Angeles; Los Angeles, CA
2014-Present	UCLA Business of Science Center Venture Team Program Coordinator; University of California Los Angeles; Los Angeles, CA
2015	Broad Stem Cell Research Center Pre-Doctoral Fellowship Award; University of California Los Angeles; Los Angeles, CA
2016	Broad Stem Cell Research Center Pre-Doctoral Fellowship Award; University of California Los Angeles; Los Angeles, CA
2016	Whitcome Pre-Doctoral Fellowship Award; University of California Los Angeles; Los Angeles, CA
2017	Dissertation Year Fellowship Award; University of California Los Angeles; Los Angeles, CA
2018	Jules Brenner Fellowship Award, Molecular Biology Institute; University of California Los Angeles; Los Angeles, CA

Publications

Flores A, Schell J, Krall A, Jelinek D, Miranda M, Grigorian M, Braas D, White AC, Zhou JL, Graham N, Graeber T, Seth P, Evseenko D, Coller H, Rutter J, Christofk H, Lowry WE. **Lactate dehydrogenase activity drives hair follicle stem cell activation.** Nature Cell Biology. 2017 Sep;19(9):1017-1026. doi: 10.1038/ncb3575. Epub 2017 Aug 14.

Schell J, Wisidagama D, Bensard C, Zhao H, Wei P, Tanner J, **Flores A**, Mohlman J, Sorensen L, Earl C, Olson K, Miao R, Waller T, Delker D, Kanth P, Jiang L, DeBerardinis R, Bronner M, Li D, Cox J, Christofk H, Lowry WE, Thummel C, Rutter J. **Control of intestinal stem cell function and proliferation by mitochondrial pyruvate metabolism**. Nature Cell Biology. 2017 Sep;19(9):1027-1036. doi: 10.1038/ncb3593. Epub 2017 Aug 14.

Lowry WE, **Flores A** and White AC. **Exploiting mouse models to uncover the etiology of Ras induced cutaneous squamous cell carcinoma**. J Invest Dermatol. 2016 May 7. doi: 10.1016/j.jid.2016.03.017.

Flores A, Grant W, White AC, Scumpia P, Takahashi R, and Lowry WE **Tumor suppressor identity can contribute to heterogeneity of phenotype in hair follicle stem cell induced squamous cell carcinoma**. Exp Dermatol. 2016 Apr 20. doi: 10.1111/exd.13037.

Ambrus A, Lemons J, Raitman I, Krishnan N, Jelinek D, Suh E, Remillard M, Shilo N, Haley E, Sun L, Xiao R, **Flores A**, Wang D, White AC, Lowry W and Coller HA. **The NADPH-Production Enzyme Isocitrate Dehydrogenase Maintains Quiescence in Hair Follicle Stem Cells**. FASEB. April 2016. vol. 30 no.1

White AC*, **Flores A***, Ong J and Lowry WE. **HMGA2 is dispensable for cutaneous squamous cell carcinoma**. Exp Dermatol. 2016 Feb 22. doi: 10.1111/exd.12978.

Jelinek D, **Flores A**, Uebelhoer M, Pasque V, Plath K, Iruela-Arispe L, Christofk H, Lowry WE, and Coller H. **Mapping metabolism: Monitoring lactate dehydrogenase activity directly in tissue**. JoVE. "in press"

Flores A, Sandoval-Gonzalez S, Takahashi, R, Sathe L and Lowry WE. **Defining the Role of Lactate dehydrogenase activity in cutaneous squamous cell carcinoma**. Nature Comunications. "in review"

Sullivan WJ, **Flores A**, Sharpley M, Ayer D, Banerjee U, Lowry WE, Braas D, Christofk H. **Extracellular matrix remodeling regulates glucose metabolism through TXNIP destabilization**. Cell. "in review"

Presentations

Broad Stem Cell Research Center 14th Annual Stem Cell Symposium. February 2018. UCLA DeNeve Auditorium. **Flores A**, Schell J, Krall A, Jelinek D, Miranda M, Grigorian M, Braas D, White AC, Zhou JL, Graham N, Graeber T, Seth P, Evseenko D, Coller H, Rutter J, Christofk H, Lowry WE. **Metabolic Control of Hair Follicle Stem Cell Activation**. (Poster)

International Society for Stem Cell Research Annual Meeting. June 2017. Boston Convention Center. **Flores A**, Jelinek D, Grigorian M, Braas D, White AC, Krall A, Coller H, Christofk H, and Lowry WE. **Lactate dehydrogenase activity drives hair follicle stem cell activation**. (Poster)

UCLA Molecular Biology Institute Retreat. April 2017. Crowne Plaza Ventura County California. **Flores A**, Jelinek D, Grigorian M, Braas D, White AC, Krall A, Coller H, Christofk H, and Lowry WE. **Lactate dehydrogenase activity drives hair follicle stem cell activation.** (Talk)

Broad Stem Cell Research Center 13th Annual Stem Cell Symposium. February 2017. UCLA DeNeve Auditorium. **Flores A**, Schell J, Krall A, Jelinek D, Coller H, Rutter J, Christofk H, Lowry WE. **Role of Metabolism in Tissue Homeostasis and Tumor Initiation by Hair Follicle Stem Cells**. (Poster)

UCLA Molecular Biology Institute Retreat. April 2016. UCLA Conference Center Lake Arrowhead. **Flores A**, Jelinek D, Grigorian M, Braas D, White AC, Krall A, Coller H, Christofk H, and Lowry WE. **The Role of Metabolism in Tissue Homeostasis and Tumor Initiation by Hair Follicle Stem Cells**. (Talk)

Broad Stem Cell Research Center 12th Annual Stem Cell Symposium. February 2016. UCLA DeNeve Auditorium. **Flores A**, Jelinek D, Grigorian M, Braas D, White AC, Krall A, Coller H, Christofk H, and Lowry WE. **The Role of Metabolism in Tissue Homeostasis and Tumor Initiation by Hair Follicle Stem Cells**. (Poster)

Chapter 1: Introduction

Adult Stem Cells

Adult stem cells, or somatic stem cells, are found in many different tissues throughout the body of nearly all living organisms. Unlike embryonic stem cells, which are pluripotent and can give rise to any cell type in the body, adult stem cells are lineage restricted and multipotent. Resident adult stem cells are responsible for maintaining and repairing the tissue in which they are found, and as such adult stem cells can divide to renew themselves and can differentiate to yield some or all the various cell types found in a tissue or organ. Adult stem cells have been identified in many organs and tissues, including the brain, bone marrow, skeletal muscle, skin, heart, gut, and liver. These tissue-specific stem cells are believed to reside in specific areas or niches of each tissue and can remain quiescent for long periods of time until they are activated for maintenance of tissue homeostasis, in disease or after injury.

Research on adult stem cells began many decades ago when researchers first discovered that the bone marrow contains at least two kinds of stem cells: hematopoietic stem cells which can give rise to the various types of blood cells found throughout the body, and stromal or mesenchymal stem cells which can generate bone, cartilage, and fat cells that aid in the formation of blood and fibrous connective tissue [1-3]. Adult hematopoietic stem cells from the bone marrow have since been used successfully in transplants, and adult stem cells have been an active area of research in the hope that these cells may become the basis of other transplantation-based therapies and can be used for modeling various diseases in the laboratory.

To maintain tissue homeostasis and wound repair throughout an organism's life, a continuous pool of adult stem cells is required. Both quiescence and self-renewal through cell division are necessary to maintain adult stem cell populations in tissues and organs. A mechanistic understanding of stem cell

quiescence is crucial for elucidating its role in human diseases such as cancer and investigating the potential use of adult stem cells in transplantation therapy and regenerative medicine. Over the years, hair follicle stem cells have emerged as an ideal model system to investigate the various mechanisms that regulate dividing and quiescent adult stem cells.

Hair Follicle Stem Cells

The hair follicle can undergo continuous regeneration throughout life. The hair follicle undergoes cyclical rounds of rest (telogen phase), regeneration (anagen phase), and degeneration (catagen phase). The ability of the hair follicle to maintain this cycle depends on the presence of hair follicle stem cells which reside in a specific niche called the bulge. Hair follicle stem cells can give rise to all the different cell types of the hair follicle, and upon injury can contribute to wound repair of the epidermis and to the formation of sebaceous gland cells, although both are believed to have their own resident stem cells[4] (Figure 1)[5].

At the start of anagen, hair follicle stem cells are activated by signals received from the dermal papilla, which at that stage borders the bulge area. Activated stem cells exit the bulge and proliferate downwards, creating a trail that becomes the outer root sheath of the hair follicle. During anagen the transit amplifying cells, found in the matrix of the hair follicle, differentiate and give rise to a new hair shaft. This stage is followed by catagen, when massive cell death via apoptosis and a regression of the dermal papilla occurs. Telogen or a rest stage follows, before the cycle is repeated.

Hair follicle stem cells are an ideal system to investigate the underlying mechanisms that regulate stem cell quiescence and activation in mice as hair growth is largely synchronized during early adult life between

post-natal days 18 and 70. Several studies have shown that around three weeks post-natal, hair follicles are in a short telogen phase before entering the first anagen at four weeks. This first anagen phase lasts only a few days before the hair follicle starts to regress and enters a transient catagen phase. During this phase the lower part of the hair follicle is degraded, and the dermal papilla moves upward below the bulge stem cell compartment. By six weeks, the hair follicle enters a prolonged telogen phase that lasts up to four weeks before the hair follicle enters the next anagen phase by post-natal week ten. Although the exact timeline for the synchronized hair cycle varies slightly across genders and mouse strains, the quiescent and activated hair follicle stem cells can be isolated and examined by FACS sorting, and distinct morphological features of the hair follicle can be observed in the tissue across the hair cycle. Hair follicle stem cells are marked by distinct cell surface markers such as CD34 and CD49/alpha6 integrin, and many groups have taken advantage of these surface markers to isolate stem cells at specific timepoints in the hair cycle to perform transcriptome analyses [6-11]. These analyses and others have been instrumental in providing mechanistic insights into the various signaling pathways involved in regulating the quiescence and activation of these stem cells.

Signaling pathways such as BMP, Wnt and FGF signaling have been shown to play important roles in determining hair follicle stem cell states. BMP signaling has been shown to be important for governing hair follicle stem cell quiescence. Deletion of Bmpr1a in hair follicle stem cells led to a loss of quiescence and hyperproliferation of these stem cells. Bmpr1a knockout mice also fail to regenerate hair shafts, indicating that BMP signaling is involved in both quiescence and differentiation of hair follicle stem cells[12-14]. When beta-catenin or Wntless genes, necessary for activation of the Wnt pathway and for secretion of Wnt ligands, respectively, are deleted in the skin, hair follicle stem cell activation is interrupted. When Wnt signaling is induced, hair growth is stimulated through the stabilization of beta-catenin [15-17]. And while the BMP and Wnt signaling pathways have been shown to have distinct effects on hair follicle stem

cell quiescence and activation, FGF signaling pathways have shown more diverse regulatory outcomes and additional studies are still necessary to elucidate the mechanisms involved in their governing of stem cell states[18]. The Shh signaling pathway has also been shown to play a critical role in promoting hair follicle stem cell division shortly after the activation of the hair cycle[19]. Shh is predominantly produced by a subset of transit amplifying cells located in the hair follicle matrix. Transit amplifying cells are generated during the anagen phase, and as such represent an example of regulatory interactions that take place between stem cells and their progenies.

In addition to the role signaling pathways have been shown to play in regulating stem cell states such as those described in hair follicle here, more recent studies have revealed that metabolic pathways may also play a crucial role in the regulation of stem cell function as well[20]. Metabolic adaptations observed in stem cells have always been believed to be because of the changes in cell state, from quiescence to activation for example, but recent studies now suggest that metabolism itself can also dictate stem cell fate [(21-23)].

Metabolic Regulation of Stem Cell Function

Metabolism is now known to be a key regulator of pluripotency and differentiation in pluripotent stem cells, and stimulation or inhibition of glycolysis has been shown to directly determine stem cell fate through the promotion or inhibition of pluripotency. Pluripotent stem cells use glycolysis to generate ATP and demonstrate the hallmarks of glycolytic metabolism such as elevated levels of hexokinase II and decreased activity of pyruvate dehydrogenase. During differentiation, however, cells show decreased levels of uncoupling protein 2 known to increase mitochondrial respiration, and ATP is produced primarily in the mitochondria by oxidative phosphorylation. The precise mechanism by which metabolic states control pluripotency is still unclear, but it is believed that metabolites might directly regulate the

epigenetic machinery to maintain pluripotency in these cells. Acetyl-CoA and α-ketoglutarate are required for the function of histone acetyltransferases and demethylases, for example, and threonine catabolism is necessary for the synthesis of S-adenosylmethionine, key for maintaining pluripotency through the trimethylation of histone H3 lysine 4[24-29].

While extensive studies have been done to elucidate the role of metabolism in pluripotent stem cell function, there have been far fewer studies investigating the metabolic regulation of adult stem cells in different tissues or organisms. Like pluripotent stem cells, hematopoietic stem cells have been shown to rely on glycolytic metabolism, though there are mechanistic differences. Hematopoietic stem cells rely on glycolysis during quiescence but upregulate oxidative phosphorylation during activation and differentiation. The hypoxic bone marrow niche where hematopoietic stem cells reside is key for maintaining stem cell quiescence through the oxygen-sensing transcription factor hypoxia-inducible factor 1 alpha. In hematopoietic stem cells, hypoxia-inducible factor 1 alpha promotes glycolysis by upregulating glycolytic genes such as lactate dehydrogenase A and pyruvate activating pyruvate dehydrogenase kinases which inhibit pyruvate dehydrogenase and prevents the entry of pyruvate into the TCA cycle. This limits mitochondrial respiration and elevates glycolytic flux by inhibiting pyruvate dehydrogenase and preventing the entry of pyruvate into the TCA cycle. Conversely, more differentiated blood cells show reduced pyruvate dehydrogenase kinase levels, increased oxidative phosphorylation and ATP production [30-35].

While these studies give insight into the metabolic control of stem cell fate, hematopoietic stem cells are largely quiescent, and can remain dormant for months at a time. The regulation of stem cell function is often dependent on the requirements of the tissue, and so additional studies are necessary to improve

our understanding of the role metabolism can play in the stem cells of different tissues and organisms as well as under various conditions. Stem cell populations vary across tissues and organisms, and so while studies show that hematopoietic stem cells rely on glycolysis for quiescence, increasing mitochondrial activity and oxidative phosphorylation promotes quiescence in intestinal stem cells of Drosophila, and muscle stem cells appear to activate glycolysis during activation and differentiation in mice. Whether these differences are due to intrinsic variations within stem cells or simply their microenvironment is a topic under investigation.

In Chapter 2 of this manuscript, I describe my own efforts to gain a better understanding of the role of metabolism in tissue homeostasis using the hair follicle as a model system. Although normally dormant, hair follicle stem cells quickly become activated to divide during a new hair cycle. The quiescence of hair follicle stem cells is known to be regulated by several intrinsic and extrinsic mechanisms, but in this manuscript, I provide several lines of evidence to demonstrate that hair follicle stem cells utilize glycolytic metabolism and produce significantly more lactate than other cells in the epidermis. Furthermore, lactate generation appears to be critical for the activation of hair follicle stem cells as deletion of lactate dehydrogenase prevented their activation. Conversely, genetically promoting lactate production in these stem cells through mitochondrial pyruvate carrier 1 deletion accelerated their activation and the hair cycle. These data suggest that hair follicle stem cells maintain a metabolic state that allows them to remain dormant and yet quickly respond to appropriate proliferative stimuli.

Cells of Origin in Cancer

The deadliest human cancers most often form in epithelial tissues such as the skin, colon, breast, prostate or lung. The tissues in which these cancers arise are made up of a wide variety of cell types including

resident adult stem cells, progenitors and non-dividing terminally differentiated cells. And while many cancer-causing gene mutations have been identified, the cells that initiate tumor formation and the sequence of events following these mutations have remained poorly understood. Identification of the cells of origin in tumors has important implications for therapeutic approaches to suppress or reverse the initial phase of disease and would serve to alleviate the enormous challenges associated with the treatment of late-stage disease. It is well documented that tumors display vast heterogeneity both within and across tissues, and the molecular and cellular mechanisms behind this heterogeneity has remained an active area of research for decades.

Recently developed methods have allowed for the delivery of various cancer-causing genetic mutations to specific cell types *in vivo*. By conditionally expressing oncogenes or deleting tumor suppressor genes through the targeted activation of Cre recombinase expression in different cell populations, it is now possible to determine the cellular origin of various tumors in mice. This can be coupled with genetic lineage-tracing allowing for the conditional expression of a reporter gene such as β-galactosidase or a fluorescent protein in the cell lineage of interest and all its future progeny [36-41]. These experiments have provided insights into whether cancers are initiated by stem cells or other cell types in the tissue and have highlighted the ability of specific genetic hits to serve as tumor initiators or promoters. For an increasing number of cancers, the cell of origin has been demonstrated to be the resident adult stem cell. One such cancer is squamous cell carcinoma, for which recent studies in our lab traced its origin to the hair follicle stem cells.

Hair Follicle Stem Cells in Squamous Cell Carcinoma

Squamous cell carcinoma is the second most prevalent type of skin cancer and exhibits a significant risk for metastasis. Aggressive squamous cell carcinoma found on the lips and ears account for 2500 deaths

every year. In fact, squamous cell carcinoma is not just a disease of the skin but can form in all stratified squamous epithelia including those of the oral cavity (7600 deaths annually), the esophagus (14,530 deaths annually), and the anus (710 deaths annually). Mutations in the Ras gene family are found in 30% of all human cancers and are often found in human cases of squamous cell carcinoma. Both murine and human squamous cell carcinoma have been linked to activating mutations in Ras (including both Hras and Kras) and mutations in the tumor suppressor gene p53[42-45].

To define the cell of origin for squamous cell carcinoma in the skin, our lab compared delivery of constitutively active Kras (KrasG12D) and loss of p53 to various cell types in the hair follicle, either the stem cells or lineage-restricted transit amplifying populations [46-48]. Oncogenic mutations were driven in conjunction with either K15CrePR or ShhCreER to determine the relative capacity of hair follicle stem cells or lineage-restricted transit amplifying cells to serve as epidermal cancer cells of origin in SCC. Activation of the K15CrePR allele with mifepristone led to profound induction of hyperplasia, epithelial to mesenchymal transition, cysts, and eventually high-grade SCC routinely within 5 to 10 weeks. In contrast, induction of the same oncogenic stimulus in the transit amplifying cells using ShhCreER resulted in no abnormal epithelial structures. These data indicated that hair follicle stem cells, before becoming lineage-restricted transit amplifying cells, can serve as cells of origin for squamous cell carcinoma.

In addition to showing that hair follicle stem cells can serve as cells of origin for squamous cell carcinoma, subsequent studies in our lab demonstrated that they will only do so when in a permissive, activated state [49]. Induction of oncogenic Kras alone or oncogenic Kras combined with deletion of tumor suppressor p53 is sufficient to initiate tumorigenesis when the stem cells have been activated, but not when they are quiescent in the telogen phase. When oncogenic stimuli are delivered to the hair follicle stem cells during

telogen, there is no tumorigenic response until the initiation of a new hair cycle during the telogen to anagen transition phase. This observation was consistent with previous efforts showing a dependence on the hair cycle for cutaneous chemical carcinogenesis induction of squamous cell carcinoma [50]. Finally, this study demonstrated that quiescent hair follicle stem cells use the phosphatase Pten to dull the response to activated Ras, as deletion of this tumor suppressor allowed for tumor formation at any stage in the hair cycle.

Understanding why some cells are more sensitive to oncogenic stimuli and vulnerable to transformation while others are resistant is crucial for the development of effective therapeutic strategies to prevent cancer initiation and block tumor progression. Whether these mechanisms are conserved across different tissues and if they contribute to tumor heterogeneity is also a topic under intense investigation.

In Chapter 3 of this manuscript, I describe my efforts in gaining a better understanding of some of the mechanisms governing tumor initiation and progression using the hair follicle as a model for tumorigenesis. For over two decades, HMGA2 has been implicated as a player in human cancer; however, the question of whether HMGA2 is required for tumor initiation or progression has not been addressed. Hmga2 functions as a chromatin-associated factor during development but is not expressed in most adult tissues. Numerous studies have implicated Hmga2 in epithelial-to-mesenchymal transition (EMT) and cancer progression through gain of function studies, but it is unclear whether Hgma2 is necessary for EMT, tumor formation or tumor progression. We deleted Hmga2 in two mouse models of squamous cell carcinoma and found this gene to be dispensable. In fact, EMT, tumor initiation and progression all appeared to be mostly unaffected by the absence of Hmga2. Tumors lacking the ability to induce Hmga2

proceeded to initiate cutaneous spindle cell and squamous cell carcinomas with all the typical pathological and molecular hallmarks of these cancers.

Sources of Tumor Diversity

The cellular and molecular mechanisms that contribute to tumor heterogeneity remain key areas of research in cancer biology. Variability is observed not only between tumors arising in the same tissue or organ but within individual tumors as well. Tumors can show great variability in their cellular morphology, gene-expression profiles, metabolic profiles, proliferation, metastatic potential and therapeutic response. Whether the marked heterogeneity observed across tumors reflects distinct cells of origin, genetic lesions, the relationship between the tumor and its microenvironment or any combination of these remains unclear. Numerous studies on human cancers and in mouse models have highlighted the influence of various genetic lesions on tumor heterogeneity and function. The most common mutations seen in cancers are found in oncogenes and tumor-suppressors involved in cellular growth, survival, and proliferation such as PI3 kinase, MYC, RAS, p53, and PTEN. Both murine and human squamous cell carcinoma have been linked to activating mutations in Ras (including both Hras and Kras) and mutations in the tumor suppressor gene p53[51-63].

Squamous cell carcinoma is one example of a cancer that shows marked tumor heterogeneity and up to 12 different diagnoses are routinely made by pathology and histological examination of these tumors. Various hypotheses have been made to account for such tumor diversity from the cell of origin, to the identity of the genetic hits, contribution of an immune response, and vascularization, but little experimental evidence exists to support adequate conclusions. Studies in our lab have investigated the roles different cells of origin and genetic lesions play in tumor initiation and progression (Figure 2)[64]. We

performed experiments with a variety of inducible Cre lineages to determine whether hair follicle stem cells respond differently to constitutively active Kras (KrasG12D) or Hras (HrasG12V). As shown in Figure 2, delivery of HrasG12V generated barely detectable phenotypes in the hair follicle, even after extended periods of time, and this was the case whether K15CrePR or Lgr5CreER was used. This suggests that at least in murine models, hair follicle stem cells are less sensitive to mutations of Hras compared to Kras. Expression of HrasG12V in LGR6+ cells of the isthmus, sebaceous gland, and interfollicular epidermis also showed only minor hyperplasia of upper portions of the follicle and the interfollicular epidermis. Expression of KrasG12D in the same population, however, showed prominent upper follicle hyperplasia and occasional papillomas. While other groups have shown that mutant Hras targeted to hair follicle cells or interfollicular cells leads to squamous cell carcinomas or papillomas respectively, differences in results can likely be attributed to the differences in the transgenic approach used[65-68]. These studies used direct transgene injection into blastocysts which can potentially lead to supraphysiologic doses of the oncogenic Hras due to multiple integration sites into the genome. In our model, genetic knock-in mice were used which allowed for oncogenic Hras or Kras to be expressed from their native loci as is typical in patients with squamous cell carcinoma.

In another study, described in Chapter 4 of this manuscript, we sought to identify additional sources of tumor heterogeneity by fixing both the cell of origin (K15CrePR or Lgr5CreER) and the initial oncogenic driver (KrasG12D), while altering the identity of the second genomic hit, the tumor suppressor (p53, PTEN, or RB). In doing so, we sought to identify whether a specific population of cells within the epidermis, namely the hair follicle stem cells, can generate different types of tumors, and elucidate the role tumor suppressors play in tumor heterogeneity. In this study we show that hair follicle stem cells can drive a variety of squamous cell carcinoma phenotypes that correlate strictly with the type of tumor suppressor

deleted, and tumor suppressor deletion correlates with distinct phenotypes in proliferation, dedifferentiation and immune response.

Cellular Metabolism in Cancer

Mouse models of oncogenesis have been crucial in elucidating the cellular origins of cancer and the impact of various mutations on tumor initiation and progression. Despite the great genetic and histological heterogeneity observed across tumors, tumorigenesis seems to involve the common induction of pathways that support fundamental cellular functions like anabolism, catabolism, and redox balance. The reprogramming of pathways for nutrient acquisition and metabolism in tumors provides a selective advantage for cancer cells during tumorigenesis, and these metabolic alterations can have profound effects on gene expression, cellular differentiation, and the tumor microenvironment. Studies have shown that some metabolic alterations support malignant transformation while others are necessary for the maintenance and propagation of the tumor cells [69-71]. Understanding the metabolic pathways that may be limiting for cancer initiation and progression is key for guiding the development of more effective therapeutic approaches. A classic example of a metabolic adaptation seen across most cancers is the Warburg effect, or aerobic glycolysis. This phenomenon, first described by a German physiologist named Otto Warburg in the 1920s, states that tumors have an increased ability to use glucose to create lactate even in the presence of oxygen [72]. In normal tissues, glycolysis is a physiological response to hypoxia, but Warburg observed that cancer cells continuously take up glucose and produce lactate regardless of oxygen availability. The increase in glycolytic flux allows glycolytic intermediates to fulfill the metabolic demands of proliferating cells, and this observation has led to significant efforts to inhibit aerobic glycolysis to inhibit tumor formation or progression.

In many cases, the metabolic adaptations observed in cancer cells are carried out by the effectors of oncogenes and tumor suppressors. The transcriptional targets of MYC, for example, include metabolite transporters and enzymes required for glycolysis, fatty acid synthesis, glutaminolysis, serine metabolism, and mitochondrial metabolism. Oncogenes like KRAS have also been shown to regulate nutrient acquisition, macromolecular synthesis, and redox homeostasis by taking advantage of both PI3K and MYC pathways to promote tumorigenicity. Tumor suppressors such as p53 have also been shown to regulate metabolism and oxidative stress as loss of p53 increases glycolytic flux to promote anabolism and redox balance, two key processes that promote tumorigenesis [73-79] (Figure 3)[80].

To support the biosynthetic and bioenergetic demands associated with proliferation, a cell must increase the import of nutrients from the environment. A hallmark of cancer cells is the ability to acquire the necessary nutrients to both support cell survival and increase biomass even in nutrient-poor conditions. Glucose, glutamine and more recently lactate have all been described to be important fuels that support the metabolic functions of cancer cells[80-82]. Through the catabolism of these nutrients, cells can both maintain pools of diverse carbon intermediates necessary for the synthesis of various macromolecules and harness reducing power to mediate the transfer of electrons to the electron transport chain to fuel ATP generation (Figure 4)[94]. Biosynthetic or anabolic pathways enable cells to produce macromolecules including proteins, lipids, and nucleic acids required for cell division and tumor growth. Oncogenic mutations, particularly in the PI3K-mTOR signaling pathway, have been shown to promote macromolecular biosynthesis in cancer cells. Both glutamine uptake and glutaminase activity are stimulated by mTORC1 to generate glutamate for transamination reactions, the TCA cycle, and amino acid synthesis. When nutrients are scarce, cells also have access to several catabolic pathways to degrade macromolecules and resupply key pools of intracellular metabolic intermediates from inside and outside of the cell. Cancer calls have been shown to take advantage of autophagy, micropinocytosis and lipid

scavenging pathways to survive nutrient-poor environments [83-89]. Cancer cells show great metabolic flexibility, and we are only beginning to understand the extent to which these cells can make use of other nutrients such as including essential fatty acids, choline, trace metals, and vitamins for their survival.

Glycolysis has been an attractive target for therapeutic intervention given the widespread observation that many tumors show a significant increase in glucose uptake compared to normal tissue. Lactate dehydrogenase, responsible for the conversion of pyruvate to lactate in glycolysis, is as a direct metabolic target of MYC, and genetic or pharmacologic inhibition of this enzyme has been shown to diminish MYC-driven tumors in xenograft models. Additional studies show that inhibition of lactate dehydrogenase leads to the regression of established tumors in mouse models of non-small cell lung cancer and delayed progression of myeloid leukemia [90-96]. Lactate has also been shown to inhibit cytotoxic T cells and reprogram macrophages to promote tumorigenesis [97-98]. While dependence on lactate dehydrogenase has been demonstrated both genetically and pharmacologically in a variety of tumor models, success of lactate dehydrogenase inhibitors has been limited.

In Chapter 5 of this manuscript, I describe the most recent efforts in our lab to target glycolytic metabolism in a squamous cell carcinoma tumor model. Murine squamous cell carcinoma can be initiated by hair follicle stem cells through induction of active Kras and loss of p53. As described in Chapter 2, hair follicle stem cells are now known to use glucose to make more lactate than other cell types in the epidermis, and the activity of lactate dehydrogenase acts to promote hair follicle activation. Therefore, we sought to determine whether lactate dehydrogenase activity in squamous cell carcinoma tumors is a marker of the cell type from which these cells arise, or a key metabolic pathway important for tumor initiation or progression. Deletion of lactate dehydrogenase enzyme activity in hair follicle stem cell-mediated

tumorigenesis in fact showed no effect on tumor number, time to tumor formation, tumor proliferation, epithelial to mesenchymal transition in tumors, gene expression in tumors, or the immune response to tumors. Tumors null for lactate dehydrogenase showed dramatically reduced levels of most glycolytic metabolites by metabolomics, and significantly reduced glucose uptake as shown by FDG-PET live animal imaging. Finally, deletion of lactate dehydrogenase in existing tumors or genetic induction of its activity also had no effect on tumor initiation or progression. These surprising results suggest that squamous cancer cells of origin do not require lactate dehydrogenase activity to generate cancers.

Figures

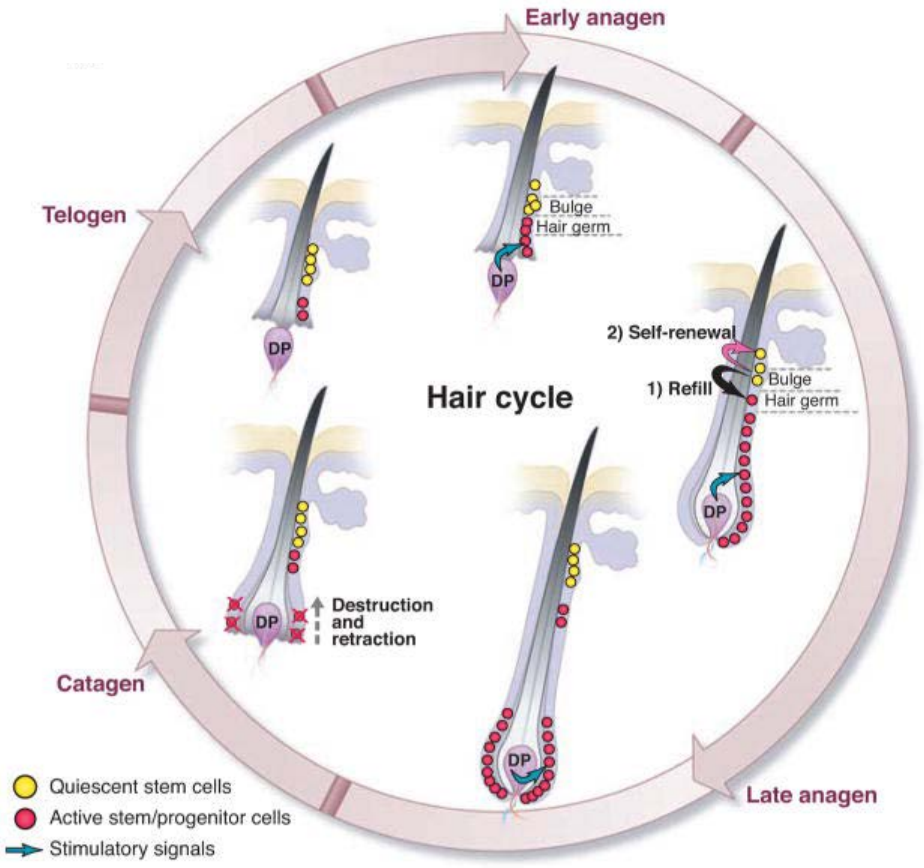

Figure 1. Stages of the Hair Cycle[5].

At the start of anagen, the dermal papilla (DP) is proximal to the hair germ and bulge. Stem/ progenitor cells in hair germ (a structure below the bulge) are activated by the DP first, whereas stem cells remain quiescent in bulge. When hair germ cells enter the hair matrix, then stem cells in bulge are activated to replenish lost hair germ cells. During anagen, active hair germ cells give rise to transit amplifying (TA) cells, which in turn support hair growth. DP is pushed down from bulge because of fast expansion of progenitor cells. In catagen, DP retracts toward bulge.

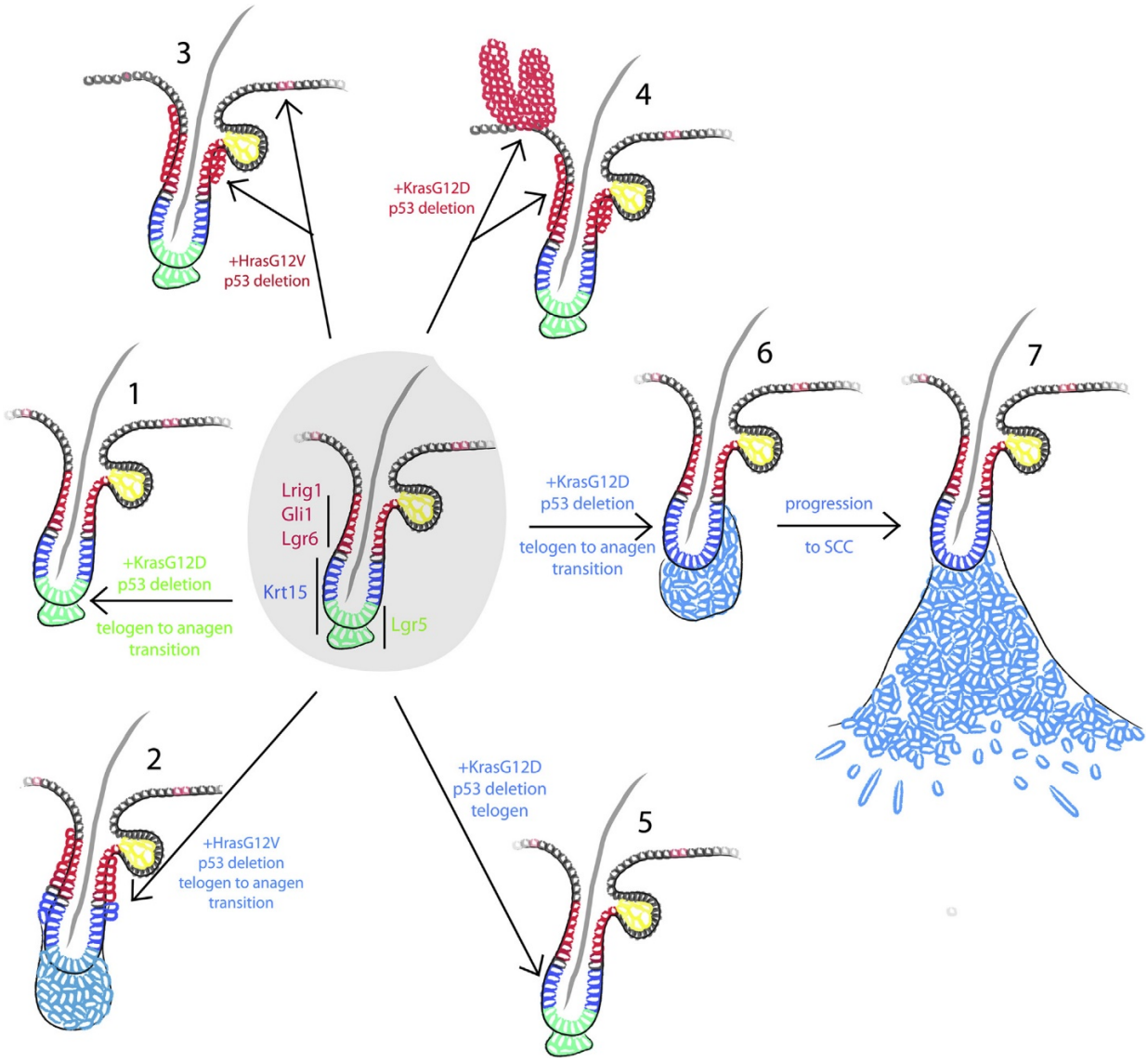

Figure 2. This image depicts several scenarios for modeling tumor initiation by various transgenic means[64].

(1) Constitutive Kras is induced and p53 is deleted in Lgr5+ cells of the bulge, but there is no effect in the short term, even after a telogen to anagen transition. (2) Induction of Hras and deletion of p53 in Krt15+ cells leads to only minor follicular hyperplasia. (3) Induction of constitutive Hras and deletion of p53 in Lgr6+ cells drives infundibular hyperplasia. (4) Induction of constitutive Kras and deletion of p53 in Lgr6+ cells generates infundibular hyperplasia and papilloma. (5) Induction of constitutive Kras and deletion of p53 in telogen has no effect until the next hair cycle. (6) Induction of Kras and deletion of p53 before or during a telogen-to-anagen transition drives tumor initiation, and eventually leads to (7) carcinoma. Note that only cell types with defined Cre lineage drivers are depicted in the image, and that the image does not fully depict all the types of phenotype that arise from the indicated genotype.

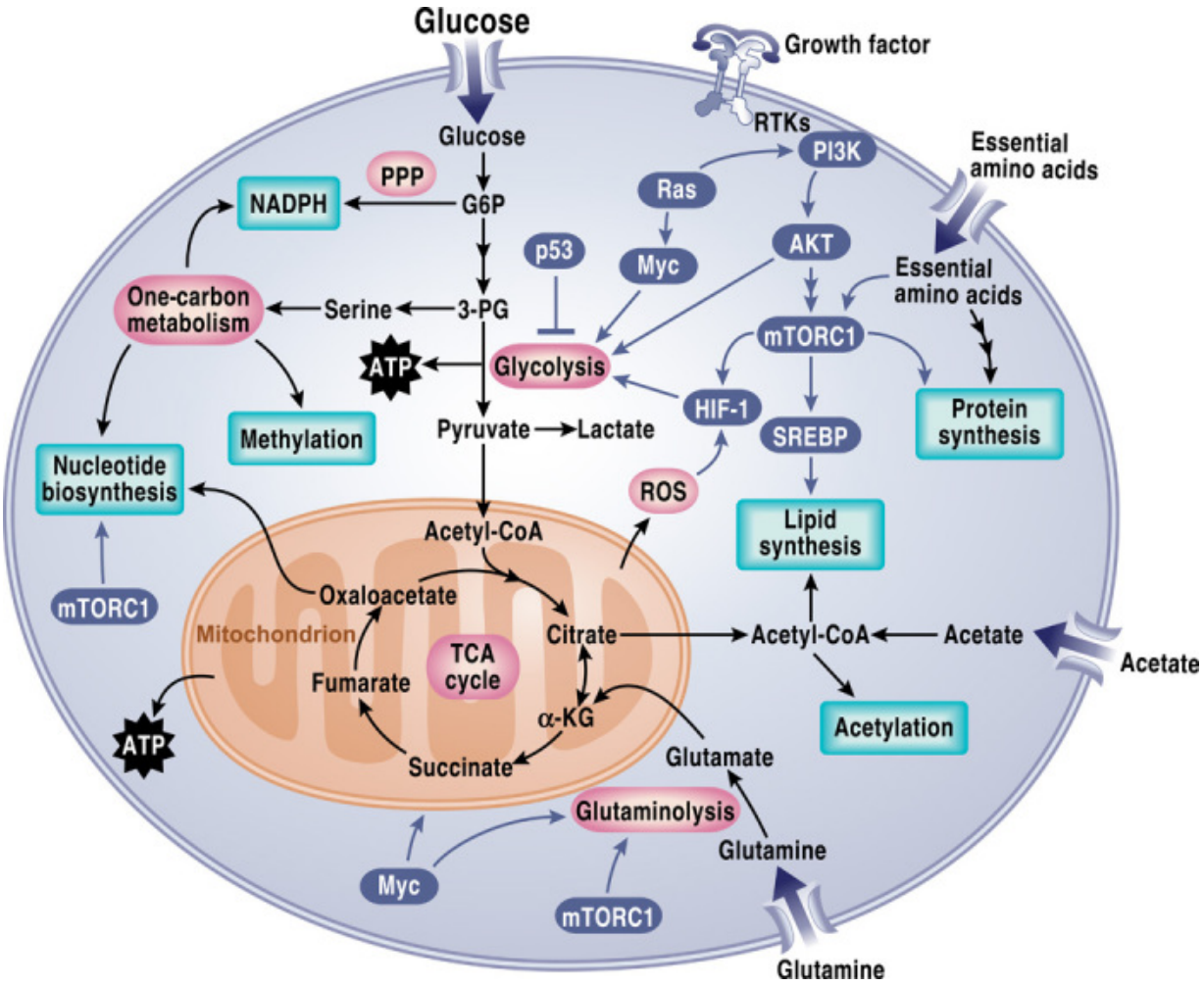

Figure 3. Signaling pathways that regulate cancer metabolism[80].

Tumor cells have aberrant activation of mTORC1 that induces an anabolic growth program resulting in nucleotide, protein, and lipid synthesis. Loss of tumor suppressors like p53 or activation of oncogenes like MYC further promotes anabolism through transcriptional regulation of metabolic genes. Metabolism controls signaling through regulating reactive oxygen species (ROS), acetylation, and methylation. PPP, pentose phosphate pathway; G6P, glucose-6-phosphate; 3-PG, 3-phosphoglycerate; ATP, adenosine 5´-triphosphate; mTORC1, mTOR complex 1; α-KG, α-ketoglutarate; RTK, receptor tyrosine kinase.

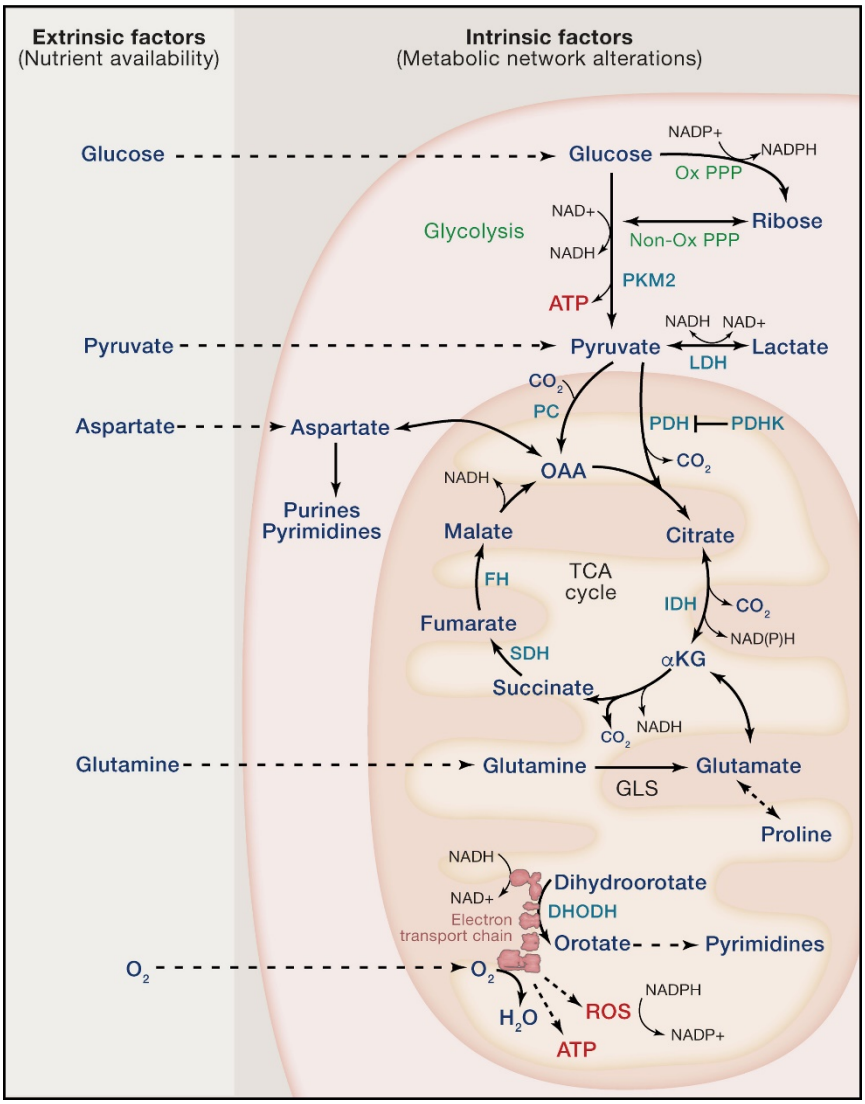

Figure 4. Nutrient Availability and the Metabolic Network Both Influence Metabolic Phenotypes[94].

Both nutrient availability and metabolic network configuration affect how cells use metabolism to produce ATP, generate macromolecules, and regulate redox state. Key reactions in central carbon metabolism are shown, including how the TCA cycle and the electron transport chain are involved in purine and pyrimidine synthesis. Some of the reactions catalyzed by enzymes and metabolites discussed in this Review are also shown for reference. PKM2, pyruvate kinase M2; LDH, lactate dehydrogenase; PDH, pyruvate dehydrogenase; PDHK, pyruvate dehydrogenase kinase; PC, pyruvate carboxylase; IDH, isocitrate dehydrogenase; SDH, succinate dehydrogenase; FH, fumarate hydratase; GLS, glutaminase; DHODH, dihydroorotate dehydrogenase; Ox PPP, oxidative pentose phosphate pathway; Non-Ox PPP, non-oxidative pentose phosphate pathway; αKG, α-ketoglutarate; OAA, oxaloacetate; ROS, reactive oxygen species.

References

1. Till JE, McCulloch EA. A direct measurement of the radiation sensitivity of normal mouse bone marrow cells. Radiat Res 1961; 14: 213–222.

2. Becker AJ, McCulloch EA, Till JE. Cytological demonstration of the clonal nature of spleen colonies derived from transplanted mouse marrow cells. Nature 1963; 197: 452–454.

3. Morrison SJ, Scadden DT. The bone marrow niche for haematopoietic stem cells. Nature 2014; 505: 327–334.

4. Nowak, J. A., Polak, L., Pasolli, H. A. & Fuchs, E. Hair follicle stem cells are specified and function in early skin morphogenesis. Cell Stem Cell 3, 33-43 (2008).

5. Li L, Clevers H. Coexistence of Quiescent and Active Adult Stem Cells in Mammals. Science 29 Jan 2010: Vol. 327, Issue 5965, pp. 542-545 DOI: 10.1126/science.1180794

6. Cotsarelis G, Sun TT, Lavker RM. Label retaining cells reside in the bulge area of pilosebaceous unit: Implications for follicular Mechanisms of Quiescent Hair Follicle Stem Cell Regulation. Cell 1990; 61:1329–1337.

7. Oshima H, Rochat A, Kedzia C et al. Morphogenesis and renewal of hair follicles from adult multipotent stem cells. Cell 2001; 104:233–245.

8. Tumbar T, Guasch G, Greco V et al. Defining the epithelial stem cell niche in skin. Science 2004; 303:359–363.

9. Blanpain C, Lowry WE, Geoghegan A et al. Self-renewal, multipotency, and the existence of two cell populations within an epithelial stem cell niche. Cell 2004;118:635

10. Liu Y, Lyle S, Yang Z et al. Keratin 15 promoter targets putative epithelial stem cells in the hair follicle bulge. J Invest Dermatol 2003;121:963–968.

11. Morris RJ, Bortner CD, Cotsarelis G et al. Enrichment for living murine keratinocytes from the hair follicle bulge with the cell surface marker CD34. J Invest Dermatol 2003; 120:501–511.

12. Deschene ER, Myung P, Rompolas P et al. b-Catenin activation regulates tissue growth non-cell autonomously in the hair stem cell niche. Science 2014;343:1353– 1356

13. Andl T, Ahn K, Kairo A et al. Epithelial Bmpr1a regulates differentiation and proliferation in postnatal hair follicles and is essential for tooth development. Development 2004;131:2257–2268.

14. Greco V, Chen T, Rendl M et al. A two-step mechanism for stem cell activation during hair regeneration. Cell Stem Cell 2009;4: 155–169.

15. Lowry WE, Blanpain C, Nowak JA et al. Defining the impact of beta-catenin/Tcf transactivation

16. Ito M, Yang Z, Andl T et al. Wnt-dependent de novo hair follicle regeneration in adult mouse skin after wounding. Nature 2007;447:316–320.

17. Yuhki M, Yamada M, Kawano M et al. BMPR1A signaling is necessary for hair follicle cycling and hair shaft differentiation in mice. Development 2004;131:1825–1833.

18. Kobielak K, Stokes N, de la Cruz J et al. Loss of a quiescent niche but not follicle stem cells in the absence of bone morphogenetic protein signaling. Proc Natl Acad Sci USA 2007;104:10063–10068.

19. Plikus MV, Mayer JA, de la Cruz D et al. Cyclic dermal BMP signaling regulates stem cell activation during hair regeneration. Nature 2008;451:340–344.

20. Chandel N.S., JasperH, Ho T.H. and Passegue E. Metabolic regulation of stem cell function in tissue homeostasis and organismal ageing. Nature Cell Biology. Vol. 18 (8) August 2016.

21. Zhang, J., Nuebel, E., Daley, G. Q., Koehler, C. M. & Teitell, M. A. Metabolic regulation in pluripotent stem cells during reprogramming and self-renewal. Cell Stem Cell 11, 589–595 (2012).

22. Teslaa, T. & Teitell, M. A. Pluripotent stem cell energy metabolism: an update. EMBO J. 34, 138–153 (2015).

23. Folmes, C. D. et al. Somatic oxidative bioenergetics transitions into pluripotency dependent glycolysis to facilitate nuclear reprogramming. Cell Metab. 14, 264–271 (2011).

24. Zhang, J. et al. UCP2 regulates energy metabolism and differentiation potential of human pluripotent stem cells. EMBO J. 30, 4860–4873 (2011).

25. Son, M. J. et al. Mitofusins deficiency elicits mitochondrial metabolic reprogramming to pluripotency. Cell Death Differ. 22, 1957–1969 (2015).

26. Kaelin, W. G. Jr & McKnight, S. L. Influence of metabolism on epigenetics and disease. Cell 153, 56–69 (2013).

27. Wang, J. et al. Dependence of mouse embryonic stem cells on threonine catabolism. Science 325, 435–439 (2009).

28. Sperber, H. et al. The metabolome regulates the epigenetic landscape during naïve to-primed human embryonic stem cell transition. Nat. Cell Biol. 17, 1523–1535 (2015).

29. Cheung, T. H. & Rando, T. A. Molecular regulation of stem cell quiescence. Nat. Rev. Mol. Cell Biol. 14, 329–340 (2013).

30. Pietras, E. M., Warr, M. & Passegué, E. Cell cycle regulation in hematopoietic stem cells. J. Cell Biol. 195, 709–720 (2011).

31. Simsek, T. et al. The distinct metabolic profile of hematopoietic stem cells reflects their location in a hypoxic niche. Cell Stem Cell 7, 380–390 (2010).

32. Takubo, K. et al. Regulation of glycolysis by Pdk functions as a metabolic checkpoint for cell cycle quiescence in hematopoietic stem cells. Cell Stem Cell 12, 49–61 (2013).

33. Yu, W. M. et al. Metabolic regulation by the mitochondrial phosphatase PTPMT1 is required for hematopoietic stem cell differentiation. Cell Stem Cell 12, 62–74 (2013).

34. Maryanovich, M. et al. An MTCH2 pathway repressing mitochondria metabolism regulates haematopoietic stem cell fate. Nat. Commun. 6, 7901 (2015).

35. Takubo, K. et al. Regulation of the HIF-1alpha level is essential for hematopoietic stem cells. Cell Stem Cell 7, 391–402 (2010).

36. Brownell I, Guevara E, Bai CB, Loomis CA, Joyner AL. Nerve-derived sonic hedgehog defines a niche for hair follicle stem cells capable of becoming epidermal stem cells. Cell Stem Cell 2011;8:552e65.

37. Grachtchouk M, Pero J, Yang SH, Ermilov AN, Michael LE, Wang A, et al. Basal cell carcinomas in mice arise from hair follicle stem cells and multiple epithelial progenitor populations. J Clin Invest 2011;121: 1768e81.

38. Jaks V, Barker N, Kasper M, van Es JH, Snippert HJ, Clevers H, et al. Lgr5 marks cycling, yet long-lived, hair follicle stem cells. Nat Genet 2008;40:1291e9.

39. Jensen KB, Collins CA, Nascimento E, Tan DW, Frye M, Itami S, et al. Lrig1 expression defines a distinct multipotent stem cell population in mammalian epidermis. Cell Stem Cell 2009;4:427e39.

40. Kasper M, Jaks V, Are A, Bergstrom A, Schwager A, Barker N, et al. Wounding enhances epidermal tumorigenesis by recruiting hair follicle keratinocytes. Proc Natl Acad Sci USA 2011;108:4099e104.

41. Morris RJ, Liu Y, Marles L, Yang Z, Trempus C, Li S, et al. Capturing and profiling adult hair follicle stem cells. Nat Biotechnol 2004;22:411e7.

42. Alam, M. & Ratner, D. Cutaneous squamous-cell carcinoma. N Engl J Med 344, 975-983, doi:10.1056/NEJM200103293441306 (2001).

43. Pickering CR, Zhou JH, Lee JJ, Drummond JA, Peng SA, Saade RE, et al. Mutational landscape of aggressive cutaneous squamous cell carcinoma. Clin Cancer Res 2014;20:6582e92.

44. South AP, Purdie KJ, Watt SA, Haldenby S, den Breems NY, Dimon M, et al. NOTCH1 mutations occur early during cutaneous squamous cell carcinogenesis. J Invest Dermatol 2014;134:2630e8.

45. Durinck S, Ho C, Wang NJ, Liao W, Jakkula LR, Collisson EA, et al. Temporal dissection of tumorigenesis in primary cancers. Cancer Discov 2011;1: 137e43.

46. White AC, Lowry WE. Exploiting the origins of Ras mediated squamous cell carcinoma to develop novel therapeutic interventions. Small GTPases 2011;2:318e21.

47. White AC, Lowry WE. Refining the role for adult stem cells as cancer cells of origin. Trends Cell Biol 2015;25:11e20.

48. White AC, Tran K, Khuu J, Dang C, Cui Y, Binder SW, et al. Defining the origins of Ras/p53-mediated squamous cell carcinoma. Proc Natl Acad Sci USA 2011;108:7425e30.

49. White AC, Khuu JK, Dang CY, Hu J, Tran KV, Liu A, et al. Stem cell quiescence acts as a tumour suppressor in squamous tumours. Nat Cell Biol 2014;16: 99e107.

50. Miller SJ, Wei ZG, Wilson C, Dzubow L, Sun TT, Lavker RM. Mouse skin is particularly susceptible to tumor initiation during early anagen of the hair cycle: possible involvement of hair follicle stem cells. J Invest Dermatol 1993;101:591e4.

51. Ma, X. J. et al. Gene expression profiles of human breast cancer progression. Proc. Natl Acad. Sci. USA 100, 5974–5979 (2003).

52. Weigelt, B. et al. Gene expression profiles of primary breast tumors maintained in distant metastases. Proc. Natl Acad. Sci. USA 100, 15901–15905 (2003).

53. Tlsty, T. D. & Coussens, L. M. Tumor stroma and regulation of cancer development. Annu. Rev. Pathol. 1, 119–150 (2006).

54. Weinstein, I. B. Addiction to oncogenes—the Achilles heal of cancer. Science 297, 63–64 (2002).

55. Lapouge G, Youssef KK, Vokaer B, Achouri Y, Michaux C, Sotiropoulou PA, et al. Identifying the cellular origin of squamous skin tumors. Proc Natl Acad Sci USA 2011;108:7431e6.

56. Nassar D, Latil M, Boeckx B, Lambrechts D, Blanpain C. Genomic landscape of carcinogen-induced and genetically induced mouse skin squamous cell carcinoma. Nat Med 2015;21:946e54.

57. Nichols AC, Yoo J, Palma DA, Fung K, Franklin JH, Koropatnick J, et al. Frequent mutations in TP53 and CDKN2A found by next-generation sequencing of head and neck cancer cell lines. Arch Otolaryngol Head Neck Surg 2012;138:732e9.

58. South AP, Purdie KJ, Watt SA, Haldenby S, den Breems NY, Dimon M, et al. NOTCH1 mutations occur early during cutaneous squamous cell carcinogenesis. J Invest Dermatol 2014;134:2630e8.

59. Stransky N, Egloff AM, Tward AD, Kostic AD, Cibulskis K, Sivachenko A, et al. The mutational landscape of head and neck squamous cell carcinoma. Science 2011;333:1157e60.

60. Su F, Viros A, Milagre C, Trunzer K, Bollag G, Spleiss O, et al. RAS mutations in cutaneous squamous-cell carcinomas in patients treated with BRAF inhibitors. N Engl J Med 2012;366:207e15.

61. van der Schroeff JG, Evers LM, Boot AJ, Bos JL. Ras oncogene mutations in basal cell carcinomas and squamous cell carcinomas of human skin. J Invest Dermatol 1990;94:423e5.

62. Yoneda K, Yokoyama T, Yamamoto T, Hatabe T,Osaki T. p53 gene mutations and p21 protein expression induced independently of p53, by TGF-beta and gamma-rays in squamous cell carcinoma cells. Eur J Cancer 1999;35:278e83.

63. Ziegler A, Jonason AS, Leffell DJ, Simon JA, Sharma HW, Kimmelman J, et al. Sunburn and p53 in the onset of skin cancer. Nature 1994;372:773e6.

64. Lowry WE, Flores A, and White AC. Exploiting Mouse Models to Study Ras-Induced Cutaneous Squamous Cell Carcinoma. Journal of Investigative Dermatology (2016) 136, 1543e1548; doi:10.1016/j.jid.2016.03.017

65. Bailleul B, Surani MA, White S, Barton SC, Brown K, Blessing M, et al. Skin hyperkeratosis and papilloma formation in transgenic mice expressing a ras oncogene from a suprabasal keratin promoter. Cell 1990;62:697e708.

66. Greenhalgh DA, Rothnagel JA, Quintanilla MI, Orengo CC, Gagne TA, Bundman DS, et al. Induction of epidermal hyperplasia, hyperkeratosis, and papillomas in transgenic mice by a targeted v-Ha-ras oncogene. Mol Carcinog 1993;7:99e110.

67. Hansen LA, Tennant RW. Follicular origin of epidermal papillomas in v-Ha-ras transgenic TG.AC mouse skin. Proc Natl Acad Sci USA 1994;91:7822e6.

68. Owens DM, Spalding JW, Tennant RW, Smart RC. Genetic alterations cooperate with v-Ha-ras to accelerate multistage carcinogenesis in TG.AC transgenic mouse skin. Cancer Res 1995;55:3171e8.

69. Boroughs L. K., DeBerardinis R. J., Metabolic pathways promoting cancer cell survival and growth. Nat. Cell Biol. 17, 351–359 (2015).

70. Ward P. S., Thompson C. B., Metabolic reprogramming: A cancer hallmark even Warburg did not anticipate. Cancer Cell 21, 297–308 (2012).

71. Lunt S. Y., Vander Heiden M. G., Aerobic glycolysis: Meeting the metabolic requirements of cell proliferation. Annu. Rev. Cell Dev. Biol. 27, 441–464 (2011).

72. Koppenol W. H., Bounds P. L., Dang C. V., Otto Warburg's contributions to current concepts of cancer metabolism. Nat. Rev. Cancer 11, 325–337 (2011).

73. Stine Z. E., Walton Z. E., Altman B. J., Hsieh A. L., Dang C. V., MYC, metabolism, and cancer. Cancer Discov. 5, 1024–1039 (2015). [PMC free article]

74. Kruiswijk F., Labuschagne C. F., Vousden K. H., p53 in survival, death and metabolic health: A lifeguard with a licence to kill. Nat. Rev. Mol. Cell Biol. 16, 393–405 (2015).

75. Jiang L., Kon N., Li T., Wang S. J., Su T., Hibshoosh H., Baer R., Gu W., Ferroptosis as a p53-mediated activity during tumour suppression. Nature 520, 57–62 (2015).

76. Li T., Kon N., Jiang L., Tan M., Ludwig T., Zhao Y., Baer R., Gu W., Tumor suppression in the absence of p53-mediated cell-cycle arrest, apoptosis, and senescence. Cell 149, 1269–1283 (2012).

77. B.J. Altman, Z.E. Stine, C.V. Dang. From Krebs to clinic: glutamine metabolism to cancer therapy. Nat. Rev. Cancer, 16 (2016), pp. 619-634

78. E. White. Exploiting the bad eating habits of Ras-driven cancers. Genes Dev., 27 (2013), pp. 2065-2071

79. J.J. Howell, S.J. Ricoult, I. Ben-Sahra, B.D. Manning. A growing role for mTOR in promoting anabolic metabolism. Biochem. Soc. Trans., 41 (2013), pp. 906-912

80. R.J. DeBerardinis, N.S. Chandel. Fundamentals of cancer metabolism. Sci. Adv., 2 (2016), p. e1600200

81. M.G. Vander Heiden, L.C. Cantley, C.B. Thompson. Understanding the Warburg effect: the metabolic requirements of cell proliferation. Science, 324 (2009), pp. 1029-103

82. R.J. DeBerardinis, A. Mancuso, E. Daikhin, I. Nissim, M. Yudkoff, S. Wehrli, C.B. Thompson. Beyond aerobic glycolysis: transformed cells can engage in glutamine metabolism that exceeds the requirement for protein and nucleotide synthesis. Proc. Natl. Acad. Sci. USA, 104 (2007), pp. 19345-19350

83. McCracken A. N., Edinger A. L., Nutrient transporters: The Achilles' heel of anabolism. Trends Endocrinol. Metab. 24, 200–208 (2013)

84. Nicklin P., Bergman P., Zhang B., Triantafellow E., Wang H., Nyfeler B., Yang H., Hild M., Kung C., Wilson C., Myer V. E., MacKeigan J. P., Porter J. A., Wang Y. K., Cantley L. C., Finan P. M., Murphy L. O., Bidirectional transport of amino acids regulates mTOR and autophagy. Cell 136, 521–534 (2009).

85. Galluzzi L., Pietrocola F., Levine B., Kroemer G., Metabolic control of autophagy. Cell 159, 1263–1276 (2014).

86. White E., The role for autophagy in cancer. J. Clin. Invest. 125, 42–46 (2015).

87. Galluzzi L., Pietrocola F., Bravo-San Pedro J. M., Amaravadi R. K., Baehrecke E. H., Cecconi F., Codogno P., Debnath J., Gewirtz D. A., Karantza V., Kimmelman A., Kumar S., Levine B., Maiuri M. C., Martin S. J., Penninger J., Piacentini M., Rubinsztein D. C., Simon H.-U., Simonsen A., Thorburn A. M., Velasco G., Ryan K. M., Kroeme G.r, Autophagy in malignant transformation and cancer progression. EMBO J. 34, 856–880 (2015).

88. Commisso C., Davidson S. M., Soydaner-Azeloglu R. G., Parker S. J., Kamphorst J. J., Hackett S., Grabocka E., Nofal M., Drebin J. A., Thompson C. B., Rabinowitz J. D., Metallo C. M., Vander Heiden M. G., Bar-Sagi D., Macropinocytosis of protein is an amino acid supply route in Ras-transformed cells. Nature 497, 633–637 (2013).

89. Palm W., Park Y., Wright K., Pavlova N. N., Tuveson D. A., Thompson C. B., The utilization of extracellular proteins as nutrients is suppressed by mTORC1. Cell 162, 259–270 (2015).

90. V.R. Fantin, J. St-Pierre, P. Leder. Attenuation of LDH-A expression uncovers a link between glycolysis, mitochondrial physiology, and tumor maintenance

91. A. Boudreau, H.E. Purkey, A. Hitz, K. Robarge, D. Peterson, S. Labadie, M. Kwong, R. Hong, M. Gao, C. Del Nagro, et al.Metabolic plasticity underpins innate and acquired resistance to LDHA inhibition. Nat. Chem. Biol., 12 (2016), pp. 779-786

92. A. Le, C.R. Cooper, A.M. Gouw, R. Dinavahi, A. Maitra, L.M. Deck, R.E. Royer, D.L. Vander Jagt, G.L. Semenza, C.V. Dang. Inhibition of lactate dehydrogenase A induces oxidative stress and inhibits tumor progression. Proc. Natl. Acad. Sci. USA, 107 (2010), pp. 2037-2042

93. H. Shim, C. Dolde, B.C. Lewis, C.S. Wu, G. Dang, R.A. Jungmann, R. Dalla-Favera, C.V. Dang. c-Myc transactivation of LDH-A: implications for tumor metabolism and growth. Proc. Natl. Acad. Sci. USA, 94 (1997), pp. 6658-6663

94. Vander Heiden M. G. and DeBerardinis R. J.Understanding the intersections between metabolism and cancer biology.Cell. 168, February 2017.

95. Xie H., Hanai J.-., Ren J.-G., Kats L., Burgess K., Bhargava P., Signoretti S., Billiard J., Duffy K. J., Grant A., Wang X., Lorkiewicz P. K., Schatzman S., Bousamra M. II, Lane A. N., Higashi R. M., Fan T. W. M., Pandolfi P. P., Sukhatme V. P., Seth P., Targeting lactate dehydrogenase-a inhibits tumorigenesis and tumor progression in mouse models of lung cancer and impacts tumor-initiating cells. Cell Metab. 19, 795–809 (2014).

96. Wang Y.-H., Israelsen W. J., Lee D., Yu V. W. C., Jeanson N. T., Clish C. B., Cantley L. C., Vander Heiden M. G., Scadden D. T., Cell-state-specific metabolic dependency in hematopoiesis and leukemogenesis. Cell 158, 1309–1323 (2014).

97. Haas R., Smith J., Rocher-Ros V., Nadkarni S., Montero-Melendez T., D'Acquisto F., Bland E. J., Bombardieri M., Pitzalis C., Perretti M., Marelli-Berg F. M., Mauro C., Lactate regulates metabolic and pro-inflammatory circuits in control of T cell migration and effector functions. PLOS Biol. 13, e1002202 (2015).

98. Colegio O. R., Chu N.-Q., Szabo A. L., Chu T., Rhebergen A. M., Jairam V., Cyrus N., Brokowski C. E., Eisenbarth S. C., Phillips G. M., Cline G. W., Phillips A. J., Medzhitov R., Functional polarization of tumour-associated macrophages by tumour-derived lactic acid. Nature 513, 559–563 (2014).

Chapter 2: Lactate dehydrogenase activity drives hair follicle stem cell activation

nature cell biology

ARTICLES

Lactate dehydrogenase activity drives hair follicle stem cell activation

Aimee Flores[1,2,3], John Schell[4], Abigail S. Krall[5], David Jelinek[1], Matilde Miranda[1], Melina Grigorian[6], Daniel Braas[5,7], Andrew C. White[8], Jessica L. Zhou[9], Nicholas A. Graham[5,9], Thomas Graeber[5,10], Pankaj Seth[11], Denis Evseenko[12], Hilary A. Coller[1,2,3,13,14], Jared Rutter[4,15], Heather R. Christofk[2,5,7,13,14,16] and William E. Lowry[1,2,3,13,16]

Although normally dormant, hair follicle stem cells (HFSCs) quickly become activated to divide during a new hair cycle. The quiescence of HFSCs is known to be regulated by a number of intrinsic and extrinsic mechanisms. Here we provide several lines of evidence to demonstrate that HFSCs utilize glycolytic metabolism and produce significantly more lactate than other cells in the epidermis. Furthermore, lactate generation appears to be critical for the activation of HFSCs as deletion of lactate dehydrogenase (Ldha) prevented their activation. Conversely, genetically promoting lactate production in HFSCs through mitochondrial pyruvate carrier 1 (Mpc1) deletion accelerated their activation and the hair cycle. Finally, we identify small molecules that increase lactate production by stimulating Myc levels or inhibiting Mpc1 carrier activity and can topically induce the hair cycle. These data suggest that HFSCs maintain a metabolic state that allows them to remain dormant and yet quickly respond to appropriate proliferative stimuli.

The hair follicle is able to undergo cyclical rounds of rest (telogen), regeneration (anagen) and degeneration (catagen). The ability of the hair follicle to maintain this cycle depends on the presence of the hair follicle stem cells, which reside in the bulge (Fig. 1). At the start of anagen, bulge stem cells are activated by signals received from the dermal papilla, which at that stage abuts the bulge area[1,2]. These stem cells exit the bulge and proliferate downwards, creating a trail that becomes the outer root sheath. Bulge stem cells are capable of giving rise to all the different cell types of the hair follicle. The ability of HFSCs to maintain quiescence and yet become proliferative for a couple days before returning to quiescence is unique in this tissue, and the precise mechanism by which these cells are endowed with this ability is not fully understood. While significant effort has produced a wealth of knowledge on both the transcriptional and epigenetic mechanisms by which HFSCs are maintained and give rise to various lineages[3,4], little is known about metabolic pathways in the hair follicle or adult stem cells *in vivo*.

Considering the fact that there are essentially no published data on metabolic states of any cell in the hair follicle, a detailed study of metabolism was necessary to understand the nature of HFSCs and their progeny. Several previous studies employed genetic disruption of the mitochondrial electron transport chain in the epidermis by deletion under the control of a pan-epidermal keratin promoter and found that mitochondrial function was essential for maintenance of the follicle[5–8]. However, these studies did not explore the metabolic requirements for specific cell types within the tissue, nor did they explore a role for glycolytic metabolism. In this study, we present methods to study the metabolism of HFSCs *in vivo*, and provide evidence that these cells take advantage of a distinct mode of metabolism not found in their progeny. In the process, we also define small molecules that can take advantage of the unique metabolism of HFSCs to ignite the hair cycle in otherwise quiescent follicles.

RESULTS

Numerous studies have uncovered unique gene expression signatures in HFSCs versus other follicle cells or cells of the interfollicular epidermis[9–12]. Many of these signatures are regulated by transcription factors that were later shown to play important roles in HFSC

[1]Department of Molecular Cell and Developmental Biology, UCLA, 90095, USA. [2]Eli and Edythe Broad Center for Regenerative Medicine, UCLA, 90095, USA. [3]Molecular Biology Institute, UCLA, 90095, USA. [4]Department of Biochemistry, University of Utah, 84322, USA. [5]Department of Molecular and Medical Pharmacology, UCLA, 90095, USA. [6]Stanford School of Medicine, Stanford University, 94305, USA. [7]UCLA Metabolomics Center, UCLA, 90095, USA. [8]School of Veterinary Medicine, Cornell University, 14853, USA. [9]Mork Family Department of Chemical Engineering, University of Southern California, 90089, USA. [10]Crump Institute for Molecular Imaging, UCLA, 90095, USA. [11]Division of Interdisciplinary Medicine and Biotechnology, Beth Israel Deaconess Cancer Center, Harvard Medical School, 02215, USA. [12]Broad Center for Regenerative Medicine, University of Southern California, 90089, USA. [13]Jonsson Comprehensive Cancer Center, UCLA, 90095, USA. [14]Department of Biological Chemistry, UCLA, 90095, USA. [15]Howard Hughes Medical Institute, 20815, USA. [16]Correspondence should be addressed to H.R.C. or W.E.L. (e-mail: HChristofk@mednet.ucla.edu or blowry@ucla.edu)

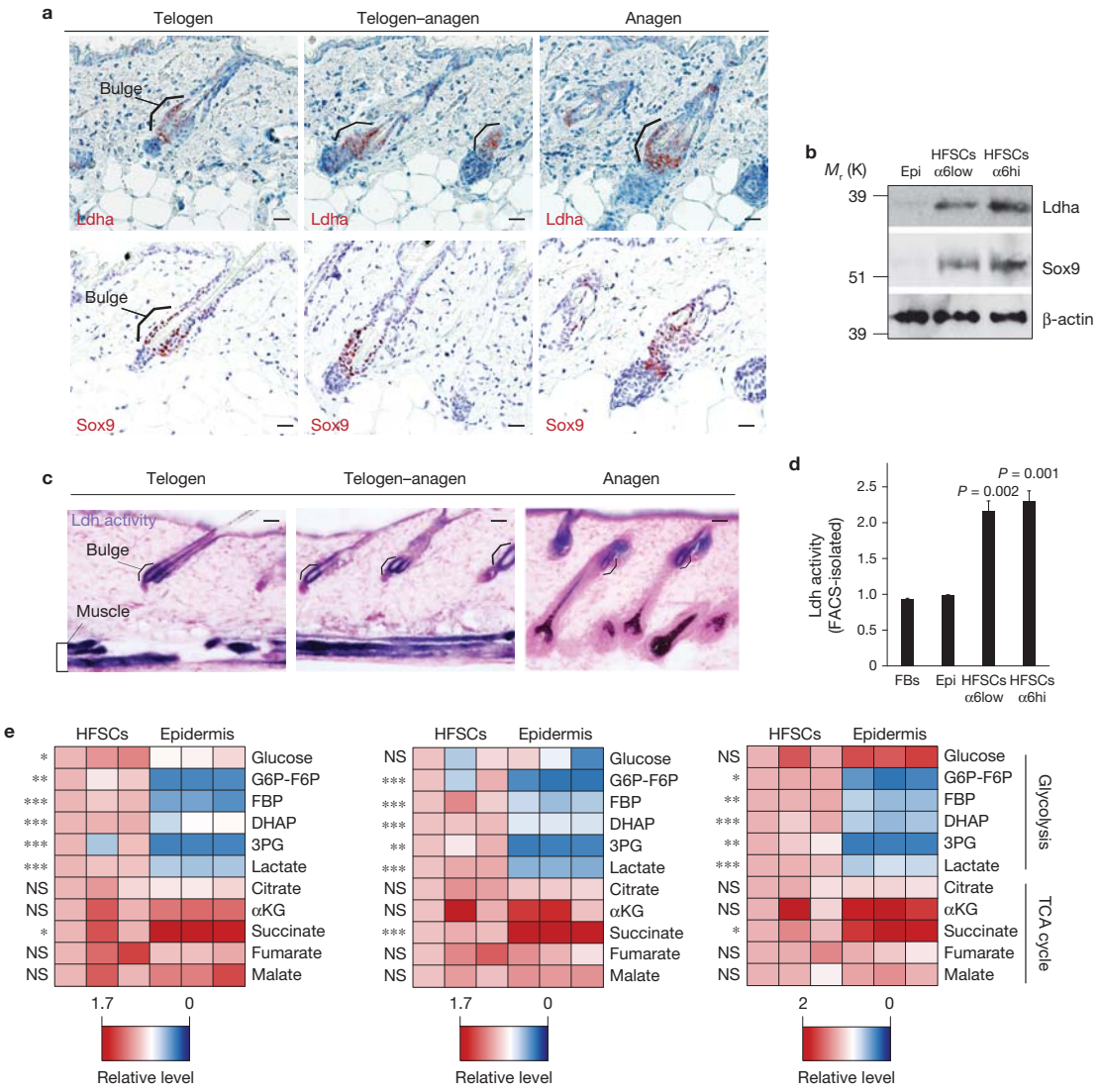

Figure 1 Lactate dehydrogenase activity is enriched in HFSCs. (**a**) IHC staining for Ldha expression across the hair cycle shows Ldha protein confined to the HFSC niche, the bulge, indicated by the bracket. IHC staining for Sox9 on serial sections demarcates the HFSC population. Scale bars, 20 μm. (**b**) Immunoblotting on FACS-isolated HFSC populations (α6low/Cd34$^+$ and α6hi/Cd34$^+$) versus total epidermis (Epi) shows differential expression of Ldha in the stem cell niche. Sox9 is a marker of HFSCs, and β-actin is a loading control. (**c**) Colorimetric assay for Ldh enzyme activity in the epidermis shows highest activity in the bulge (brackets) and subcuticular muscle layer (bracket). This activity is enriched in the bulge across different stages of the hair cycle. Activity is indicated by purple colour; pink is a nuclear counterstain. Note also that developing hair shafts in pigmented mice show strong deposits of melanin as observed here; hair shafts never displayed any purple stain indicative of Ldh activity. Scale bars, 50 μm. (**d**) Ldh activity in sorted cell populations, measured using a plate-reader-based assay, also shows the highest Ldh activity in two separate HFSC populations (α6hi/Cd34$^+$ and α6low/Cd34$^+$) compared with epidermal cells (Epi) and fibroblasts (FBs). Each bar represents the average signal for each cell type where $n=9$ mice pooled from 3 independent experiments. Shown as mean ± s.e.m. Paired t-test was performed, $P<0.05$ shown for each cell type versus epidermal cells. (**e**) HFSCs and epidermal cells were isolated during telogen (day 50) by FACS, and metabolites were extracted and analysed by LC–MS. Heatmaps show relative levels of glycolytic and TCA cycle metabolites from cells isolated from different mice in independent experiments with cells from three animals in each. G6P-F6P, glucose-6-phosphate and fructose-6-phosphate; FBP, fructose-bisphosphate; DHAP, dihydroxyacetone phosphate; 3PG, 3-phosphoglycerate; and αKG, alpha-ketoglutarate. Asterisks indicate significant difference in metabolite levels between epidermal cells and HFSCs. For (**e**) paired t-test was performed; $^*P<0.05$; $^{**}P<0.01$; $^{***}P<0.001$; NS, $P>0.05$; $n=9$ mice pooled from 3 independent experiments. Unprocessed original scans of blots are shown in Supplementary Fig. 6.

homeostasis[13]. Lactate dehydrogenase is most commonly encoded by the *Ldha* and *Ldhb* genes in mammals, the protein products of which form homo- or hetero-tetramers to catalyse the NADH-dependent reduction of pyruvate to lactate and NAD$^+$-dependent oxidation of lactate to pyruvate[14]. By immunostaining, Ldha appeared to be enriched in quiescent HFSCs *in situ* (telogen) (Fig. 1a), and

immunohistochemistry (IHC) with an antibody that recognizes both Ldha and Ldhb showed that only Ldha appears to be localized to the HFSC niche (Supplementary Fig. 1a).

HFSCs are known to go through successive rounds of quiescence (telogen) punctuated by brief periods of proliferation correlating with the start of the hair cycle (telogen–anagen transition)[4,15]. Proliferation or activation of HFSCs is well known to be a prerequisite for advancement of the hair cycle. IHC analysis also showed that Ldha expression was enriched in HFSCs (Sox9$^+$) at three stages of the hair cycle (Fig. 1a). Consistently, immunoblotting of lysates from sorted cells showed strong expression of Ldha in the basal HFSCs (α6hi/CD34$^+$), and suprabasal (α6lo/CD34$^+$) HFSC populations relative to total epidermis (Fig. 1b)[9] (the sorting strategy is outlined in Supplementary Fig. 1b).

To determine whether Ldha expression patterns correlate with activity of the Ldh enzyme, we used a colorimetric-based enzymatic assay to assess Ldh activity capacity *in situ*. Typically performed on protein lysates or aliquots with a plate reader[16], we adapted the Ldh activity assay to work *in situ* on frozen tissue sections. Note that since both the *in situ* and *in vitro* Ldh activity assays employ use of excess substrate (lactate), the results from these assays reflect the capacity for Ldh activity, and not the steady-state activity.

Applying this assay to skin samples demonstrated that Ldh activity capacity was significantly higher in HFSCs, consistent with the expression pattern of Ldha (Fig. 1c). Furthermore, Ldh activity was enriched in HFSCs across the hair cycle (Fig. 1c). As a control, assays conducted without the enzymatic substrate (lactate) or on acid-treated tissue yielded zero activity (Supplementary Fig. 1c). To further validate these results, we sorted epidermal populations, generated cell lysates on the sorted cells, and performed a similar colorimetric-based enzymatic assay on the sorted cell lysates, which also showed increased Ldh activity in HFSCs (Fig. 1d). To better characterize the metabolism of HFSCs, we performed metabolomics analysis on sorted populations from mouse skin by liquid chromatography–mass spectrometry (LC–MS) (Fig. 1e). Several glycolytic metabolites, including glucose/fructose-6-phosphate, fructose-bisphosphate, dihydroxyacetone phosphate, 3-phosphoglycerate and lactate, were routinely higher in HFSCs relative to total epidermis across three independent experiments (isolated from different mice on different days). Conversely, most TCA cycle metabolites were not consistently different between the epidermis and HFSCs (Fig. 1e). Collectively these results suggest that while all cells in the epidermis use the TCA cycle extensively to generate energy, HFSCs also have increased Ldha expression, Ldh activity and glycolytic metabolism.

Measuring metabolism across the hair cycle therefore would capture any dynamic changes that occur in HFSCs that correlate with activation or quiescence. Analysis of RNA-seq data from HFSCs isolated during either telogen or the telogen–anagen transition demonstrated not only that *Ldha* is the predominant *Ldh* isoform expressed in HFSCs (Fig. 2c), but it is also induced during the telogen–anagen transition (Fig. 2a,b) (NIHGEOGSE67404 and GSE51635). To confirm that the cells analysed by RNA-seq were indeed either in telogen or the telogen–anagen transition, important markers of this transition were assessed including the Shh and Wnt pathways (*Gli1*, *2*, *3*; *Lef1*, *Axin1*, *Axin2* and *Ccnd1*) as well as proliferation markers (*Ki-67*, *Pcna* and *Sox4*) (Supplementary Fig. 2a).

The *in vitro* Ldh activity assay on lysates from sorted HFSCs uncovered a modest induction of Ldh activity correlating with the telogen–anagen transition (Fig. 2d). Hair cycle staging was validated by Ki-67 immunostaining to determine HFSC activation (Supplementary Fig. 2b). Additionally, measurements of steady-state metabolites extracted from sorted HFSCs showed an increase in lactate in HFSCs as they enter the telogen–anagen transition, and then decrease again in anagen as HFSCs return to quiescence (Fig. 2e).

To determine whether Ldh activity is functionally related to the ability of HFSCs to remain quiescent or to activate at the start of a hair cycle, we deleted *Ldha* specifically in the HFSCs. Taking advantage of mice with floxed alleles of *Ldha*[17], this enzyme was deleted in HFSCs by crossing to mice bearing the *K15-CrePR* allele[11], known to be inducible by mifepristone specifically in HFSCs. Deletion of *Ldha* in HFSCs was initiated by administration of mifepristone during telogen (day 50) and led to a typically mosaic recombination of the floxed alleles across the backskin[11,18]. Mice with HFSC-specific deletion of *Ldha* failed to undergo a proper hair cycle, with most follicles remaining in telogen across at least 33 pairs of littermates 3–4 weeks after mifepristone treatment (Fig. 3a). A complete list of transgenic animals including birth date, sex and genotype is provided in Supplementary Table 1.

Histology showed that wild-type hair follicles entered into the telogen–anagen transition typically by day 70, and this was accompanied by typical expansion of the hypodermis below (Fig. 3b). However, in backskin with deletion of *Ldha*, the hypodermis did not expand, and the telogen–anagen transition was severely abrogated (Fig. 3b). In areas of strong phenotypic penetrance, Ldh activity was severely abrogated in the HFSC compartment (Fig. 3c), demonstrating that the *Ldha* allele is critically important for Ldh activity in HFSCs and consistent with the fact that isoform a of *Ldh* is expressed at the highest level. Quantification of hair cycle progression across numerous animals indicated that most follicles lacking *Ldha* remained in telogen (Fig. 3d).

In addition, to confirm the phenotypes, we also deleted *Ldha* with an independent HFSC-specific Cre strategy. *Lgr5-CreER* has been used for lineage tracing in a variety of adult stem cell models, and has been shown to mark cells with high regenerative capacity, including HFSCs[19]. *Lgr5-CreER;Ldha*$^{fl/fl}$ mice, treated with tamoxifen at postnatal day 50 prior to a synchronized hair cycle, also failed to activate anagen across at least 20 littermate pairs (Fig. 3g). *In situ* Ldh assay and metabolomics confirmed the successful deletion of *Ldha* in these animals (Fig. 3h,i).

We also monitored the effect of loss of Ldha activity in K15$^+$ cells over a six-month period and found that deletion of *Ldha* led to a mosaic, but permanent block of HFSC activation in some portions of the backskin (Supplementary Fig. 3a). These data confirm that Ldh activity is required for HFSC activation, and is not simply a marker of HFSCs. A closer look at these long-term *Ldha* deletions showed that *Ldha*-null HFSCs continued expressing typical markers, but lacked Ldh activity, and failed to initiate new hair cycles, while those follicles that escaped deletion continued to express Ldha and to cycle normally (Supplementary Fig. 3b,c).

After sorting HFSCs from animals with or without *Ldha* deletion, LC–MS-based metabolomics analysis demonstrated that lactate levels, as well as levels of other glycolytic metabolites, were strongly

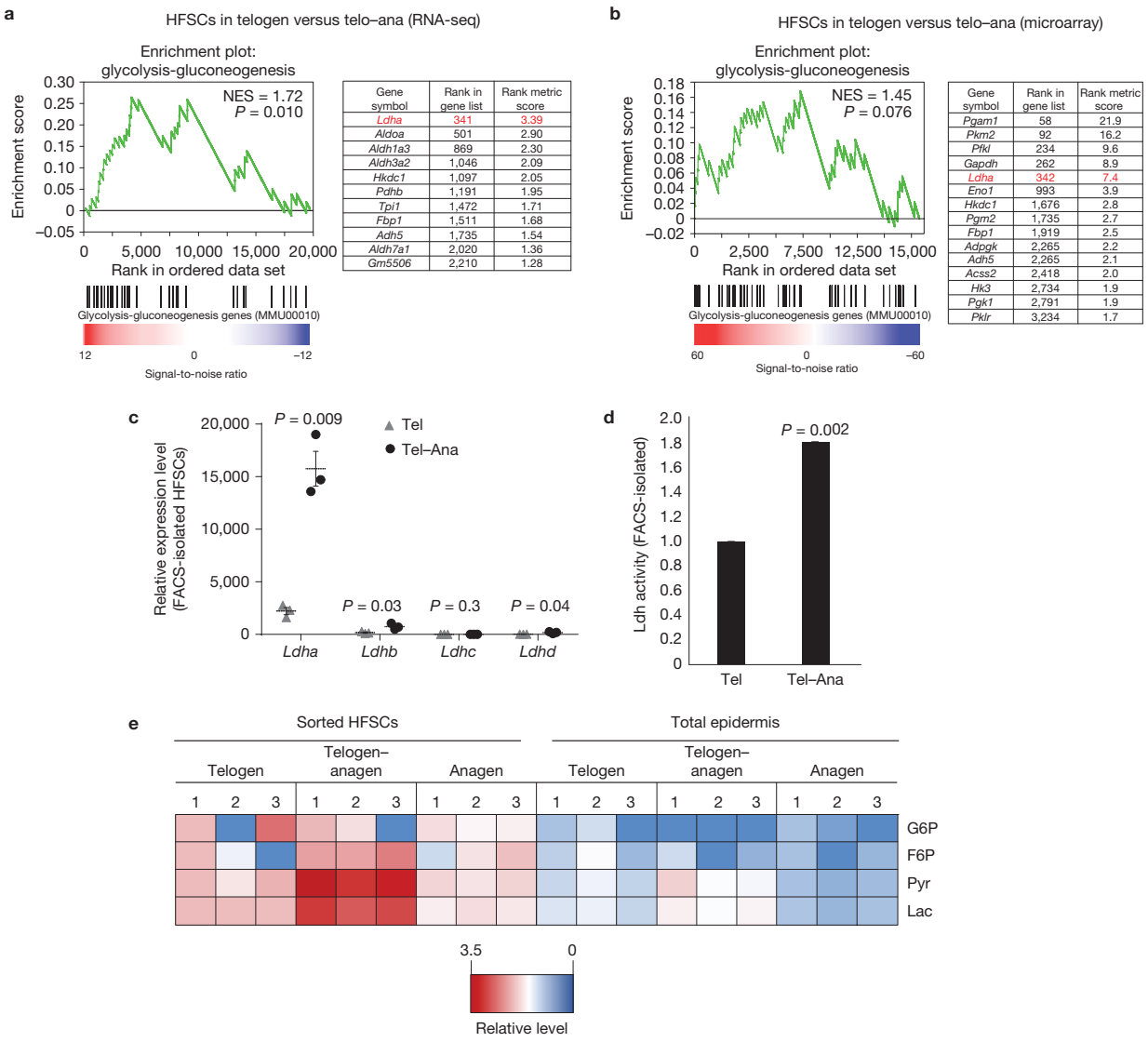

Figure 2 Ldh activity increases during HFSC activation. (**a**) Gene set enrichment analysis (GSEA) on RNA-seq transcriptome data from HFSCs versus total epidermis shows enrichment for glycolysis-related genes in HFSCs (normalized enrichment score (NES) = 1.72). (**b**) GSEA on microarray transcriptome data from HFSCs versus total epidermis shows enrichment for glycolysis-related genes in HFSCs (NES = 1.45). Results were generated from three mice of each condition. (**c**) RNA-seq data from HFSCs sorted during telogen or telogen–anagen transition (Tel–Ana) show induction of *Ldha*[35]. Data represent the average of three separate animals at each time point ($n=3$), and subjected to Student's *t*-test for significance ($P<0.05$). (**d**) Ldh activity in sorted stem cell populations, measured using a plate-reader-based assay, shows elevated Ldh activity as stem cells become activated in telogen–anagen transition. Each bar represents the average signal for each condition where $n=9$ mice pooled from 3 independent experiments. Shown as mean ± s.e.m. Paired *t*-test was performed, $P<0.05$. (**e**) Heatmap showing relative levels of glycolytic and TCA cycle metabolites extracted from quiescent (Telogen, day 50), activated (Telogen–Anagen, day 70) and HFSCs that have returned to the quiescent state (Anagen, day 90). Pyr, pyruvate; Lac, lactate. Data shown were generated from $n=3$ animals per time point in 3 independent experiments.

reduced in the absence of Ldha (Fig. 3e), functional evidence that the targeting strategy was successful. The fact that glycolytic metabolites upstream of lactate were also suppressed suggests that HFSCs could be adapting their metabolism to account for the loss of Ldh activity. Immunostaining for markers of HFSC activation and proliferation indicated a failure of HFSC activation. Ki-67 and pS6 have been clearly demonstrated to be abundant in the HFSC niche at the start of the hair cycle[20], and both of these markers were absent in *Ldha*-deleted backskin (Fig. 3f). Immunostaining for Ldha also confirmed successful deletion of this protein, while staining for Sox9, a marker of HFSCs, indicated that these cells remained in their niche, but just failed to activate in the absence of Ldha (Fig. 3f). Induction of the hair cycle is also thought to be regulated by signalling from the Shh, Wnt and Jak–Stat pathways.

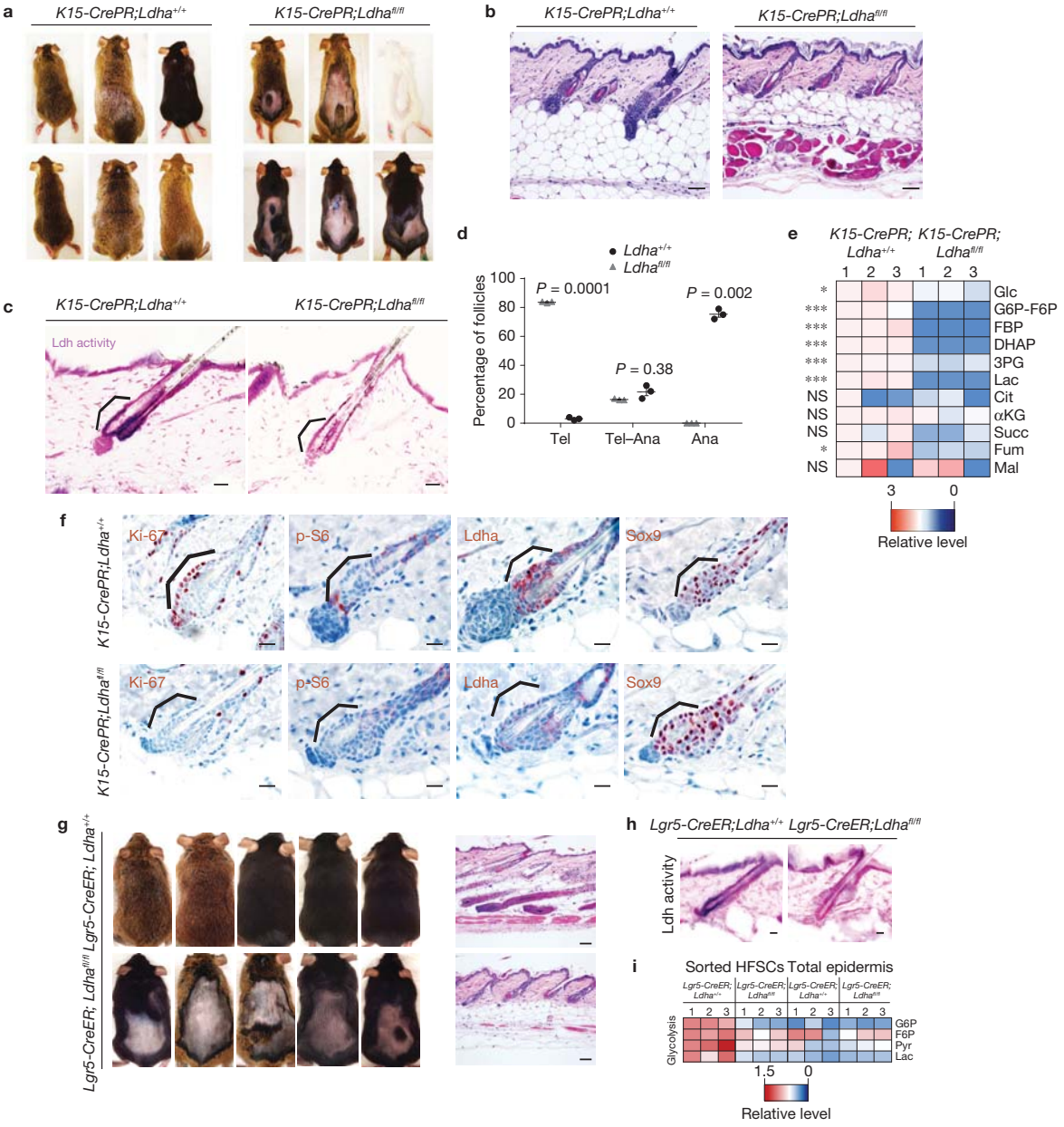

Figure 3 Deletion of Ldha blocks HFSC activation. (**a**) *Ldha*$^{+/+}$ animals enter the hair cycle synchronously around day 70 as measured by shaving and observation beginning at day 50. *K15-CrePR;Ldha*$^{fl/fl}$ animals treated with mifepristone show defects in anagen entry. Results are representative of at least 33 animals of each genotype. (**b**) Skin pathology showing that *K15-CrePR;Ldha*$^{fl/fl}$ animals remained in telogen. Scale bars, 50 μm. (**c**) Ldh enzyme activity assay showed that *K15-CrePR;Ldha*$^{fl/fl}$ animals lacked this activity in the HFSCs (indicated by bracket). Scale bars, 20 μm. (**d**) Graph showing percentage of follicles in telogen, telogen–anagen transition and anagen in *K15-CrePR;Ldha*$^{+/+}$ mice versus *K15-CrePR;Ldha*$^{fl/fl}$ mice (n=225 follicles from 3 mice per genotype). Shown as mean ± s.e.m. Paired t-test was performed, $P<0.05$. (**e**) Heatmap showing relative levels of glycolytic and TCA cycle metabolites extracted from *Ldha*$^{+/+}$ HFSCs and *Ldha*$^{fl/fl}$ HFSCs and measured by LC–MS. Asterisks indicate significant difference in metabolite levels between genotypes. For **e**, paired t-test was performed; $^{*}P<0.05$; $^{***}P<0.001$; NS, $P>0.05$; n=9 mice pooled from 3 independent experiments. (**f**) Immunohistochemistry staining for Ki-67, a marker of proliferation, is absent in *Ldha*$^{fl/fl}$ HFSCs. Phospho-S6, a marker in HFSCs at the beginning of a new hair cycle, is absent in *Ldha*$^{fl/fl}$ HFSCs. Staining for Ldha protein shows specific deletion in HFSCs. Brackets indicate bulge. Staining for Sox9 shows that HFSCs are still present in the *Ldha*-deleted niche. Scale bars, 20 μm. (**g**) Animals with *Ldha* deletion in their HFSCs as controlled by *Lgr5-CreER* show profound defects in the entry into anagen. Right, skin pathology showing that *Lgr5-CreER;Ldha*$^{fl/fl}$ animals mostly remained in telogen. Scale bars, 100 μm. Results are representative of at least 12 animals of each genotype. (**h**) Ldh enzyme activity assay in the epidermis shows that *Lgr5-CreER;Ldha*$^{fl/fl}$ animals lacked this activity in the HFSCs. Scale bars, 20 μm. (**i**) LC–MS analysis of metabolites from the indicated mice. Data were generated from n=3 animals per condition pooled from 3 independent experiments.

We assayed each of these by IHC in normal or *Ldha*-deletion follicles and found that in general these pathways were not activated in *Ldha*-null HFSCs that failed to enter a telogen–anagen transition (Supplementary Fig. 3d).

To determine whether induction of lactate production could affect HFSC activation or the hair cycle, we crossed *K15-CrePR* animals to those floxed for mitochondrial pyruvate carrier 1 (*Mpc1*) (*K15-CrePR;Mpc1*$^{fl/fl}$). Mpc1, as a heterodimer with Mpc2, forms the mitochondrial pyruvate carrier MPC, a transporter on the inner mitochondrial membrane required for pyruvate entry into the mitochondria[21]. Loss of function of Mpc1 has been shown to drive lactate production through enhanced conversion of pyruvate to lactate by Ldh[22].

In animals with *Mpc1* deletion in HFSCs, we observed a strong acceleration of the ventral and dorsal hair cycles with all the typical features of a telogen–anagen transition (Fig. 4a) ($n = 12$ littermate pairs). Mifepristone-treated *K15-CrePR;Mpc1*$^{fl/fl}$ animals were the only ones to show any signs of dorsal anagen by day 70. Western blotting on sorted HFSCs validated the loss of Mpc1 protein (Fig. 4b). Importantly, purified HFSCs lacking *Mpc1* showed a strong induction of Ldh activity (Fig. 4c). Quantification of the dorsal hair cycle across three pairs of littermates showed a strong induction of anagen in backskin lacking *Mpc1* (Fig. 4d, right), and histology showed that the anagen induction was normal in appearance with a typical hypodermal expansion (Fig. 4d). Immunostaining demonstrated the induction in *Mpc1*-null HFSCs of various markers of hair cycle activation such as Ki-67 and pS6, while Sox9 expression was unaffected (Fig. 4e). Long-term deletion of *Mpc1* did not lead to aberrant follicles or exhaustion of HFSCs as judged by pathology and staining for Sox9 (Supplementary Fig. 4a). Furthermore, deletion of *Mpc1* with *Lgr5-CreER* showed a very similar phenotype as deletion with *K15-CrePR* (Fig. 4f,g), validating the fact that deletion of this protein in HFSCs leads to their activation ($n = 12$ pairs of littermates). Finally, immunofluorescence for the *Ires-GFP* of the *Lgr5-CreER* transgene along with Ki-67 and lineage tracing with K15-CrePR;Mpc1$^{fl/fl}$;lsl-Tomato mice also demonstrated that the HFSCs were indeed proliferative following induction of Mpc1 deletion by tamoxifen or mifepristone (Supplementary Fig. 4b).

On the other hand, deletion of *Mpc1* in the top of the follicle (infundibulum, sebaceous gland progenitors) and a limited number of interfollicular cells with *Lgr6-CreER* (ref. 23) did not appear to affect the hair cycle (*Lgr6-CreER;Mpc1*$^{fl/fl}$) ($n = 10$ littermate pairs) or general skin homeostasis over at least 2 months (Supplementary Fig. 4c). Ldh activity assay on Lgr6^{+} cells sorted from wild-type or deletion skin demonstrated that the *Mpc1* deletion was effective (Supplementary Fig. 4d). Together, these results indicate that increasing lactate production through the blockade of pyruvate into the TCA cycle has a strong effect on the ability of HFSCs, but not other cells in the hair follicle, to become activated to initiate a new hair cycle.

UK-5099 is a well-established pharmacological inhibitor of the mitochondrial pyruvate carrier and is known to promote lactate production as a result in various settings[24]. Topical treatment of animals in telogen (day 50) with UK-5099 led to a robust acceleration of the hair cycle, as well as minor hyperproliferation of the interfollicular epidermis (Fig. 5a). Quantification of the hair cycle across at least 6 pairs of animals (vehicle versus UK-5099) indicated a strong acceleration of the hair cycle, in as few as 6–9 days (Fig. 5b). Similar to genetic deletion of *Mpc1*, pharmacological blockade of the mitochondrial pyruvate carrier by UK-5099 for 48 h during telogen promoted increased Ldh activity in HFSCs and the interfollicular epidermis, consistent with increased capacity for lactate production (Fig. 5c). Finally, metabolomic analysis demonstrated that topical application of UK-5099 increases total levels of lactate in sorted HFSCs (Fig. 5d).

Because alteration of lactate production in HFSCs appeared to regulate their activation, we attempted to identify other small molecules that could take advantage of these findings to induce the hair cycle. *Ldha* is known to be transcriptionally regulated by Myc, which has been shown to play an important role in HFSC activation and the hair cycle[25–27]. RNA-seq on sorted HFSCs indicated that Myc is induced during the telogen–anagen transition (Fig. 6a). Western blotting for both c-Myc and n-Myc in sorted HFSCs versus total epidermis showed a strong increase in Myc protein in the nuclei of HFSCs (Fig. 6b).

Taking advantage of a molecule with the robust ability to promote Myc expression through binding of GP130 and activation of Jak/Stat signalling, we topically treated mice for 48 h to determine the effect of RCGD423 on Stat signalling and Myc expression. We found that RCGD423 induced levels of both c-Myc and n-Myc as well as Ldha (Fig. 6c), consistent with activation of Stat3 signalling leading to induction of Myc and Ldha protein expression. *In vitro* measurement of Ldh activity on lysates from total epidermis showed an increase in activity by RCGD423 (Fig. 6d). *In situ* staining for Ldh activity showed a strong induction following treatment with RCGD423 in both the epidermis and even in the dermis, as expected with topical treatment (Fig. 6e). LC–MS-based metabolomics on epidermis isolated from vehicle or RCGD423 showed a large increase in lactate as well, even after just 48 h (Fig. 6f).

RCGD423 binds to GP130, a co-receptor for Jak–Stat signalling, and activates Stat3. We found that Stat3 was activated in HFSCs by RCGD423 after topical treatment by immunostaining with phospho-Stat3 antibody (Fig. 6g). This also correlated with induction of Ki-67 in HFSCs in the same tissue (Fig. 6g). IHC for pStat1 and pStat5 suggested that RCGD423 does not dramatically affect these other Stat family members (Supplementary Fig. 5). Topical treatment of animals in telogen (day 50) with RCGD423 led to a robust acceleration of the hair cycle (Fig. 6h), as well as minor hyperproliferation of the interfollicular epidermis.

DISCUSSION

Together, these data demonstrate that the production of lactate, through Ldha, is important for HFSC activation, and that HFSCs may maintain a high capacity for glycolytic metabolism at least in part through the activity of Myc. Our data also demonstrate that a genetic or pharmacological disruption of lactate production can be exploited to regulate the activity of HFSCs. It is possible that these results have implications for adult stem cells in other tissues. In an accompanying manuscript, the Rutter laboratory describes a role for Mpc1 in adult intestinal stem cells[28]. Consistent with data presented here on HFSCs, deletion of Mpc1 led to an increase in the ability of intestinal stem cells to form organoids.

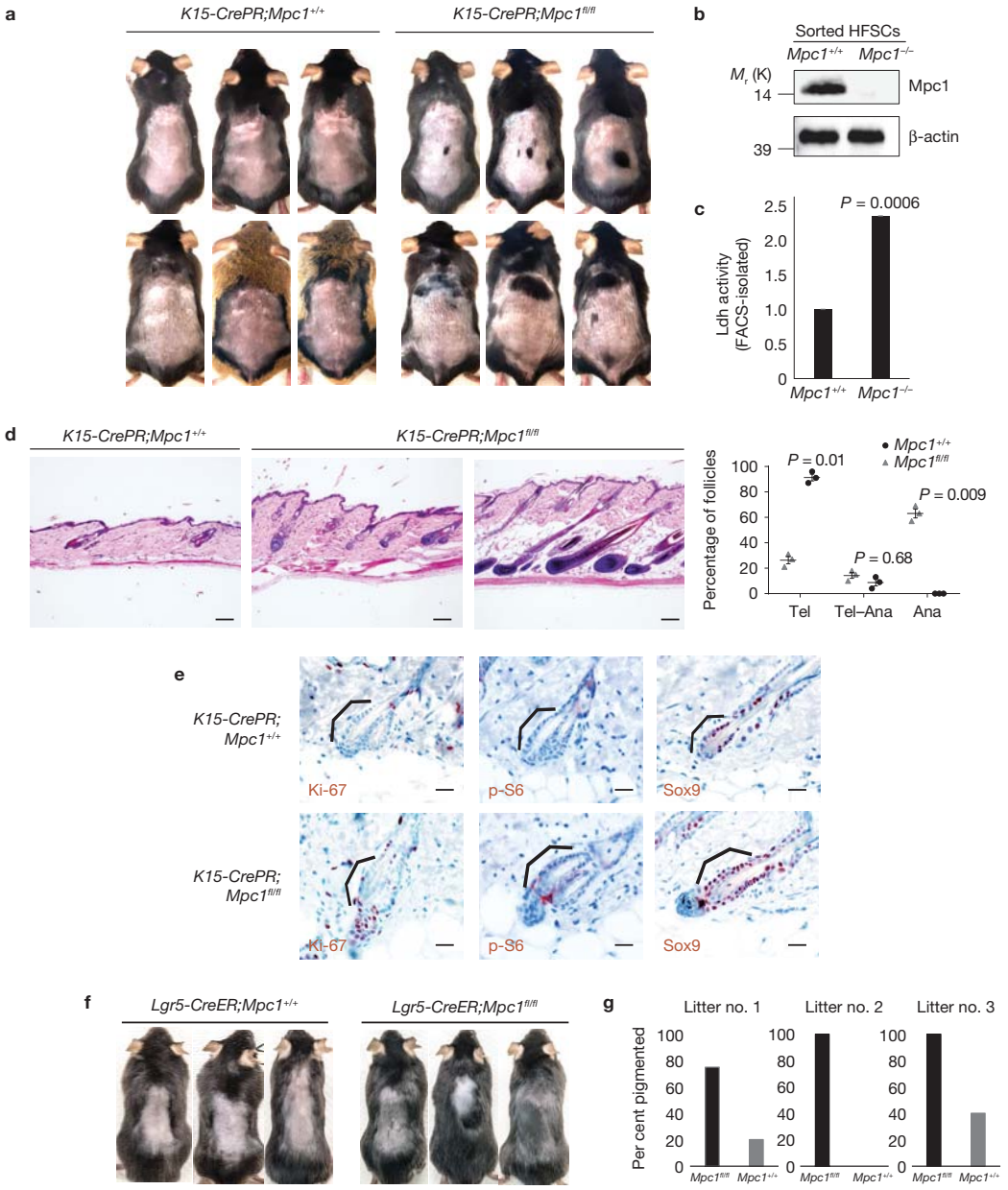

Figure 4 Deletion of Mpc1 increases lactate production and accelerates the activation of HFSCs. (**a**) *Mpc1*$^{fl/fl}$ animals show pigmentation and hair growth, consistent with entry into the anagen cycle at 8.5 weeks, whereas *Mpc1*$^{+/+}$ animals do not show dorsal pigmentation and hair growth this early. Animals shown are representative of at least 12 animals of each genotype. (**b**) FACS isolation of HFSC bulge populations in *Mpc1*$^{+/+}$ versus *Mpc1*$^{fl/fl}$ mice followed by western blotting shows successful deletion of Mpc1 protein in the stem cell niche. β-actin is a loading control. (**c**) Plate-reader assay for Ldh activity on sorted HFSC populations shows elevated activity in *Mpc1*$^{fl/fl}$ HFSCs compared with *Mpc1*$^{+/+}$ HFSCs. Each bar represents the average signal for each genotype where $n=9$ mice pooled from 3 independent experiments. Shown as mean ± s.e.m. Paired *t*-test was performed, $P<0.05$. (**d**) Histology on wild-type versus Mpc1 deletion skin shows induction of anagen in absence of Mpc1. Scale bars, 100 μm. Quantification of phenotype at right shows percentage of dorsal follicles in telogen, telogen–anagen transition and anagen in *Mpc1*$^{+/+}$ mice versus *Mpc1*$^{fl/fl}$ mice ($n=250$ follicles from 3 mice per genotype). Shown as mean ± s.e.m. Paired *t*-test was performed, $P<0.05$. (**e**) Immunohistochemistry staining for Ki-67, a marker of proliferation that is active in HFSCs only at the beginning of a new hair cycle, is present in *Mpc1*$^{fl/fl}$ HFSCs only at 8.5 weeks, consistent with their accelerated entry into a new hair cycle. Phospho-S6, another marker that is active in HFSCs only at the beginning of a new hair cycle, is present in *Mpc1*$^{fl/fl}$ HFSCs. Staining for Sox9 shows that HFSCs are present in the Mpc1-deleted niche. Images taken at ×60 magnification. (**f**) Deletion of Mpc1 in mice bearing the *Lgr5-CreER* allele shows strong induction of the hair cycle. Results are representative of at least 9 animals per genotype. (**g**) Quantification of pigmentation in the indicated genotypes across three independent litters ($n=5$ mice per genotype). Unprocessed original scans of blots are shown in Supplementary Fig. 6.

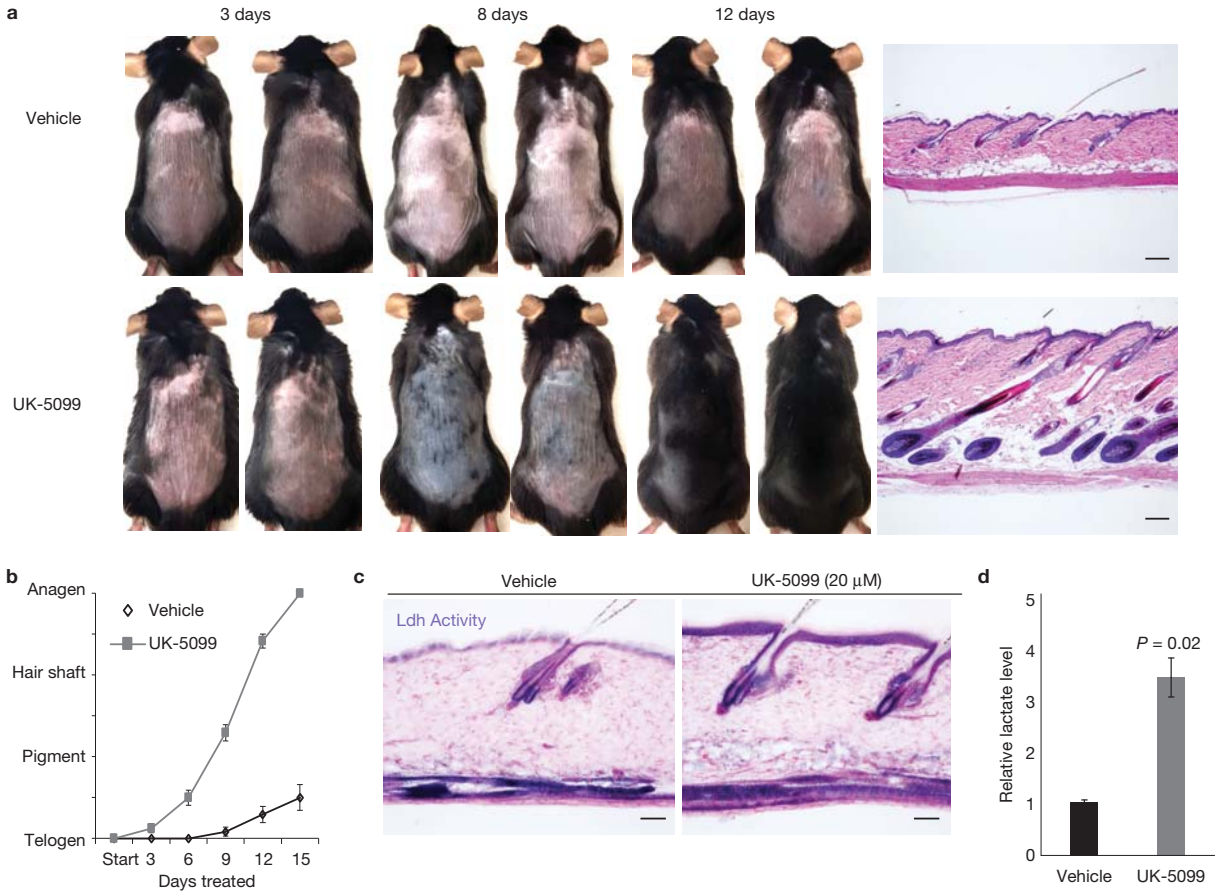

Figure 5 Pharmacological inhibition of Mpc1 promotes HFSC activation. (**a**) Animals treated topically with UK-5099 (20 μM) show pigmentation and hair growth, indicative of entry into anagen, after 8 days of treatment. Full anagen, indicated by a full coat of hair, is achieved after 14 days of treatment. Mice treated topically with vehicle control do not show pigmentation nor hair growth even after 12 days of treatment. Right, skin pathology showing that UK-5099 animals enter an accelerated anagen at 8 weeks typified by down growth of the follicle and hypodermal thickening, while vehicle control-treated animals showed neither and remained in telogen. Images shown are representative of at least 14 mice from 7 independent experiments. Scale bars, 100 μm. (**b**) Graph showing time to observed phenotype in vehicle- versus UK-5099-treated mice. $n=6$ mice per condition. Shown as mean ± s.e.m. (**c**) Ldh enzyme activity assay in the epidermis shows strong activity in HFSCs in vehicle control- and UK-5099-treated animals. Ldh enzyme activity also seen in interfollicular epidermis of UK-5099-treated animals. Ldh activity is indicated by purple stain; pink is nuclear fast red counterstain. Scale bars, 50 μm. (**d**) Metabolomic analysis of lactate on HFSCs isolated from UK-5099-treated skin for 48 h; each bar represents the average signal for each condition where $n=9$ mice pooled from 3 independent experiments. Shown as mean ± s.e.m. Paired t-test was performed, $P<0.05$.

Previous work showed that haematopoietic stem cells (HSCs) show higher glycolytic activity, but disruption of glycolysis in the HSCs led to activation of their cycling[29–32], contrary to what we find with HFSCs. While the distinction could be biological, there are technical reasons for potential discrepancies as well. First, there are no Cre transgenic lines that can delete genes specifically in HSCs, as opposed to HFSCs ($K15^+$ or $Lgr5^+$). Second, to block glycolysis in HSCs, the previous study deleted the PDK enzyme, which would only indirectly regulate glycolysis, whereas here we deleted the Ldh enzyme specifically. In addition, HSCs and HFSCs are functionally distinct in that HFSCs cycle only at well-defined moments (telogen–anagen transition), while the timing of HSC activation is not as well established or synchronized. Instead, we hypothesize that increased glycolytic rate in HFSCs allows them to respond quickly to the barrage of cues that orchestrate the onset of a new hair cycle. This has also been proposed to be the case for neural stem cells solely on the basis of RNA-seq data[33], but as of yet no *in vivo* functional evidence exists to confirm this possibility.

The fact that small molecules could be used to promote HFSC activation suggests that they could be useful for regenerative medicine. This is not only the case for hair growth, but potentially for wound healing as well. While HFSCs do not normally contribute to the interfollicular epidermis, in a wound setting, HFSCs migrate towards the wound site and make a contribution, as measured by lineage tracing[34]. Whether activation of Ldh enzyme activity by Mpc1 inhibition (UK-5099) or Myc activation (RCGD423) can promote wound healing will be the subject of intense effort going forward. □

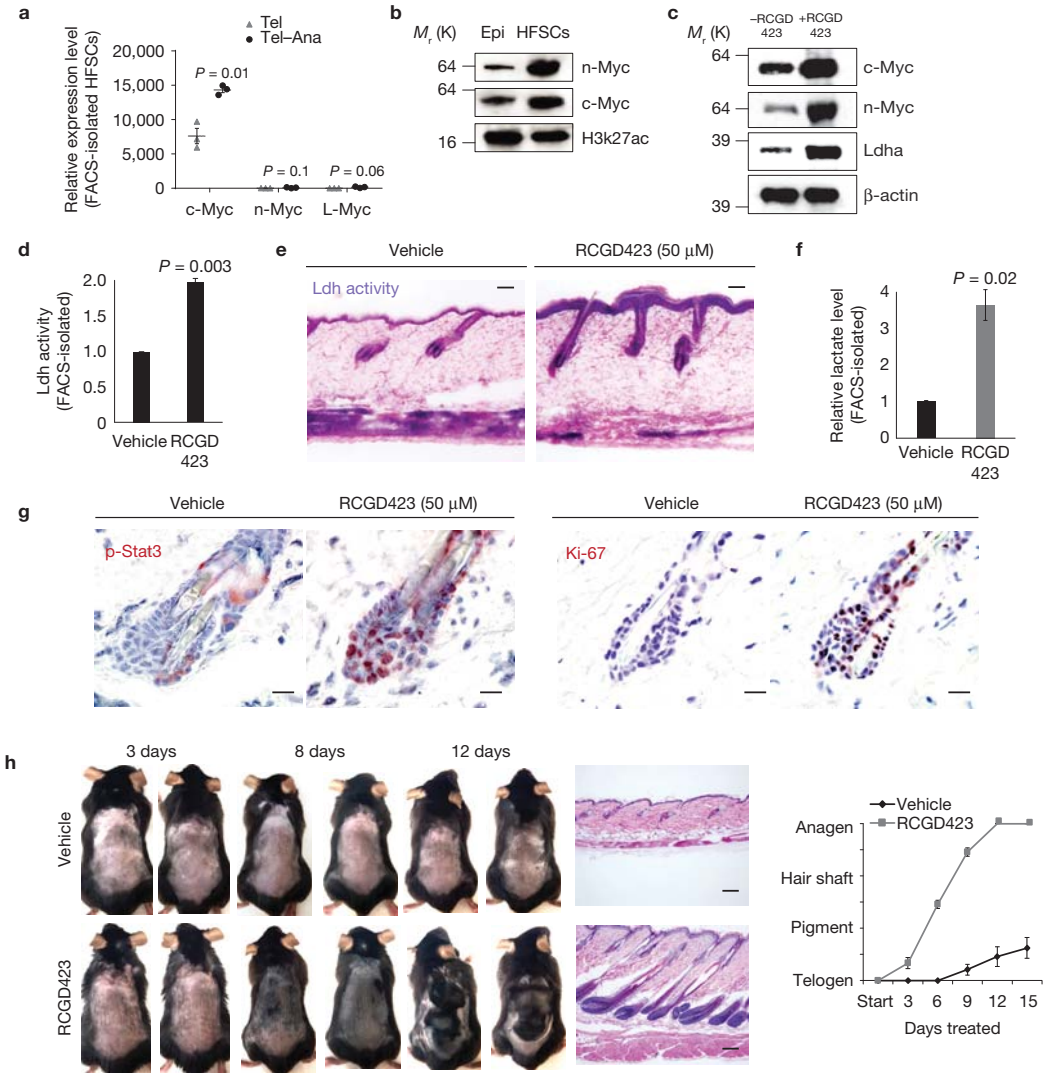

Figure 6 Stimulation of Myc levels promotes HFSC activation. (**a**) RNA-seq data from sorted HFSCs in telogen and telogen–anagen transition[35]. $n=3$ mice per time point. Shown as mean ± s.e.m. Paired t-test was performed, $P<0.05$. (**b**) Nuclear protein fractions show expression of n-Myc and c-Myc in HFSCs compared with epidermal cells. H3k27ac is a loading control for nuclear proteins. (**c**) Total protein preparations from skin treated with two topical doses of RCGD423 (50 μM) show increased c-Myc, n-Myc and Ldha protein levels compared with animals that received two topical doses of vehicle control. β-actin is a loading control. (**d**) Plate-reader assay for Ldh enzyme activity in the epidermis. Each bar represents the average signal for each condition where $n=9$ mice pooled from 3 independent experiments. Shown as mean ± s.e.m. Paired t-test was performed, $P<0.05$. (**e**) Ldh enzyme activity assay in the epidermis in vehicle control- and RCGD423-treated animals. Scale bars, 50 μm. (**f**) Metabolomic analysis of lactate on HFSCs isolated from RCGD423-treated skin for 48 h. Each bar represents the average signal for each condition where $n=9$ mice pooled from 3 independent experiments. Shown as mean ± s.e.m. Paired t-test was performed, $P<0.05$. (**g**) Immunohistochemistry staining for Ki-67 and phospho-Stat3, a downstream marker of RCGD423 activity. Scale bars, 20 μm. (**h**) Animals treated with RCGD423 (50 μM) show pigmentation and hair growth, indicative of entry into anagen, after 5 doses. Images shown are representative of at least 14 mice from 7 independent experiments. Scale bars, 100 μm. Quantification of phenotype showing time to observed phenotype in vehicle- versus RCGD423-treated mice. $n=6$ mice per condition. Shown as mean ± s.e.m. Unprocessed original scans of blots are shown in Supplementary Fig. 6.

METHODS

Methods, including statements of data availability and any associated accession codes and references, are available in the online version of this paper.

Note: Supplementary Information is available in the online version of the paper

ACKNOWLEDGEMENTS

We would like to acknowledge the significant technical support of M. Neebe, J. Cinkornpumin and A. Liu on this project. We are also particularly grateful to members of the Banerjee laboratory for guidance and development of the Ldh activity assay. A.F. and A.C.W. were supported by a fellowship from the Eli and Edythe Broad Center for Regenerative Medicine at UCLA. A.C.W. and M.G. were supported by a fellowship from the Tumor Cell Biology programme

at UCLA (NIH). A.C.W. was also supported by a training grant from CIRM. D.J. was supported by awards from a New Idea Award from the Leukemia Lymphoma Society, the Jonsson Comprehensive Cancer Center, the UCLA Clinical Translational Science Institute UL1TR000124, the Prostate Cancer SPORE at UCLA P50 CA092131, and the Eli & Edythe Broad Center for Regenerative Medicine & Stem Cell Research. N.A.G. is a postdoctoral trainee supported by the UCLA Scholars in Oncologic Molecular Imagining program (NCI/NIH grant R25T CA098010). A.S.K. was supported by a UCLA Dissertation Year Fellowship. H.A.C. was supported by National Institute of General Medical Sciences R01-GM081686 and R01-GM0866465. J.R. was supported by NIH (RO1GM094232). H.R.C. was supported by a Research Scholar Grant, RSG-16-111-01-MPC, from the American Cancer Society and the Eli & Edythe Broad Center of Regenerative Medicine and Stem Cell Research at UCLA and Rose Hills Foundation Research Award. W.E.L. was supported by NIH-NIAMS (5R01AR57409), an Impact award from CTSI and the Jonsson Comprehensive Cancer Foundation, and The Gaba Fund through the Eli & Edythe Broad Center of Regenerative Medicine at UCLA.

AUTHOR CONTRIBUTIONS

A.F., J.S., A.S.K., D.J., M.M., M.G. and D.B. performed experiments. A.F., A.S.K., J.L.Z., N.A.G. performed analysis and compiled data. P.S., D.E. and J.R. provided key reagents essential to the work. T.G. and H.A.C. provided important insight and advice. H.R.C. and W.E.L. provided oversight and were financially responsible for the work. A.F., H.R.C. and W.E.L. were responsible for assembling the figures and writing the manuscript.

COMPETING FINANCIAL INTERESTS

The use of RCGD423 to promote hair growth is covered by a provisional patent application filed by UC Regents and this technology has been licensed by Carthronix LLC. W.E.L. is a member of the board of advisers and a shareholder of Carthronix LLC. None of the work in this study was supported by Carthronix. The use of UK-5099 to promote hair growth is covered by a separate provisional patent filed by UC Regents with W.E.L. and H.R.C. as inventors.

Published online at http://dx.doi.org/10.1038/ncb3575

1. Hsu, Y. C., Pasolli, H. A. & Fuchs, E. Dynamics between stem cells, niche, and progeny in the hair follicle. *Cell* **144,** 92–105 (2011).
2. Morris, R. J. & Potten, C. S. Highly persistent label-retaining cells in the hair follicles of mice and their fate following induction of anagen. *J. Invest. Dermatol.* **112,** 470–475 (1999).
3. Fuchs, E. The tortoise and the hair: slow-cycling cells in the stem cell race. *Cell* **137,** 811–819 (2009).
4. Fuchs, E., Merrill, B. J., Jamora, C. & DasGupta, R. At the roots of a never-ending cycle. *Dev. Cell* **1,** 13–25 (2001).
5. Kloepper, J. E. *et al.* Mitochondrial function in murine skin epithelium is crucial for hair follicle morphogenesis and epithelial-mesenchymal interactions. *J. Invest. Dermatol.* **135,** 679–689 (2015).
6. Hamanaka, R. B. & Chandel, N. S. Mitochondrial metabolism as a regulator of keratinocyte differentiation. *Cell. Logist.* **3,** e25456 (2013).
7. Hamanaka, R. B. *et al.* Mitochondrial reactive oxygen species promote epidermal differentiation and hair follicle development. *Sci. Signal.* **6,** ra8 (2013).
8. Baris, O. R. *et al.* The mitochondrial electron transport chain is dispensable for proliferation and differentiation of epidermal progenitor cells. *Stem Cells* **29,** 1459–1468 (2011).
9. Blanpain, C., Lowry, W. E., Geoghegan, A., Polak, L. & Fuchs, E. Self-renewal, multipotency, and the existence of two cell populations within an epithelial stem cell niche. *Cell* **118,** 635–648 (2004).
10. Tumbar, T. *et al.* Defining the epithelial stem cell niche in skin. *Science* **303,** 359–363 (2004).
11. Morris, R. J. *et al.* Capturing and profiling adult hair follicle stem cells. *Nat. Biotech.* **22,** 411–417 (2004).
12. Trempus, C. S. *et al.* Enrichment for living murine keratinocytes from the hair follicle bulge with the cell surface marker CD34. *J. Invest. Dermatol.* **120,** 501–511 (2003).
13. Nguyen, H., Rendl, M. & Fuchs, E. Tcf3 governs stem cell features and represses cell fate determination in skin. *Cell* **127,** 171–183 (2006).
14. Fromm, H. J. The nature of pyruvate involved in the enzymic formation of L-lactate in the rabbit-muscle lactate dehydrogenase reaction. *Biochim. Biophys. Acta* **99,** 540–542 (1965).
15. Paus, R., Muller-Rover, S. & Botchkarev, V. A. Chronobiology of the hair follicle: hunting the 'hair cycle clock'. *J. Invest. Dermatol. Symp. Proc.* **4,** 338–345 (1999).
16. Chan, F. K., Moriwaki, K. & De Rosa, M. J. Detection of necrosis by release of lactate dehydrogenase activity. *Methods Mol. Biol.* **979,** 65–70 (2013).
17. Xie, H. *et al.* Targeting lactate dehydrogenase-a inhibits tumorigenesis and tumor progression in mouse models of lung cancer and impacts tumor-initiating cells. *Cell Metab.* **19,** 795–809 (2014).
18. White, A. C. *et al.* Defining the origins of Ras/p53-mediated squamous cell carcinoma. *Proc. Natl Acad. Sci. USA* **108,** 7425–7430 (2011).
19. Jaks, V. *et al.* Lgr5 marks cycling, yet long-lived, hair follicle stem cells. *Nat. Genet.* **40,** 1291–1299 (2008).
20. Kellenberger, A. J. & Tauchi, M. Mammalian target of rapamycin complex 1 (mTORC1) may modulate the timing of anagen entry in mouse hair follicles. *Exp. Dermatol.* **22,** 77–80 (2013).
21. Bricker, D. K. *et al.* A mitochondrial pyruvate carrier required for pyruvate uptake in yeast, *Drosophila*, and humans. *Science* **337,** 96–100 (2012).
22. Schell, J. C. *et al.* A role for the mitochondrial pyruvate carrier as a repressor of the Warburg effect and colon cancer cell growth. *Mol. Cell* **56,** 400–413 (2014).
23. Snippert, H. J. *et al.* Lgr6 marks stem cells in the hair follicle that generate all cell lineages of the skin. *Science* **327,** 1385–1389 (2010).
24. Patterson, J. N. *et al.* Mitochondrial metabolism of pyruvate is essential for regulating glucose-stimulated insulin secretion. *J. Biol. Chem.* **289,** 13335–13346 (2014).
25. Wang, N. *et al.* The expression and role of c-Myc in mouse hair follicle morphogenesis and cycling. *Acta Histochem.* **114,** 199–206 (2012).
26. Bull, J. J. *et al.* Ectopic expression of c-Myc in the skin affects the hair growth cycle and causes an enlargement of the sebaceous gland. *Br. J. Dermatol.* **152,** 1125–1133 (2005).
27. Zanet, J. *et al.* Endogenous Myc controls mammalian epidermal cell size, hyperproliferation, endoreplication and stem cell amplification. *J. Cell Sci.* **118,** 1693–1704 (2005).
28. Schell, J. C. *et al.* Control of intestinal stem cell function and proliferation by mitochondrial pyruvate metabolism. *Nat. Cell Biol.* http://dx.doi.org/10.1038/ncb3593 (2017).
29. Hsu, P. & Qu, C. K. Metabolic plasticity and hematopoietic stem cell biology. *Curr. Opin. Hematol.* **20,** 289–294 (2013).
30. Harris, J. M. *et al.* Glucose metabolism impacts the spatiotemporal onset and magnitude of HSC induction *in vivo*. *Blood* **121,** 2483–2493 (2013).
31. Takubo, K. *et al.* Regulation of glycolysis by Pdk functions as a metabolic checkpoint for cell cycle quiescence in hematopoietic stem cells. *Cell Stem Cell* **12,** 49–61 (2013).
32. Simsek, T. *et al.* The distinct metabolic profile of hematopoietic stem cells reflects their location in a hypoxic niche. *Cell Stem Cell* **7,** 380–390 (2010).
33. Shin, J. *et al.* Single-cell RNA-Seq with waterfall reveals molecular cascades underlying adult neurogenesis. *Cell Stem Cell* **17,** 360–372 (2015).
34. Ito, M. *et al.* Stem cells in the hair follicle bulge contribute to wound repair but not to homeostasis of the epidermis. *Nat. Med.* **11,** 1351–1354 (2005).
35. Wang, L., Siegenthaler, J. A., Dowell, R. D. & Yi, R. Foxc1 reinforces quiescence in self-renewing hair follicle stem cells. *Science* **351,** 613–617 (2016).

METHODS

Mice. Several of the animal strains came from Jackson Labs (*K15-CrePR*, *Lgr5-CreER* and *Lgr6-CreER*), while others were generated in the Rutter (*Mpc*$^{fl/fl}$) and Seth laboratories[17] (*Ldha*$^{fl/fl}$) and maintained under conditions set forth by IUCUC and UCLA ARC. For experiments that include analysis of the telogen stage of the hair cycle, animals were harvested at postnatal day 50, for telogen–anagen transition animals were harvested at day 70, and for anagen animals were harvested at postnatal day 90. For experiments that include analysis of transgenic animals, *K15-CrePR* animals were shaved and treated by injection of mifepristone and *Lgr5-CreER* and *Lgr6-CreER* animals were shaved and treated with tamoxifen (10 mg ml^{-1} dissolved in sunflower seed oil, 2 mg per day for 3 days) during telogen (postnatal day 50), and monitored for hair regrowth following shaving. For Figs 5 and 6, wild-type C57BL/6J animals were shaved at postnatal day 50 and treated topically with Transderma Plo Gel Ultramax Base (TR220) (vehicle), UK-5099 (Sigma PZ0160) (20 μM) or RCGD423 (50 μM) for the indicated periods of time. Both male and female animals were used in this study in approximately equal numbers with no apparent difference in phenotype between genders. All animal experiments were performed in compliance with ethical guidelines and approved by the UCLA Animal Research Committee (ARC) according to IACUC guidelines in facilities run by the UCLA Department of Laboratory Animal Medicine (DLAM).

Histology, immunostaining and immunoblotting. Tissues were isolated from the indicated genotypes and embedded fresh in OCT compound for frozen tissue preparations, or fixed overnight in 4% formalin and embedded in paraffin. For frozen tissue, sectioning was performed on a Leica 3200 Cryostat, and the sections were fixed for 5 min in 4% paraformaldehyde. Paraffin-embedded tissue was sectioned, de-paraffinized and prepared for histology. All sections prepared for staining were blocked in staining buffer containing appropriate control IgG (goat, rabbit and so on). Immunohistochemistry was performed on formalin-fixed paraffin-embedded tissue with citrate or Tris buffer antigen retrieval with the following antibodies: Ki-67 (Abcam ab16667, 1:50), p-S6 (Cell Signaling CST2215, 1:50), Sox9 (Abcam ab185230, 1:1,000), Ldha (Abcam ab47010, 1:100), Ldh (Abcam ab125683, 1:100), p-Stat3 (Abcam ab68153, 1:200), p-Stat1 (Abcam ab109461, 1:200), p-Stat5 (Abcam ab32364; 1:50), Gli3 (Abcam ab6050; 1:100), β-catenin (Abcam ab32572; 1:500). The DAKO EnVision+ HRP Peroxidase System (Dako K400911-2) and Dako AEC Substrate Chromogen (Dako K346430-2) was used for detection. Images were collected on an Olympus BX43 Upright Microscope and Zeiss Model Axio Imager M1 Upright Fluorescence Microscope. Protein samples for western blots and enzymatic assays were extracted from FACS-sorted epidermal populations in RIPA lysis buffer (Pierce) with Halt protease and phosphatase inhibitors (Thermo-Fisher) and precipitated in acetone for concentration. The following antibodies were used: β-actin (Abcam ab8227; 1:1,000), β-actin (Santa Cruz sc-47778; 1:1,000), c-Myc (Abcam ab32072; 1:1,000), n-Myc (Santa Cruz sc-53993; 1:200), H3K27Ac (Abcam ab177178; 1:200), Mpc1 (Sigma HPA045119).

Cell isolation and FACS. Whole dorsal and ventral mouse skin was excised and floated on trypsin (0.25%) for 1 h at 37° or overnight at 4°. The epidermis was separated from dermis by scraping and epidermal cells were mechanically dissociated using a pipette. Epidermal cells were filtered with a 70 μM cell strainer into 20% BCS, collected at 300*g* and washed twice with PBS. The cells were then filtered through a 40 μM cell strainer and stained for FACS processing with CD34 Monoclonal Antibody (RAM34), FITC, eBioscience (catalogue no. 11-0341-82) and CD49d (Integrin alpha 4) Monoclonal Antibody (R1-2), PE, eBioscience (catalogue no. 12-0492-81). The gating strategy is shown in Supplementary Fig. 1b. Cells were sorted using BD FACSAria high-speed cell sorters. Single-positive and double-positive populations were collected into 20% BCS, RIPA lysis buffer (Thermo Scientific, Pierce), or 80% methanol for enzymatic assays, western blots or mass spectrometry analyses respectively.

Cell lines. No cell lines were used in this study.

Plate-reader Ldh assay. Ldh activity was determined in cell lysates by measuring the formation of soluble XTT formazan in direct relation to production of NADH over time at 475 nm at 37 °C using a Synergy-MX plate reader (Biotek Instruments). Lysates were prepared in RIPA Buffer (Thermo Scientific Pierce). Protein content was determined using the BCA Protein Assay Kit (Thermo Scientific Pierce). Ten micrograms of protein was used per well. The staining solution contained 50 mM Tris buffer pH 7.4, 150 μM XTT (Sigma), 750 μM NAD (Sigma), 80 μM phenazine methosulfate (Sigma) and 10 mM of substrate lactate (Sigma). Ldh activity was determined in cell lysates by measuring the change in absorbance of their common substrate or product, NADH, over time at 340 nm at 25 °C using a Synergy-MX plate reader (Biotek Instruments).

***In situ* Ldh assay.** Cryostat sections of mouse skin were briefly fixed (4% formalin for 5 min), washed with PBS pH 7.4, and then incubated with the appropriate solution for LDH activity. Staining medium contained 50 mM Tris pH 7.4, 750 μM NAD (Sigma), 80 μM phenazine methosulfate (Sigma), 600 μM nitrotetrazolium blue chloride (Sigma), 10 mM $MgCl_2$ (Sigma) and 10 mM of the substrate lactate (Sigma). Slides were incubated with staining medium at 37 °C until they reached the desired intensity, then counterstained using Nuclear Fast Red (Vector) and mounted using VectaMount (Vector). Control reactions were performed by using incubation medium that lacked the substrate mixture or NAD.

Mass spectrometry-based metabolomics analysis. The experiments were performed as described in ref. 17. To extract intracellular metabolites, FACS-sorted cells were briefly rinsed with cold 150 mM ammonium acetate (pH 7.3), followed by addition of 1 ml cold 80% methanol on dry ice. Cell suspensions were transferred into Eppendorf tubes and 10 nmol D/L-norvaline was added. After rigorously mixing, the suspension was pelleted by centrifugation (18,000*g*, 4 °C). The supernatant was transferred into a glass vial, metabolites dried down under vacuum, and resuspended in 70% acetonitrile. For the mass spectrometry-based analysis of the sample, 5 μl was injected onto a Luna NH2 (150 mm × 2 mm, Phenomenex) column. The samples were analysed with an UltiMate 3000RSLC (Thermo Scientific) coupled to a Q Exactive mass spectrometer (Thermo Scientific). The Q Exactive was run with polarity switching (+3.50 kV/−3.50 kV) in full scan mode with an m/z range of 65–975. Separation was achieved using A) 5 mM NH_4AcO (pH 9.9) and B) ACN. The gradient started with 15% A) going to 90% A) over 18 min, followed by an isocratic step for 9 min and reversal to the initial 15% A) for 7 min. Metabolites were quantified with TraceFinder 3.3 using accurate mass measurements (≤3 ppm) and retention times. Normalized metabolite data are available at figshare.com (https://doi.org/10.6084/m9.figshare.c.3801271).

Statistics and reproducibility. Experiments were performed on male and female animals in approximately equal numbers with no apparent difference in phenotype between sexes. All phenotypes described are representative of a minimum of $n = 3$ littermate pairs as indicated in the description of each experiment. For analysis of the hair regrowth phenotype no statistical measure was used to determine the sample size beforehand, nor were statistics used to measure effects, as the results were essentially positive or negative as represented in the figures. The results described include data from all treated animals. Investigators were not blinded to allocation during the experimental data collection. Experiments were not randomized. All results shown are representative images from at least three independently treated animals, and genotyping was performed both before and after animal treatment for confirmation. For graphs, all comparisons are shown by Student's two-tailed unpaired t-test and all graphs, bars or lines indicate mean and error bars indicate standard error of the mean (s.e.m.).

Data availability. Previously published transcriptomics data that were reanalysed here are available under accession code GSE67404 and GSE51635 (refs 35,36). Normalized metabolite data are available at figshare.com (https://doi.org/10.6084/m9.figshare.c.3801271). All other data supporting the findings of this study are available from the corresponding author on reasonable request.

36. White, A. C. *et al.* Stem cell quiescence acts as a tumour suppressor in squamous tumours. *Nat. Cell Biol.* **16,** 99–107 (2014).

nature cell biology

DOI: 10.1038/ncb3575

In the format provided by the authors and unedited.

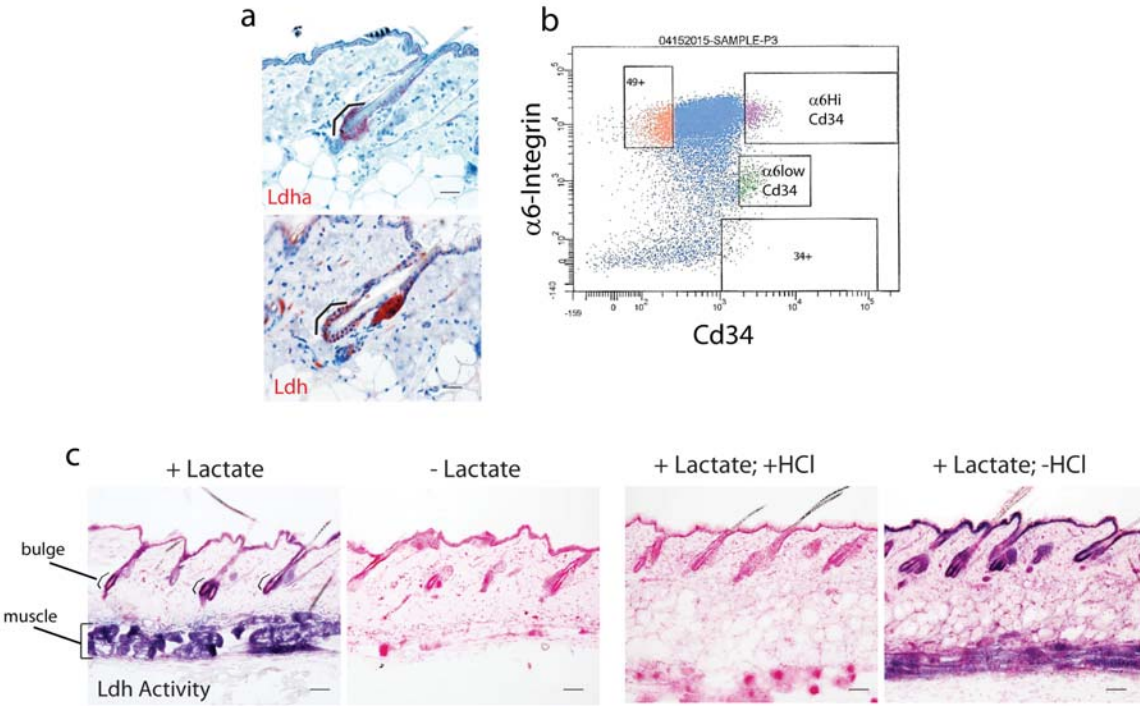

Supplementary Figure 1 Validation of key reagents and assays **a**, top, IHC with antibody recognizing specifically Ldha (same as used in Fig 1a). bottom, IHC with antibody recognizing multiple isoforms of Ldh protein. Scale bars indicate 20 micrometers. **b**, the sorting strategy employed to isolate two populations of cells from the bulge. This particular sort was used to isolate the protein samples shown by western blot in Fig 1b. **c**, Validation of colorimetric Ldh enzyme activity assay. The highest Ldh enzyme activity was observed in HFSC bulge and in the muscle. Activity indicated by purple stain; pink color is nuclear fast red counterstain. In absence of substrate lactate there was no detectable activity (purple stain). **right**, Additional validation of colorimetric Ldh enzyme activity assay. Enzyme activity inhibited by treating skin with HCl before addition of staining solution with substrate lactate. No Ldh activity (purple stain) detected. Skin in which enzyme activity is not inhibited by Hydrochloric Acid (HCl) shows highest Ldh enzyme activity in HFSC bulge and in the muscle. Scale bars indicate 50 micrometers.

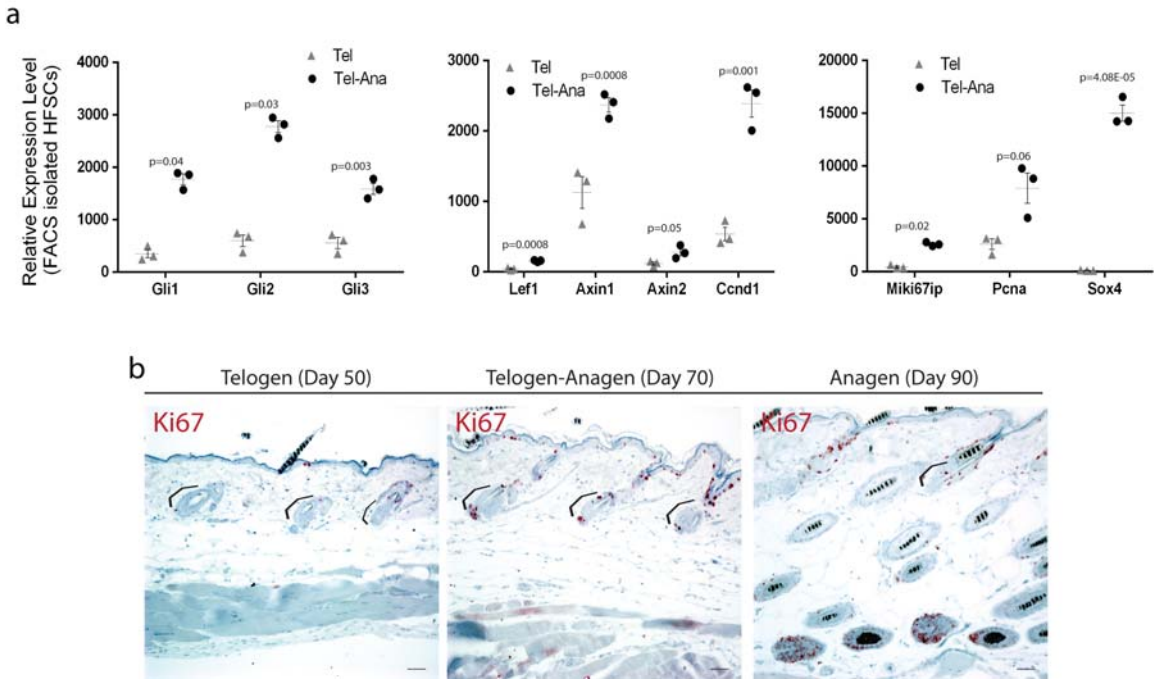

Supplementary Figure 2 Validation of hair cycle stage **a**, Analysis of RNA-seq data to validate that HFSCs in telogen-anagen transition were in fact in such a transition. The telogen-anagen transition is known to be driven by Shh (Gli factors are targets) and Wnt (Lef1, Axin, Ccnd1 are targets) signaling, and correlate with increased proliferation (Ki67 and Pcna). In addition, Sox4 was previously identified as a regulator of the telogen-anagen transition. n=3 mice per timepoint. Shown as mean ± SEM. Paired t-test was performed, $p < 0.05$. **b**, staining for Ki-67 marks dividing cells during various stages of the hair cycle. Brackets indicate the HFSC niche. Scale bars indicate 100 micrometers.

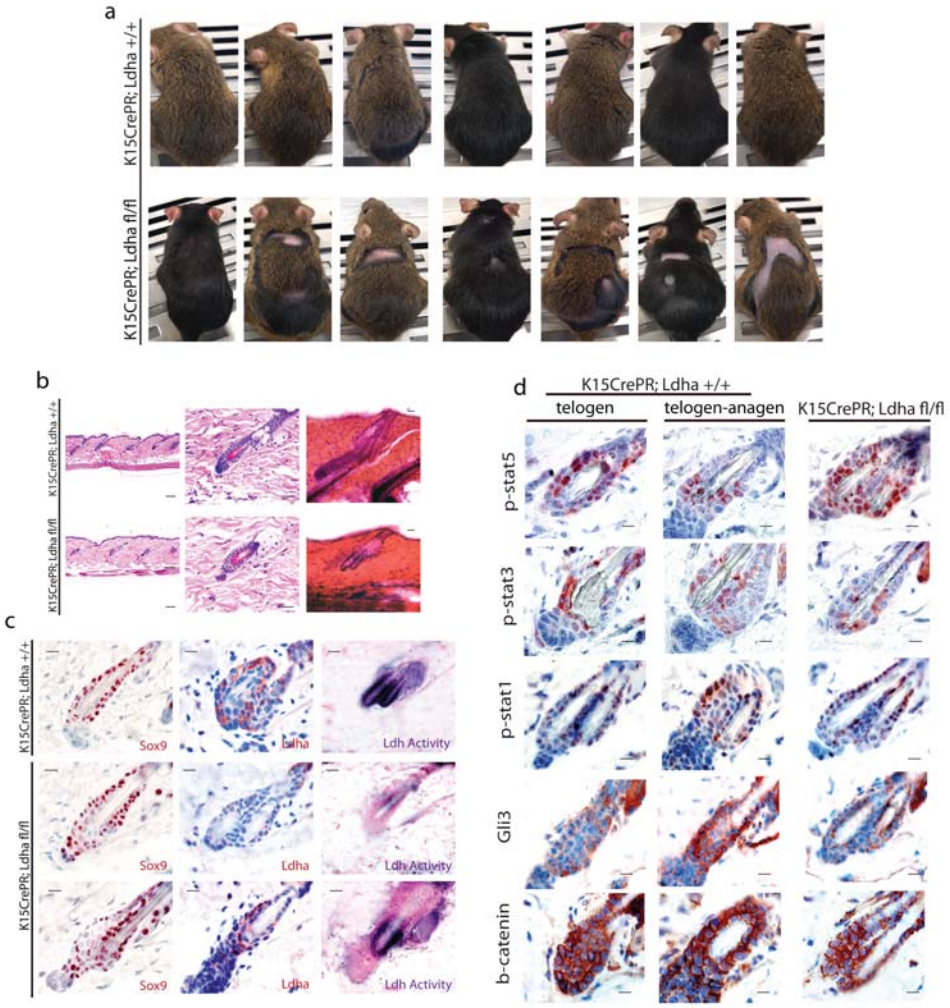

Supplementary Figure 3 Long term deletion of Ldha in HFSCs **a**, *K15CrePR;Ldha*$^{fl/fl}$ animals treated with Mifepristone during telogen (day 50) were allowed to develop for 6 months. None of the *K15CrePR;Ldha*$^{fl/fl}$ mice showed complete hair regrowth, compared to control animals that all grew their hair coats back completely. Images are representative of at least 12 animals per genotype. **b**, Histological examination of the long term *K15CrePR;Ldha*$^{fl/fl}$ mice showed that Ldha-null HFSCs remained in telogen while WT HFSCs went through anagen and then returned to telogen. This is apparent from thick sections (50 micron, right) that show an increased number of club hairs in the WT relative to *Ldha*-null follicles. Scale bars indicate 100 micrometers (left), and 20 micrometers (middle and right). **c**, IHC for HFSC marker Sox9 showed that deletion of *Ldha* from HFSCs does not affect their presence in the bulge even after 6 months. In addition, IHC and Ldh activity assay demonstrate that the deletion of *Ldha* was sustained. Because of the mosaicism of the deletion, in some portions of *K15CrePR;Ldha*$^{fl/fl}$ skin *Ldha* was not deleted. Shown on the bottom row is tissue from hair bearing skin in the *K15CrePR;Ldha*$^{fl/fl}$ mice where *Ldha* was still expressed, showing that new hair growth in *K15CrePR;Ldha*$^{fl/fl}$ mice was due to lack of deletion of *Ldha* caused by the mosaic approach used to mediate Cre recombination. Scale bars indicate 20 micrometers. **d,** To determine how various signaling pathways previously linked to the hair cycle are affected by loss of *Ldha* in HFSCs, we performed IHC for markers that indicate activity of these pathways in telogen and telogen-anagen transition. Note that pStat5 appears to be suppressed in normal telogen-anagen transition, and this does not seem to occur in *Ldha*-null HFSCs. pStat1 and pStat3 did not seem to be affected by loss of *Ldha*. Expression of Gli3, a target of Shh signaling, is typically induced in an activated hair germ derived from HFSCs, but *Ldha*-null HFSCs do not make an active hair germ. Activation of the Wnt pathway is indicated by nuclear localization of β-catenin, and very little nuclear β-catenin was detected in Ldha-null HFSCs. Scale bars indicate 6 micrometers.

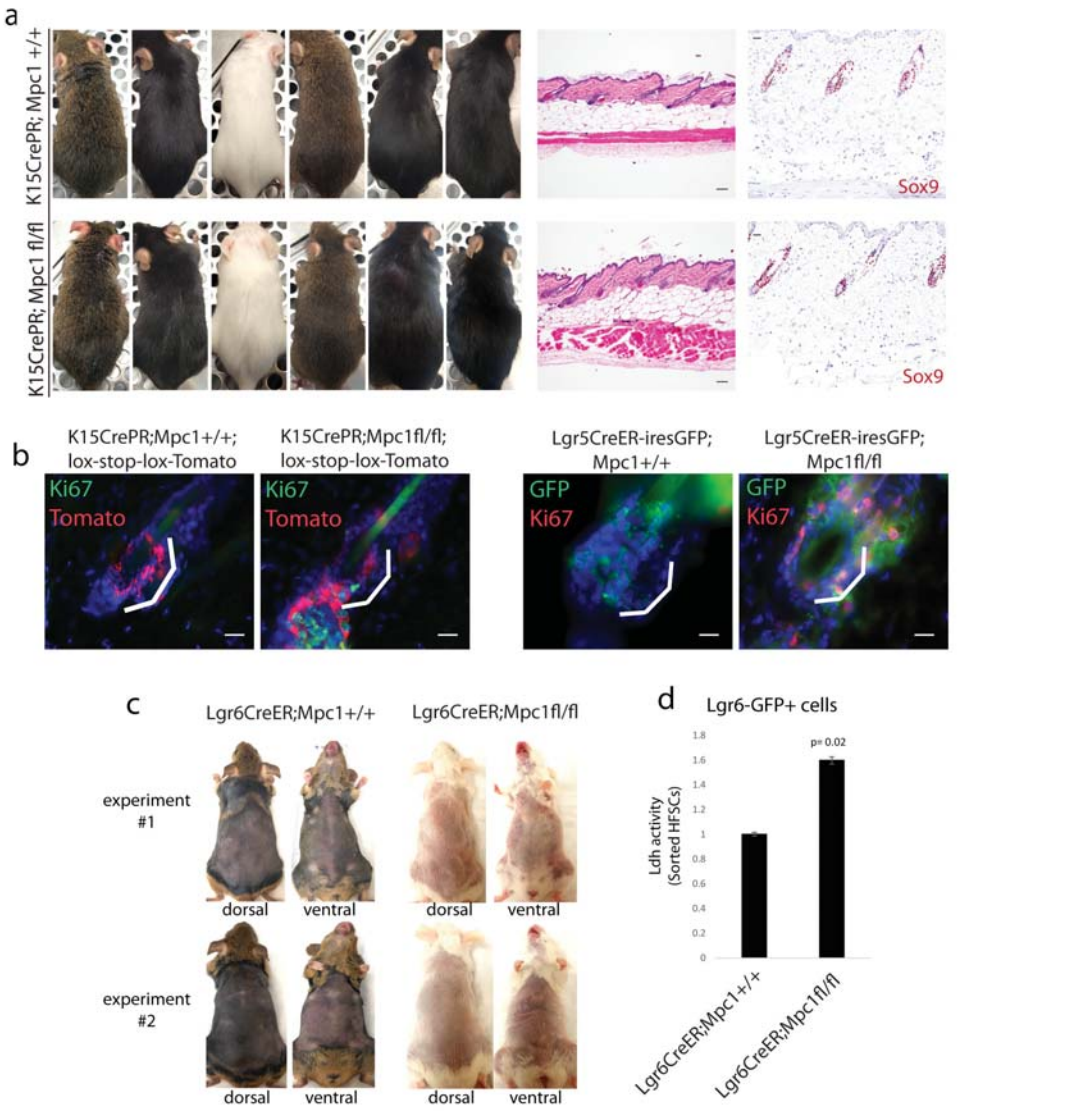

Supplementary Figure 4 Long term deletion of Mpc1 in HFSCs **a**, Six months after initiation of deletion of Mpc1 in HFSCs (*K15CrePR;Mpc1fl/fl),* mice lacking Mpc1 show no deleterious effects as measured by the hair cycle (left), pathology (middle, H and E), or staining for HFSCs (right, Sox9). Scale bars indicate 100 micrometers in middle panel, and 50 micrometers in right panel. Images are representative of at least 12 animals per genotype. **b,** To demonstrate that the deletion of Mpc1 promotes proliferation specifically in HFSCs, we used *K15CrePR;Ldha*$^{fl/fl}$ mice bearing a lox-stop-lox-Tomato allele to look at K15+ HFSCs and proliferation with and without Mpc1 deletion (left). In addition, we took advantage of the ires-GFP within the *Lgr5CreER* allele to stain for Ki-67 and GFP and look for co-localization with and without Mpc1 deletion (right). White brackets denote bulge area. Scale bars represent 20 micrometers. **c**, Deletion of *Mpc1* in mice bearing the *Lgr6CreER* allele shows no premature induction of the hair cycle. **d**, Ldh activity assay on sorted HFSCs from either control or *Lgr6CreER* mediated *Mpc1* deletion mice showed increased activity in cells lacking Mpc1. n=6 mice per genotype pooled from 2 independent experiments. Shown as mean ± SEM. Paired t-test was performed, $p < 0.05$.

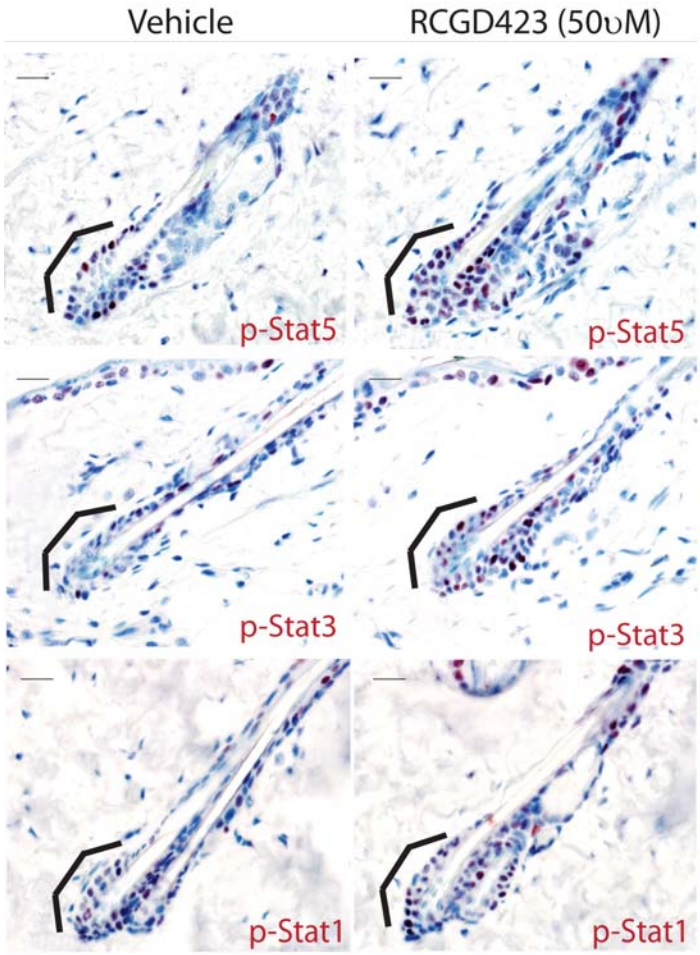

Supplementary Figure 5 Stimulation of Jak-Stat signaling and the hair cycle. RCGD423 was applied topically to shaved mice at day 50. 48 hours after treatment, the skin was harvested and prepared for IHC. IHC with the indicated antibodies demonstrates relative activity of Stat signaling in vehicle vs RCGD423 treated skin. Scale bars indicate 20 micrometers.

SUPPLEMENTARY INFORMATION

Fig1

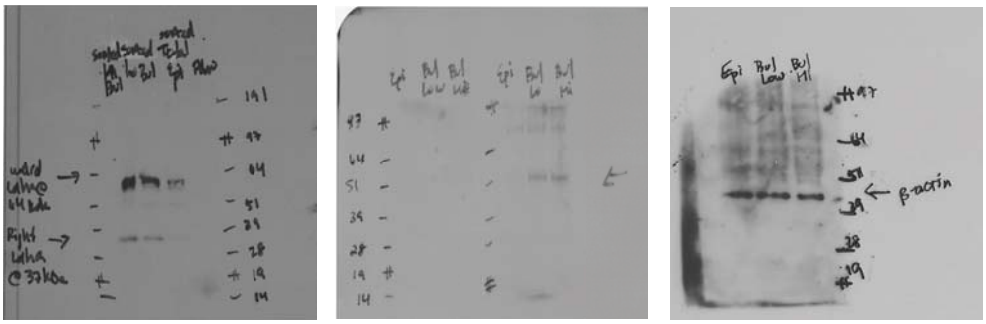

Fig 4

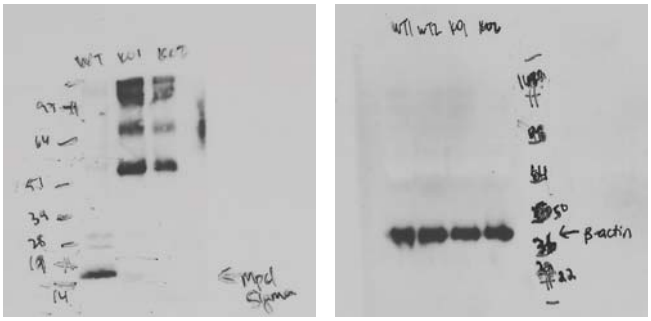

Fig 6

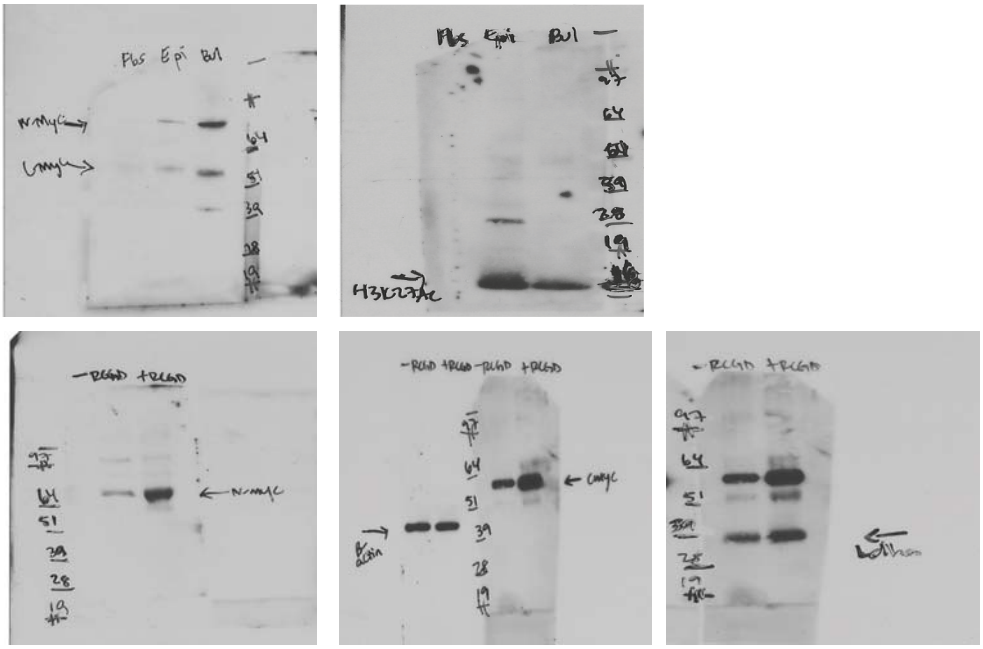

Supplementary Figure 6 Unprocessed Blots. Unprocessed scans of the blots shown in Figures 1, 4, 6 are shown.

Supplementary Table Legend

Supplementary Table 1 Presented is an inventory of mice that are described in Figures 1-6 (and Supplementary Figures 1-5), including age, sex, and genotype.

Animal ID	DOB	K15CrePR	Ldha	Sex
2990	6/11/2015	+	fl/fl	M
2991	6/11/2015	-	+/+	M
125	7/16/2015	-	+/+	F
126	7/16/2015	+	fl/fl	F
127	7/16/2015	+	fl/fl	F
128	7/16/2015	+	fl/fl	F
129	7/16/2015	+	fl/fl	F
130	7/16/2015	+	fl/fl	F
131	7/16/2015	-	fl/fl	F
132	7/16/2015	+	fl/fl	M
133	7/16/2015	-	fl/fl	M
134	7/16/2015	-	+/+	M
278	8/30/2015	-	+/+	F
279	8/30/2015	+	fl/fl	F
280	8/30/2015	+	fl/fl	F
281	8/30/2015	-	+/+	F
473	1/3/2016	+	fl/fl	F
474	1/3/2016	+	+/+	F
475	1/3/2016	+	+/+	F
476	1/3/2016	+	+/+	F
477	1/3/2016	+	fl/fl	F
478	1/3/2016	+	+/+	M
479	1/3/2016	+	fl/fl	M
480	1/4/2016	-	+/+	F
481	1/4/2016	+	fl/fl	F
482	1/4/2016	+	fl/fl	M
483	1/4/2016	+	+/+	M
484	1/4/2016	-	fl/fl	M
485	1/4/2016	+	+/+	M
486	1/4/2016	-	+/+	M
487	1/4/2016	+	+/+	M
488	1/4/2016	-	+/+	M
489	1/4/2016	+	fl/fl	M
507	1/25/2016	+	fl/fl	F
508	1/25/2016	+	fl/fl	F
509	1/25/2016	-	+/+	F
510	1/25/2016	+	fl/fl	F
511	1/25/2016	+	+/+	F
751	6/9/2016	+	fl/fl	F
755	6/9/2016	+	fl/fl	M
758	6/13/2016	+	fl/fl	F
759	6/13/2016	-	+/+	F
760	6/13/2016	+	fl/fl	F
761	6/13/2016	+	fl/fl	M
762	6/13/2016	+	+/+	M
763	6/13/2016	-	+/+	M
813	7/13/2016	+	fl/fl	M
814	7/13/2016	+	fl/fl	M
815	7/13/2016	-	+/+	M
816	7/13/2016	+	fl/fl	M
818	7/13/2016	+	+/+	M
819	7/13/2016	-	fl/fl	M
820	7/13/2016	+	fl/fl	M
822	7/13/2016	-	+/+	M
1050	10/17/2016	-	+/+	M
1051	10/17/2016	+	fl/fl	M
1052	10/17/2016	-	+/+	M
1028	10/14/2016	+	fl/fl	M
1029	10/14/2016	-	fl/fl	M
1032	10/14/2016	-	fl/fl	M
1033	10/14/2016	+	fl/fl	M
1191	10/19/2016	+	fl/fl	F
1192	10/19/2016	-	fl/fl	F
1193	10/19/2016	+	fl/fl	F
1194	10/19/2016	+	+/+	F
1195	10/19/2016	+	fl/fl	F

Animal ID	DOB	Lgr5CreER	Ldha	Sex
2780	3/31/2015	-	fl/fl	M
2787	3/31/2015	+	fl/fl	M
13	6/15/2015	+	+/+	F
14	6/15/2015	+	fl/fl	F
86	7/3/2015	+	fl/fl	F
92	7/3/2015	+	fl/fl	M
93	7/3/2015	-	+/+	M
81	7/10/2015	+	+/+	M
83	7/10/2015	+	fl/fl	M
84	7/3/2015	+	+/+	F
663	4/26/2016	+	fl/fl	F
664	4/26/2016	+	+/+	F
717	5/22/2016	-	fl/fl	F
718	5/22/2016	+	fl/fl	F
778	6/16/2016	-	+/+	F
779	6/16/2016	-	fl/fl	F
780	6/16/2016	+	fl/fl	F
781	6/16/2016	-	fl/fl	F
782	6/16/2016	-	+/+	F
783	6/16/2016	-	+/+	M
784	6/16/2016	+	fl/fl	M
785	6/16/2016	+	fl/fl	M
786	6/16/2016	+	fl/fl	M
845	8/4/2016	-	+/+	M
846	8/4/2016	+	fl/fl	M
850	8/4/2016	-	fl/fl	M
851	8/4/2016	+	+/+	M
892	8/23/2016	+	fl/fl	F
893	8/23/2016	-	fl/fl	F
987	11/15/2016	+	+/+	F
988	11/15/2016	+	fl/fl	F
989	11/15/2016	+	+/+	F
990	11/15/2016	+	+/+	M
1069	10/16/2016	+	fl/fl	F
1070	10/16/2016	-	fl/fl	M
1071	10/16/2016	+	fl/fl	M
1072	10/16/2016	+	fl/fl	M
1073	10/16/2016	+	fl/fl	M
1074	10/16/2016	+	fl/fl	M
1075	10/16/2016	-	fl/fl	M
1076	10/16/2016	+	fl/fl	M

Animal ID	DOB	Lgr6CreER	Mpc1	Sex
659	4/26/2016	-	fl/fl	M
660	4/26/2016	+	fl/fl	F
661	4/26/2016	+	fl/fl	M
662	4/26/2016	-	fl/fl	M
693	4/28/2016	-	fl/fl	M
694	4/28/2016	-	fl/fl	M
696	4/28/2016	+	fl/fl	M
697	4/28/2016	+	fl/fl	M
701	5/9/2016	+	+/+	F
702	5/9/2016	+	+/+	F
703	5/9/2016	+	fl/fl	F
704	5/9/2016	-	fl/fl	M
705	5/9/2016	+	fl/fl	M
735	6/4/2016	+	fl/fl	M
736	6/4/2016	-	fl/fl	M
737	6/4/2016	+	fl/fl	M
777	6/4/2016	+	+/+	M
793	7/12/2016	+	fl/fl	F
794	7/12/2016	-	fl/fl	F
795	7/12/2016	+	fl/fl	F

Animal ID	DOB	K15CrePR	Mpc1	Sex
493	1/8/2016	+	+/+	M
494	1/8/2016	+	fl/fl	M
495	1/8/2016	-	fl/fl	M
550	2/17/2016	-	+/+	F
551	2/17/2016	+	fl/fl	F
552	2/17/2016	-	+/+	F
631	3/24/2016	+	fl/fl	F
633	3/24/2016	+	+/+	F
634	3/24/2016	-	+/+	F
680	4/27/2016	+	fl/fl	F
681	4/27/2016	+	+/+	F
682	4/27/2016	-	fl/fl	F
683	4/27/2016	+	fl/fl	F
684	4/27/2016	-	fl/fl	F
768	6/12/2016	-	fl/fl	F
769	6/12/2016	+	fl/fl	F
770	6/12/2016	+	fl/fl	F
860	7/18/2016	+	+/+	F
861	7/18/2016	+	fl/fl	F
875	7/22/2016	+	fl/fl	M
876	7/22/2016	+	+/+	M
880	8/22/2016	+	fl/fl	M
881	8/22/2016	+	+/+	M
991	9/18/2016	+	fl/fl	M
992	9/18/2016	+	+/+	M
993	9/18/2016	+	+/+	F
994	9/18/2016	+	fl/fl	F
995	9/18/2016	+	+/+	M
996	9/18/2016	+	fl/fl	M
997	9/18/2016	-	fl/fl	M

Animal ID	DOB	Lgr5CreER	Mpc1	Sex
5652	7/6/2016	+	fl/fl	M
5653	7/6/2016	+	fl/fl	M
5654	7/6/2016	-	fl/fl	M
5655	7/6/2016	+	fl/fl	F
5656	7/6/2016	-	fl/fl	F
5657	7/6/2016	-	fl/fl	F
5658	7/6/2016	-	fl/fl	F
5659	7/6/2016	-	fl/fl	F
5660	7/6/2016	+	fl/fl	F
5661	7/6/2016	+	fl/fl	F
5662	7/6/2016	-	fl/fl	F
5663	7/6/2016	+	fl/fl	M
5664	7/6/2016	+	fl/fl	M
5665	7/6/2016	-	fl/fl	M
5666	7/6/2016	+	fl/fl	F
5667	7/6/2016	+	fl/fl	F
5668	7/9/2016	+	+/+	F
5672	7/9/2016	+	+/+	M
5673	7/9/2016	+	+/+	M
5674	7/9/2016	+	+/+	M
5675	7/9/2016	+	+/+	M
5882	8/17/2016	+	fl/fl	M
5883	8/17/2016	+	fl/fl	M
5884	8/21/2016	+	+/+	F
5886	8/21/2016	+	+/+	F
5890	8/21/2016	+	+/+	M
5891	8/21/2016	+	+/+	M
5892	8/24/2016	+	+/+	F
5893	8/24/2016	+	+/+	F
5896	8/24/2016	+	+/+	M
5897	8/24/2016	+	+/+	M
5898	8/27/2016	+	fl/fl	F

Chapter 3: Hmga2 is dispensable for cutaneous squamous cell carcinoma

Author contributions

Wim Verkruijsse (principal scientist, Philips Research, Eindhoven, the Netherlands) contributed to the design of the research study, is an employee of Royal Philips Electronics B.V., the Netherlands, and has no conflict of interest to declare. Jan Willem Bikker (statistical consultant, CQM consultancy, Eindhoven, the Netherlands) assisted in the analysis of questionnaire data, which were used to select subjects with sensitive skin and subjects with non-sensitive skin, and has no conflict of interest to declare.

Funding and disclosures

The costs made to conduct this study were paid by Royal Philips Electronics B.V, the Netherlands Natallia Uzunbajakava is an employee of Royal Philips Electronics B.V, the Netherlands and received salary for this study.

Supporting Information

Additional supporting data may be found in the supplementary information of this article.

Data S1. Methods and material.

Data S2. Questionnaire.

Data S3. Supplementary References.

Figure S1. Representative images of clinical presentation and immunohistochemistry.

Table S1. The observed median (range) of the biophysical measurements and the immunohistochemical markers and the estimated mean differences (95% CI) at each point of measurement by skin sensitivity, using a linear mixed model for repeated measurements adjusted for baseline values.

References

1 Misery L, Myon E, Martin N *et al.* J Eur Acad Dermatol Venereol 2007: **21**: 620–628.
2 Morizot F, Guinot C, Lopez J *et al.* Cosmet Toiletries 2000: **115**: 83–89.
3 Saint-Martory C, Roguedas-Contios A M, Sibaud V *et al.* Br J Dermatol 2008: **158**: 130–133.
4 Fartasch M. Microsc Res Tech 1997: **37**: 193–199.
5 Willis C M, Stephens C J M, Wilkinson J D. J Investig Dermatol 1989: **93**: 695–699.
6 Cho H J, Chung B Y, Lee H B *et al.* J Dermatol 2012: **39**: 295–300.
7 Diogo L, Papoila A L. Skin Res Technol 2010: **16**: 30–37.
8 Loffler H, Dickel H, Kuss O *et al.* Acta Dermato-Venereologica 2001: **81**: 343–346.
9 Robinson M K, Perkins M A. Contact Dermatitis 2001: **45**: 205–213.
10 Richters R J, Uzunbajakava N E, Falcone D *et al.* Br J Dermatol 2015: doi: 10.1111/bjd.14307 [e-pub ahead of print]

DOI: 10.1111/exd.12978
www.wileyonlinelibrary.com/journal/EXD

Letter: Mouse Mutants with Absent or Minimal Skin Phenotype
Section Editor: Michael Rendl, New York

Hmga2 is dispensable for cutaneous squamous cell carcinoma

Andrew White[1,2,3,4,*], Aimee Flores[1,2,3,4,*], Jessica Ong[1,2,3,4] and William E. Lowry[1,2,3,4]

[1]Department of Molecular Cell and Developmental Biology, UCLA, Los Angeles, CA, USA; [2]Jonsson Comprehensive Cancer Center, UCLA, Los Angeles, CA, USA; [3]Eli and Edythe Broad Center for Regenerative Medicine, UCLA, Los Angeles, CA, USA; [4]Molecular Biology Institute, UCLA, Los Angeles, CA, USA

Correspondence: William E. Lowry, 621 Charles Young Drive South, Los Angeles, CA 90095, USA, Tel.: 310-794-5175, Fax: 310 794 91323, e-mail: blowry@ucla.edu

**These authors contributed equally*

Abstract: Hmga2 functions as a chromatin-associated factor during development, but is not expressed in most adult tissues. Expression of Hmga2 in adult tissues has been associated with a variety of human cancers. Numerous studies have implicated Hmga2 in epithelial-to-mesenchymal transition (EMT) and cancer progression through gain of function studies, but it is unclear whether Hgma2 is necessary for EMT, tumor formation or tumor progression. We deleted Hmga2 in two mouse models of squamous cell carcinoma and found this gene to be dispensable. In fact, EMT, tumor initiation and progression all appeared to be mostly unaffected by the absence of Hmga2. Tumors lacking the ability to induce Hmga2 proceeded to initiate cutaneous spindle cell and squamous cell carcinomas with all the typical pathological and molecular hallmarks of these cancers.

Key words: hair follicle stem cells – Hmga2 – squamous cell carcinoma – tumor progression

Accepted for publication 2 February 2016

For over two decades, HMGA2 has been implicated as a player in human cancer (1); however, the question of whether HMGA2 is required for tumor initiation or progression has not been addressed (2). Our laboratory and others have determined that cutaneous SCC can be initiated by induction of constitutively active K-ras and loss of p53 specifically in hair follicle stem cells (3,4). Here, we studied the role of HMGA2 in epithelial-to-mesenchymal transition (EMT), tumor initiation and progression using both molecular genetics and chemical carcinogenic tumor models. Surprisingly, we did not detect any dramatic effect of the loss of Hmga2 in EMT, initiation or progression of SCC.

Shown in Fig. 1a are the top 30 upregulated genes from hyperplasia towards the high-grade tumor. Interestingly, many of the genes (8 of 30) strongly induced in this tumorigenesis model are also known to be targets of the let-7 family of miRNAs, including Hmga2, which was strongly induced in this model as shown at the

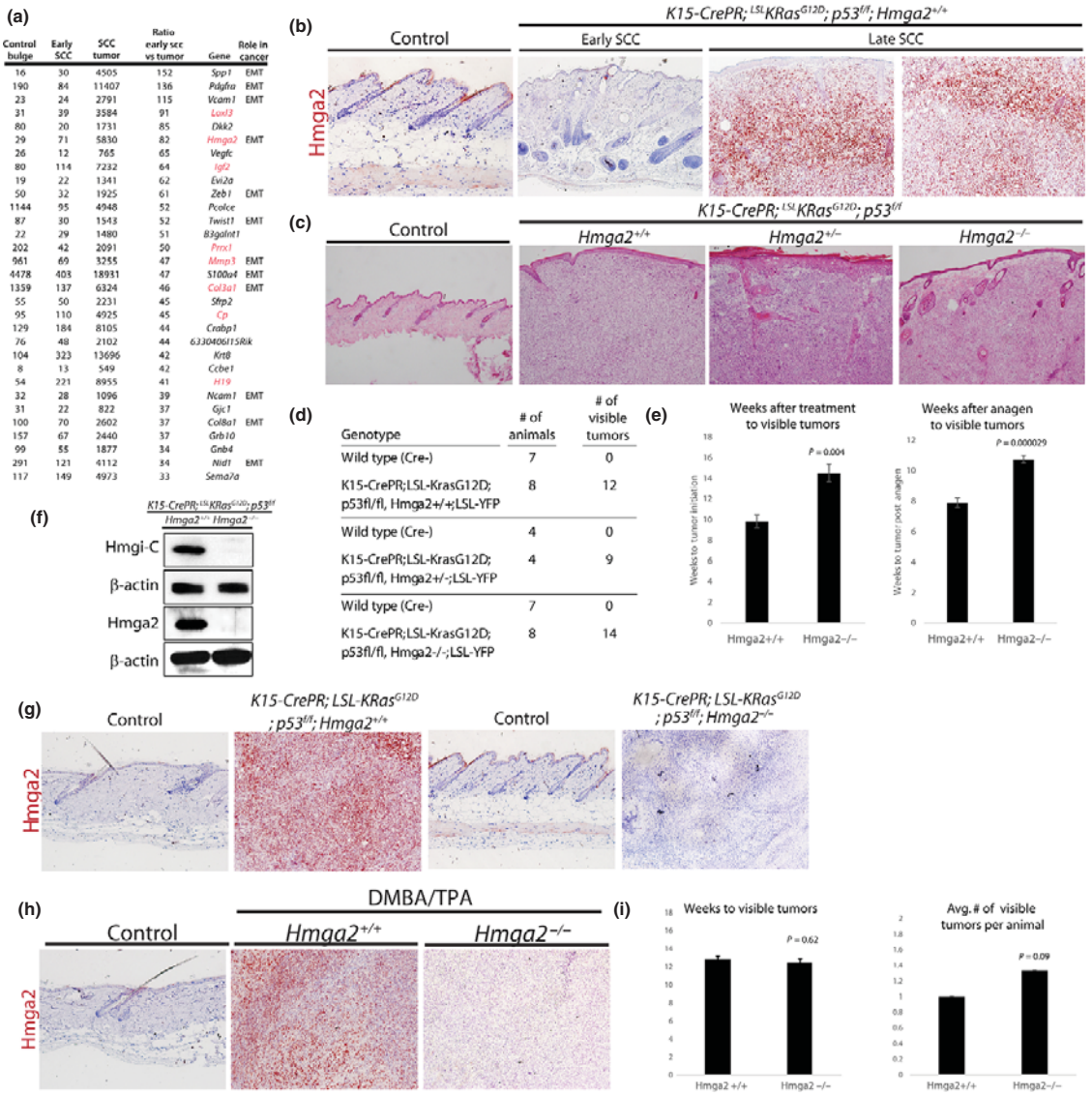

Figure 1. Defining the role for Hmga2 in SCC. (a) Gene expression profiling by microarray identified many genes induced in FACS sorted, lineage traced cancer cells as HFSCs progress from a high-grade SCC. Shown are the top 30 genes induced in high-grade tumors, many of which have been implicated in EMT. Numbers indicate the average, normalized signal intensity on the microarray from at least two replicates. Shown in RED are those that are predicted targets of the let-7 family of miRNAs. (b) immunostaining with Hmga2 confirms the expression pattern seen by transcriptional profiling. (c) Haematoxylin and eosin staining shows SCC induction upon induction of KrasG12D and loss of p53 (second panel). Loss of one or two alleles of Hmga2 generates tumors of a similar phenotype (third and fourth panels). (d) quantification of visible tumors across genotypes 10 weeks after induction is provided (bottom panels). (e) Quantification of the timing of tumor onset as measured by visual inspection is shown either from the point of induction with mifepristone (left) or the start of anagen (right). *P*-value was calculated with two-tailed Student's *t*-test with unequal variance and $n > 4$; error bars represent variation over replicate animals. (f) Western blotting with cell extract from tumors formed either in the absence or presence of Hmga2 and confirms the deletion. Note that Hmga2 antibody (ab97276) was used for the immunostainings in (b, g and h, g), immunostaining for Hmga2 shows a typical pattern expression during SCC formation, and the absence of Hmga2 protein in tumors made from mutant mice is shown. (h) mice treated with DMBA/TPA over the course of 18 weeks, and all developed tumors. (i) across $n > 7$ experiments, neither tumor initiation nor frequency was significantly affected by the loss of Hmga2 as measured by visual inspection. *P*-value was calculated with two-tailed Student's *t*-test with unequal variance and $n > 7$; error bars represent variation over replicate animals.

protein level by immunostaining (Fig. 1b). Furthermore, the induction of Hmga2 in these tumors was present in cells that were formerly hair follicle cells as shown by colocalization and lineage tracing (Figure S1). Hmga2 is not typically expressed in most postnatal tissues, but is instead induced relatively late in tumor progression, as predicted by the gene expression profiling.

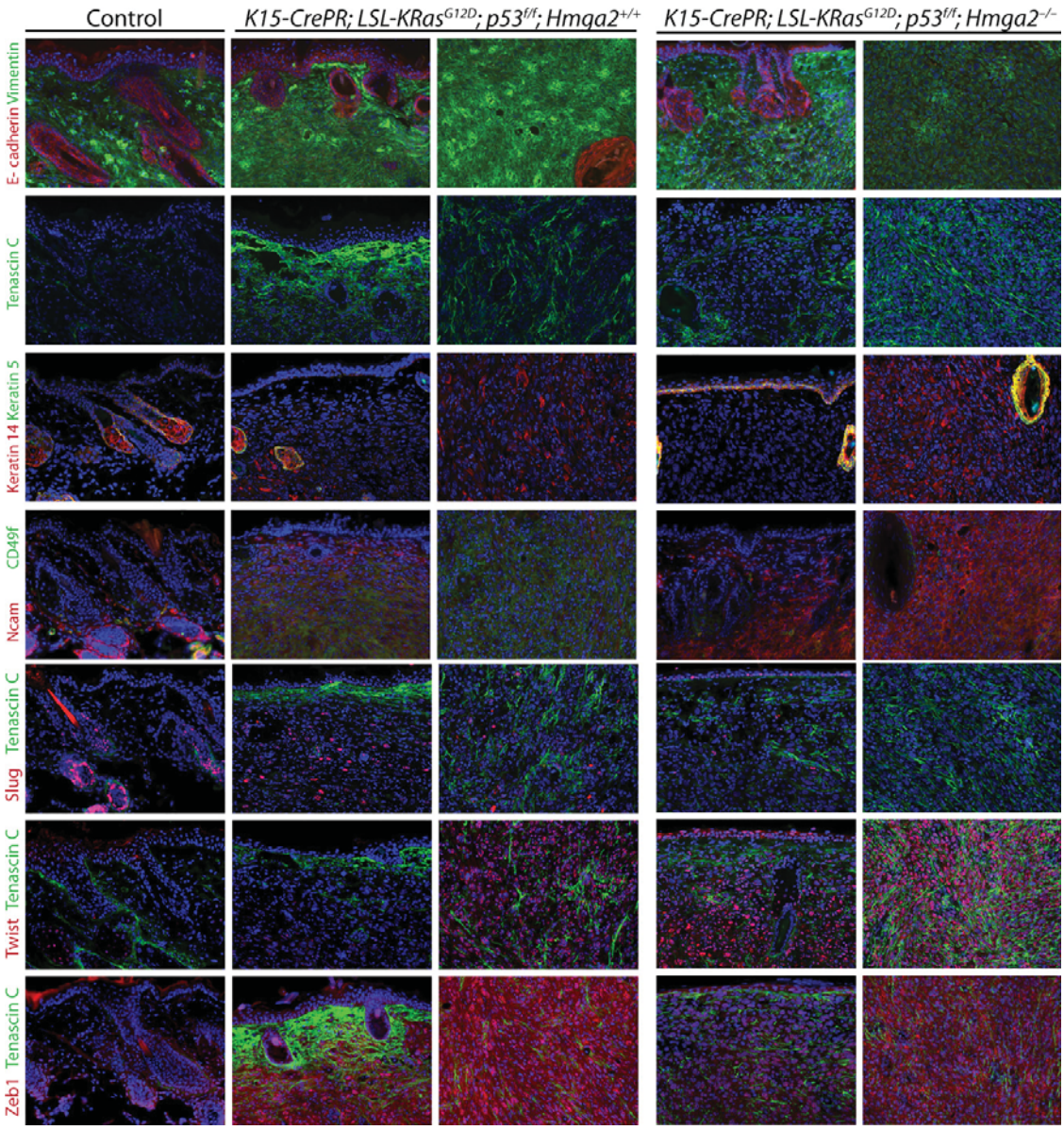

Figure 2. Loss of Hmga2 does not affect EMT in SCC. Immunostaining for a variety of EMT markers or for regulators of EMT shows that in general the epithelial program is suppressed and a mesenchymal program is induced in SCC, even in the absence of Hmga2 (E-cad, Vim, TnC, Krt5, Krt14, Ncam, Cd49f, Slug, Twist and Zeb1). Shown are two panels for each marker from both genotypes to indicate the diversity of staining patterns across individual tumors both in the WT and the Hmga2 KO.

Because of the remarkable induction of Hmga2 in our SCC model, we sought to determine whether induction of this gene is required for tumor initiation, tumor progression or induction of the mesenchymal state found in cutaneous spindle cell carcinomas. We obtained Hmga2$^{+/-}$ mice and mated them into the background of our two-hit tumor model for SCC (3). Remarkably, even with loss of either one or both alleles of Hmga2, hair follicle stem cells were still able to serve as cancer cells of origin and produced bona fide SCC (Fig. 1c). Tumor frequency, severity and pathology were not markedly affected by loss of Hmga2 (Fig. 1d). Most mice in this model presented with 1-3 macroscopically visible tumors (as quantified in Fig. 1d), and full penetrance of more subtle phenotypes upon microscopic examination across all follicles ($n > 7$) (Fig. 1d). Quantification of the timing of tumor

onset suggested that tumors appeared with a longer latency in the absence of Hmga2 (Fig. 1e). This observation could have been due to differences in tumor initiation or even hair cycle timing, as we previously showed that tumor initiation by HFSCs depends on activation of the hair cycle (5). Regardless, the longer latency observed in the absence of Hmga2 did not correlate with severity of phenotype. Western blotting with two independent antibodies confirmed the absence of Hmga2 protein in the tumors and validated the specificity of the immunostainings shown in Fig. 1b, f, g. Immunostaining confirmed the fact that Hmga2 protein was dispensable for acquisition of high-grade SCC in this model (Fig. 1g).

To determine whether Hmga2 could play a role in SCC driven by an alternative method, we employed the DMBA/TPA protocol on WT and Hmga2 null skin. After sixteen weeks of the DMBA/TPA protocol, papillomas and keratoacanthomas began to appear on both WT and Hmga2-null mice, some of which progressed towards SCC (Fig. 1h). These experiments suggested that neither the rate of initiation nor the frequency of tumor formation by DMBA/TPA was affected by the loss of Hmga2 (Fig. 1i) ($n > 7$).

We previously described some key molecular cornerstones of tumor initiation and progression from hair follicle stem cells in this model (3), including induction of signalling through Tgf beta (pSMAD2), Map Kinase (pErk), Creb (pCreb) or Akt (pS6). We failed to detect any significant change in the activation of each of these pathways in Hmga2-null tumors (Figure S2). In addition, Igf2bp1 and Keratin 8, markers of dedifferentiation, were induced in tumors produced in the absence of Hmga2, while another, Sox2, was diminished (Figure S3). These results suggest that while the loss of Hmga2 does have some molecular effects on tumor formation, these are not significant enough to strongly affect tumor initiation or progression (Figure S3).

Numerous studies have shown that Hmga2 is important in regulating factors that determine whether epithelial cells undergo an EMT during tumorigenesis (6,7). The SCC model used here adopts features of a typical EMT. Immunostaining for both epithelial (E-cad, K14, Integrin a6) and mesenchymal (Ncam, TnC, CD34) hallmarks, or regulators of EMT (Slug and Twist) demonstrated that loss of Hmga2 expression appeared to have no effect on EMT (Fig. 2). An analysis of independent samples by RT-PCR showed the same effect, namely EMT genes were still induced in tumors made without Hmga2 (Figure S4).

The lack of substantial phenotypic effect in the absence of Hmga2 raises many questions as to the role of this gene in cancer, and whether the role for this protein in SCC is typical of that of other cancers as well. It is important to note that cutaneous SCC is only rarely metastatic and thus it is difficult to assign a role for Hmga2 in metastases of SCC as has been done for numerous other cancers. In addition, we cannot rule out the fact that Hmga2 could play an important role in tumor physiology once expressed, even in SCC.

It is certainly possible that the loss of Hmga2 could be compensated for by Hmga1. Hmga1 shares significant homology with Hmga2, but has typically been ascribed to different roles in the cell. The best evidence that these genes may compensate for each other is a recent report demonstrating that while deletion of Hmga2 leads to the pygmy phenotype, deletion of both Hmga1 and 2 generates what were called super-pygmy mice that were significantly smaller still (8). It is worth noting that, according to our RNA profiling, Hmga1 is expressed throughout the epidermis at a significant level and does not change over the course of tumorigenesis, or in the absence of Hmga2 (data not shown). Regardless, we cannot rule out the possibility that the loss of Hmga2 was compensated for by Hmga1 in our experiments.

Acknowledgements

We would like to acknowledge DLAM staff for the care and maintenance of animal strains. We would like to thank Jeanny Hu and Anqi Liu for genotyping. We are grateful to Kiran Chada (UMDNJ) for providing Hmga2$^{-/-}$ mice as well as guidance for genotyping. ACW was supported by a CIRM training grant. This work was supported by NIH R01 from NIAMS, and the Jonsson Cancer Center Foundation.

Author contributions

ACW and AF designed and carried out experiments and helped write the manuscript. JO carried out experiments. WEL designed experiments and wrote the manuscript.

Funding

This work was supported by an NIH Grant (NIAMS R01AR057409).

Conflict of interest

The authors have no conflicts of interest to disclose.

Supporting Information

Additional supporting data may be found in the supplementary information of this article.

Figure 1. Hma2 is expressed in SCC cells that were once a part of the hair follicle.

Figure 2. Loss of Hmga2 does not affect markers of tumor initiation.

Figure 3. Dedifferentiation in the absence of Hmga2.

Figure 4. Loss of Hmga2 does not affect induction of the EMT program at the RNA level.

Appendix S1. Materials and Methods.

References

1 Staats B, Bonk U, Wanschura S *et al.* Breast Cancer Res Treat 1996: **38**: 299–303.
2 Hebert C, Norris K, Scheper M A *et al.* Mol Cancer 2007: **6**: 5.
3 White A C, Tran K, Khuu J *et al.* Proc Natl Acad Sci USA 2011: **108**: 7425–7430.
4 Lapouge G, Youssef K K, Vokaer B *et al.* Proc Natl Acad Sci USA 2011: **108**: 7431–7436.
5 White A C, Khuu J K, Dang C Y *et al.* Nat Cell Biol 2014: **16**: 99–107.
6 Thuault S, Valcourt U, Petersen M *et al.* J Cell Biol 2006: **174**: 175–183.
7 Morishita A, Zaidi M R, Mitoro A *et al.* Cancer Res 2013: **73**: 4289–4299.
8 Federico A, Forzati F, Esposito F *et al.* Biol Open 2014: **3**: 372–378.

Supplemental Materials and Methods

Animals

Animals were housed and treated according to protocols approved by DLAM (UCLA) and IACUC. KRasG12D, K15-CrePR, lsl-YFP, and p53fl/fl mice were acquired from Jackson Labs and described previously (10). Hmga2-/+ mice were a kind gift from Kirin Chada (UMDNJ, New Jersey). For tumor modeling, KrasG12D expression and deletion of p53 were instigated by injection with Mifepristone solubilized in sunflower seed oil and delivered by intraperitoneal injection at 7-8 weeks of age. The phenotypes described were observed by 4-10 weeks after injection. For DMBA/TPA experiments, Hmga2+/+,+/- and -/- animals were treated with DMBA at 7-8 weeks of age, followed by weekly treatments of TPA for up to 18 weeks. DMBA was re-administered at 4 weeks after initial treatment. All animals described were c57/Bl6 strain.

Gene expression profiling and RT-PCR

For RT-PCR, tumor and control tissues were isolated and lysed in Qiazol lysis buffer. Qiagen Total RNA kits were used to isolate RNA. Equal amounts of RNA were used for Reverse Transcriptase assays using the Invitrogen cDNA Synthesis kit. PCR primers for individual genes were designed to span intron/exon boundaries where possible, and PCR reactions were carried out in a Roche 480 Lightcycler. Results shown were generated by calculating crossing values (Ct) by second derivative maximum, then normalized against a housekeeping gene (either Gapdh or Actin). The results shows in Fig S3 are expressed as a function of the expression level in control tissue (gray line). For microarray profiling, RNA were isolated from FACS sorted cells positive for the YFP lineage tracing allele from the indicated genotypes, and profiled as described in the NIH GEO datasets GSE51635.

Histology and Immunostaining

Tumor, tumor adjacent, and control tissues were isolated from the indicated genotypes and embedded fresh in OCT for frozen tissue preparations, or fixed overnight in 4% formalin and embedded in paraffin. For frozen tissue, sectioning was performed on a Leica 3200 Cryostat, and fixed for 5-10 min in 4% paraformaldehyde. Paraffin embedded tissue was sectioned, de-paraffinzed, and prepared for histology. All sections prepared for staining were blocked in staining buffer containing appropriate control IgG (Goat, Rabbit etc.). Images were collected on either a Zeiss A2 upright microscope (immunofluorescence) or Olympus upright microscope (immunohistochemistry). All images presented used a 20X objective. Antibodies: E-Cadherin (CST3195), Vimentin (Covance PCK-594P), Tenascin-C (ab6346), Keratin 5 (Covance PRB-160P), Keratin 14 (Covance PRB-155P), CD49f (BD555734), Ncam (Millipore AB45032), Slug (CST9585), Twist (ab49254), Zeb1 (Bethyl Labs IHC-00419), p-Smad2 (CST3108), p-Creb (CST9198), p-Erk (CST4370), p-S6 (CST2215), IGF2BP1 (ab100999), Sox2 (Biolegend 630901/2), K8/18 Troma 1 (DSHB AB531826), Hmgi-C (FL109) (sc30223), Hmga2 (ab97276), β-catenin (sc7199), GFP (ab13970).

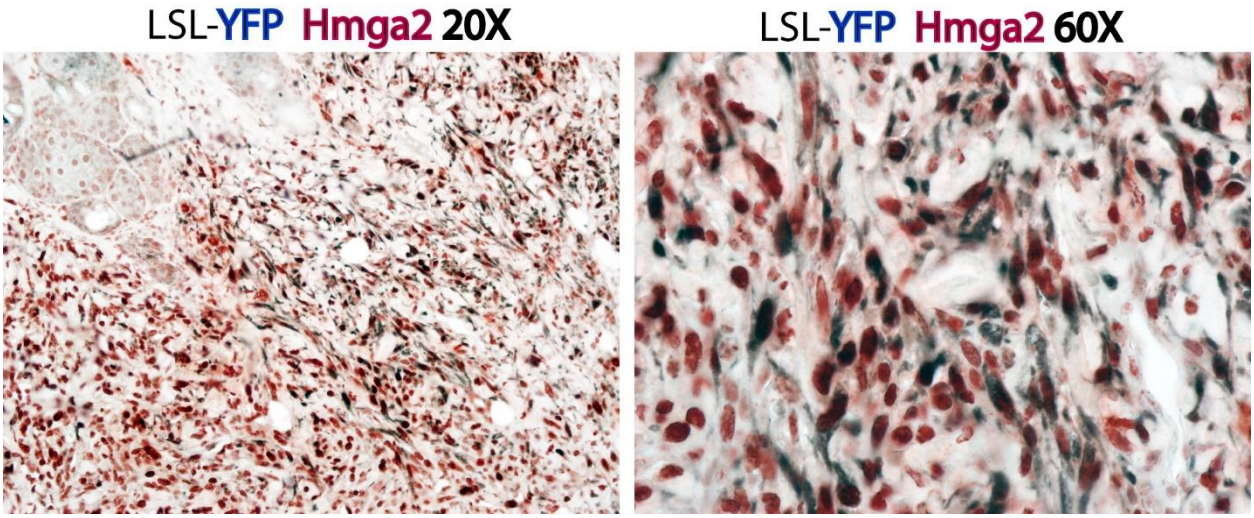

Supplemental Figure 1. Hma2 is expressed in SCC cells that were once a part of the hair follicle Taking advantage of a lineage tracing system to mark cells permanently by Cre recombination, we co-stained sections of tumors with antibodies against GFP and Hmga2. High magnification images show that many Hmga2 cells co-stained with GFP, indicating that they came from K15CrePR+ hair follicle stem cells. Note that Hmga2 is mostly expressed in the nucleus whereas the YFP allele is expressed in the cytoplasm.

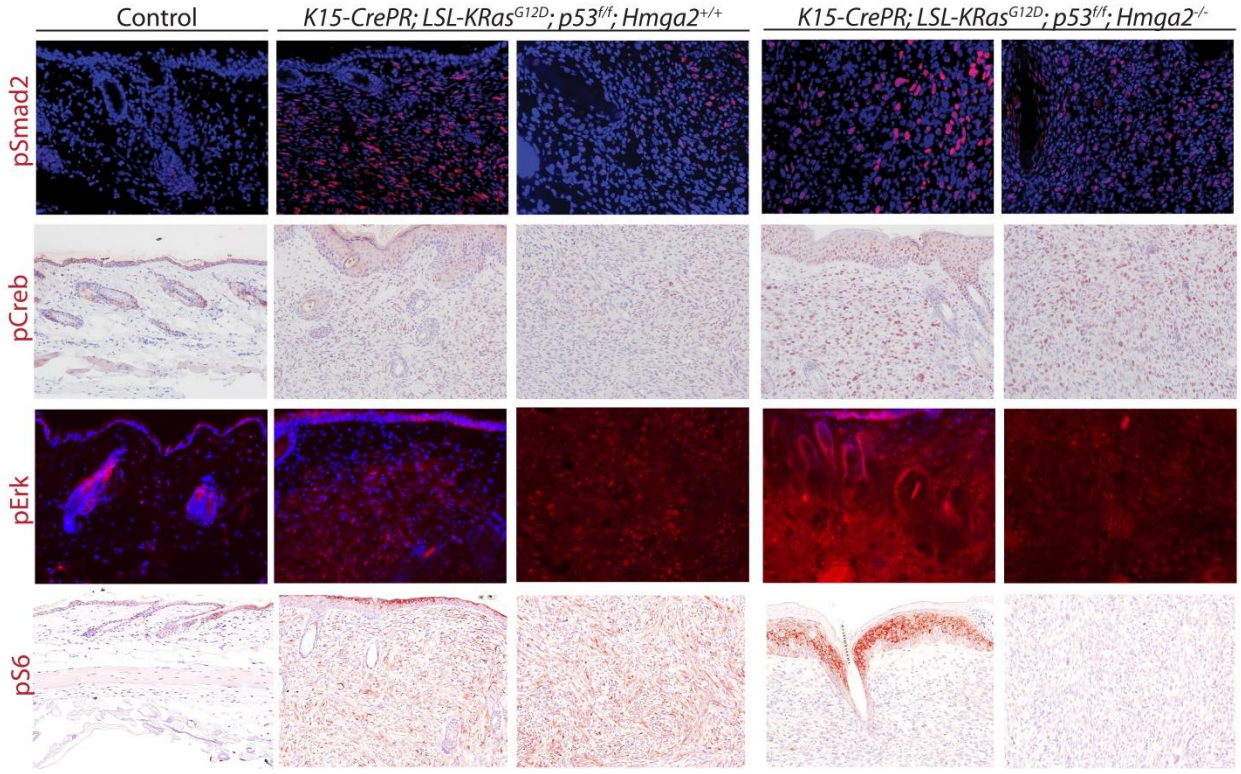

Supplemental Figure 2. Loss of Hmga2 does not affect markers of tumor initiation. Immunostaining on frozen or paraffin embedded tissue with antibodies for markers that are typically induced early in tumorigenesis demonstrated that with or without Hmga2, tumor induction was similar (pSmad2, pCreb, pErk, pS6). Shown are two panels for each marker from both genotypes to indicate the diversity of staining patterns across individual tumors both in the WT and the Hmga2 KO.

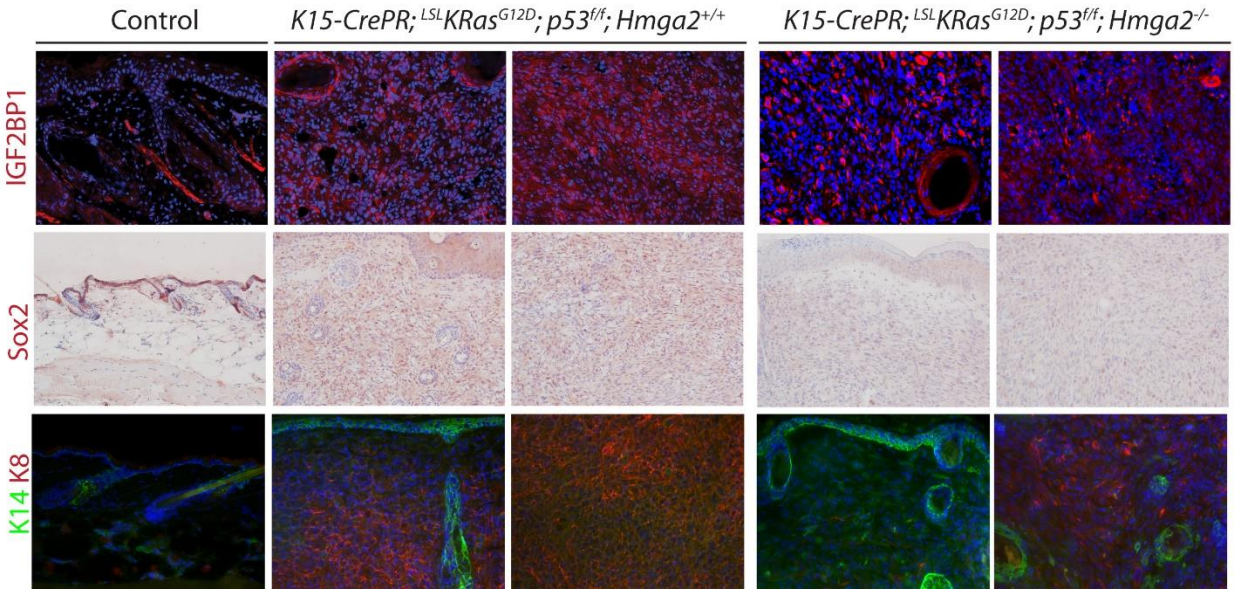

Supplemental Figure 3. Dedifferentiation in the absence of Hmga2. Immunostaining for markers of dedifferentiation shows them all to be induced in SCCs formed by induction of KrasG12D and loss of p53 in the HFSCs (Igf2bp1, Sox2, Krt8), though Sox2 induction appears to be somewhat impaired in the absence of Hmga2.

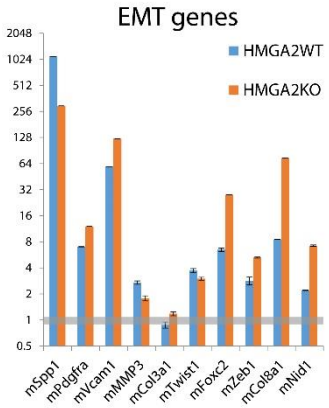

Supplemental Figure 4. Loss of Hmga2 does not affect induction of the EMT program at the RNA level RT-PCR on tumors made in tumors with or without Hmga2 demonstrated that several genes related to EMT were induced in both WT and Hmga2-/- tumors relative to control skin (the gray bar indicates two fold induction over control skin). Note that the results shown are average fold change across two independent samples.

Chapter 4: Tumor suppressor identity can contribute to heterogeneity of phenotype in hair follicle stem cell-induced squamous cell carcinoma

appears to be specific for this DSG isoform because either anti-DSG3 or IgG failed to elicit this effect. This observation is in line with earlier observations on the significance of DSG1 in HaCaT cells (8) and may also imply a specific role for DSG1 in ER stress.

Cell survival assays showed that both anti-DSG1 and anti-DSG3 – albeit at a lesser extent – were inhibitory in HaCaT cells. However, ablation of CHOP expression partially restored cell survival only for anti-DSG1. In view of the role of CHOP in mediating the proapoptotic effects of ER stress, this observation suggests that anti-DSG1-related, but not anti-DSG3-related growth inhibition is associated with UPR induction. The fact that restoration of cell viability by siRNA for CHOP was only partial may reflect the canonical UPR-associated effects and the more wide effects of anti-DSGs in cell viability. Of those, only the former are linked to anti-DSG1 and depend on CHOP, while the latter are inflicted by both anti-DSG1 and anti-DSG3 and appear to be CHOP independent. To that end, a specific association between DSG1 and ER stress induction should be considered.

It is noted that while anti-DSG1 antibodies are not causative for the PV development of mucosal lesions as opposed to the anti-DSG3 antibodies that are present in all cases of PV exhibiting mucosal lesions, their presence, which is detected in about 60% of the cases, has been associated with increased aggressiveness of the disease (9).

A limitation of the current study is that the anti-DSG antibodies used do not simulate all aspects of IgGs from patients with PV. However, they provide hints on the potential association between ER stress and pemphigus. The fact that interference with ER stress induction abrogated, even partially, anti-DSG1-induced growth arrest suggests that modulation of the UPR may provide means for the management of PV.

Acknowledgements

CM, NK, EP and EF performed the research; AS, HK and IC designed the research study; HK and IC analysed the data; CM and IC wrote the manuscript. This study was supported by a grant from Empeirikion Foundation (to IC).

Disclosure statement

The authors have nothing to declare.

Supporting Information

Additional Supporting Information may be found online in the supporting information tab for this article:

Figure S1. Densitometric analysis of the results shown in Fig. 2.

Figure S2. siRNA-mediated silencing of CHOP expression in HaCaT cells protects against during anti-Dsg1 treatment.

Data S1. Specimens, Materials and methods.

References

1 Ruocco V, Ruocco E, Lo Schiavo A *et al.* Clin Dermatol 2013: **31**: 374–381.
2 Spindler V, Waschke J. Cell Commun Adhes 2014: **21**: 77–84.
3 Lanza A, Lanza M, Santoro R *et al.* Br J Dermatol 2011: **164**: 336–343.
4 Oyadomari S, Koizumi A, Takeda K *et al.* J Clin Invest 2002: **109**: 525–532.
5 Mihailidou C, Chatzistamou I, Papavassiliou A G *et al.* Endocr Relat Cancer 2015: **22**: 217–228.
6 Mihailidou C, Chatzistamou I, Papavassiliou A G *et al.* Endocr Relat Cancer 2015: **22**: 229–238.
7 Stanley J R, Koulu L, Klaus-Kovtun V *et al.* J Immunol 1986: **136**: 1227–1230.
8 Waschke J, Bruggeman P, Baumgartner W *et al.* J Clin Invest 2005: **115**: 3157–3165.
9 Harman K E, Gratian M J, Bhogal B S *et al.* Br J Dermatol 2000: **143**: 343–348.

DOI: 10.1111/exd.13037
www.wileyonlinelibrary.com/journal/EXD

Letter to the Editor

Tumor suppressor identity can contribute to heterogeneity of phenotype in hair follicle stem cell-induced squamous cell carcinoma

Aimee Flores[1,2,*], William Grant[1,*], Andrew C. White[3,*], Phillip Scumpia[4], Rie Takahashi[4] and William E. Lowry[1,2,4,5,6]

[1]Molecular Biology Institute, UCLA, Los Angeles, CA, USA; [2]Eli and Edythe Broad Center for Regenerative Medicine, UCLA, Los Angeles, CA, USA; [3]Department of Biomedical Sciences, Cornell University, Ithaca, NY, USA; [4]Department of Dermatology, UCLA, Los Angeles, CA, USA; [5]Department of Molecular Cell and Developmental Biology, UCLA, Los Angeles, CA, USA; [6]Jonsson Comprehensive Cancer Center, UCLA, Los Angeles, CA, USA

Correspondence: William E. Lowry, Department of Molecular Cell and Developmental Biology, UCLA, 621 Charles Young Drive South, Los Angeles, CA 90095, USA, Tel.: 310 794 5175, Fax: 310 794 9323, e-mail: blowry@ucla.edu

**These authors contributed equally.*

Key words: hair follicle stem cells – Ras – squamous cell carcinoma – tumor suppressor

Accepted for publication 6 April 2016

Background

Pathological examination of cutaneous squamous cell carcinoma (cSCC) can identify up to 12 distinct features of this disease (1). An outstanding question in the field is how so many different flavours of cSCC can arise. Direct sequencing of bulk tumors has uncovered generally 10 consistent gain or loss of function mutations common to SCC, with *Ras* and *p53* mutations overrepresented (2). Years of effort have implicated *Hras* and *Kras* mutations in the aetiology of SCC (3–5), and murine models of SCC strongly suggest that *Ras* activation is critical to SCC formation (5). Work from our laboratory demonstrated that hair follicle stem cells (HFSCs) can serve as cells of origin for SCC and that gain of *KrasG12D* mutation and loss of *p53* are sufficient to generate high grade SCC typical of spindle cell carcinoma (6). These results suggest that SCC can be generated by mutations in *Ras* and *p53* in HFSCs, but this particular model does not yield the full spectrum of phenotypes known to be present in human SCC.

Question addressed

We sought to identify sources of tumor heterogeneity by fixing both the cell of origin and the initial oncogenic driver, while altering the identity of the second genomic hit, the tumor suppressor. In doing so, we could identify whether a specific population of cells within the epidermis (HFSCs) has the ability to generate different types of tumors, while also demonstrating the role tumor suppressors play in tumor heterogeneity.

Experimental design

We used mice transgenic for *lox-stop-lox-KrasG12D* to enable Cre recombinase-mediated induction of constitutively active *Ras* expressed from its endogenous locus. These mice were crossed to mice expressing inducible Cre (*Cre-PR*) under control of a promoter active specifically in HFSCs of the skin (*Keratin 15*). Double transgenic mice were then crossed to mice with floxed alleles of either *p53, Rb* or *PTEN* to produce mice that would induce expression of constitutively active *Kras* coupled with loss of a single tumor suppressor only upon treatment with a progesterone antagonist (mifepristone). These experiments have potential clinical relevance as mutations in *KRAS, TP53*, *RB1* and *PTEN* have all been shown to occur in human cutaneous SCC at varying rates (Fig. 1a) (3,7). Mice were allowed to reach adulthood, and Cre-mediated recombination was induced just prior to the second adult hair cycle which is synchronized at postnatal day 50.

Results

Between 8 and 10 weeks following delivery of genetic hits and activation of the hair cycle, tumors became apparent macroscopically. To demonstrate the efficiency of this transgenic system to delete various tumor suppressors, we immunostained each of the targeted tumor suppressors on skin from animals of all genotypes (Fig. 1b). In addition, there were not large differences in the rate of tumor initiation from either the time transgene expression was induced or from the beginning of the next hair cycle (Fig. 1c). This is important, as we previously showed that initiation of phenotype by induction of *KrasG12D* depends on the onset of the telogen-to-anagen transition (8).

Strikingly, we observed a profound difference in the type of squamous tumors formed between the animals with different deletions of tumor suppressors (Figs 1d and S1). While we ideally would look to human SCC samples for a similar correlation,

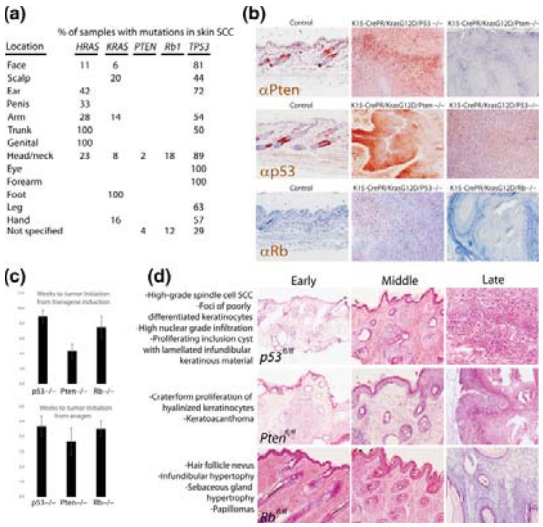

Figure 1. Hair follicle stem cells can drive different phenotypes in SCC depending on tumor suppressor identity. (a) Using data from the COSMIC database, the percentage of tumors with mutations in the genes described here are shown. These data are for SCCs from the indicated locations on the body. (b) Immunostaining with the indicated antibodies showed that transgenic deletion of each tumor suppressor was successful as shown in the resulting tumors. (c) Quantification of the time to visible tumor induction across different genotypes, either from the time in which the transgene was activated (by administration of mifepristone) (Top panel) or the time from the subsequent anagen initiation (Bottom panel). (d) Animals of the indicated genotype were induced to drive expression of oncogenic *Ras* or ablate a tumor suppressor, and phenotypes were allowed to develop. Representative images of some phenotypes are shown, and complete blinded pathological diagnoses were made based on a large number of animals analysed (Figure S1).

mutations in some of the genes examined here are rare in human SCC (Fig. 1a), and human SCC is thought to derive from the interfollicular epidermis, not the hair, precluding simple identification of a similar correlation in human.

As described previously (8), *K15CrePR;KrasG12D;p53fl/fl* mice developed significant phenotypes and eventually progressed to high grade SCC ($n > 15$) (Fig. 1d). In mice where *PTEN* was deleted instead of *p53* (*K15CrePR;KrasG12D;Ptenfl/fl*), hyperplasia developed over a similar time course but did not progress to the point of SCC within 15 weeks after induction (the time by which all animals had to be sacrificed due to tumor/phenotype burden) ($n = 6$) (8). Deletion of *PTEN* along with induction of oncogenic *Kras* led to a different type of squamous hyperplasia (Figure S1). While we previously characterized phenotypes of *K15CrePR; KrasG12D;p53fl/fl* mice (6,8), we provide a more complete description of phenotypes in *K15CrePR;KrasG12D;Ptenfl/fl* and *K15CrePR;KrasG12D;Rbfl/fl* mice in Figure S2.

In *K15CrePR;KrasG12D;Rbfl/fl* mice, the hyperplasia generated appeared to move upwards towards the infundibulum and the interfollicular epidermis ($n = 4$). This hyperplasia also did not progress to the point of *bona fide* SCC, but instead produced benign papilloma (Figs 1d and S3). In summary, when controlling for the cell of origin and the initial oncogenic stimulus, the identity of the tumor suppressor appeared to be significantly related to the type of squamous phenotype that developed.

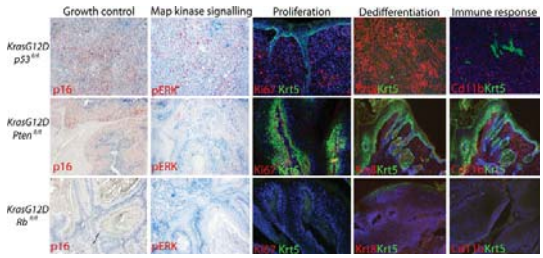

Figure 2. Tumor suppressor deletion correlates with distinct phenotypes in regard to proliferation, dedifferentiation and immune response. Immunostaining for Ki67, a marker of proliferation, showed that tumors made in the absence of *p53* or *PTEN* continue to proliferate, whereas those made in the absence of *Rb* show little proliferation once fully formed**.** Immunostaining for p16 showed that only tumors deleted for p53 or *PTEN* showed induction of this Cdk inhibitor. Staining for phospho-ERK marks cells with active map kinase signalling in tumors lacking *p53*. Keratin 8 is only expressed in adult epidermal cells upon dedifferentiation and tumorigenesis. Only tumors with deletion of p53 progressed enough to show expression of Keratin 8. Myeloid-derived suppressor cells (MDSCs) are known to facilitate tumor progression by suppressor inhibitory signals during tumorigenesis. Staining for MDSCs with Cd11b showed that only tumors with deletion of *p53* or *PTEN* recruited these immune cells. These same tumors also stained positively for Gr-1, another marker of MDSCs (not shown).

To characterize the phenotypic disparity between the genotypes tested, we assessed proliferation, growth control, MAP kinase signalling, dedifferentiation and immune response in each genotype. Staining for Ki67 showed that tumors without *p53* or *PTEN* had extensive proliferation, whereas those made without *Rb* had significantly less proliferation once the tumors were formed. Coincident with this, staining for p16, a protein known to be induced where growth control is needed, was induced in tumors without *p53* and *PTEN*, but less so in tumors lacking *Rb*. In addition, staining for phospho-Erk, a marker of activated MAP kinase signalling, showed significant activity only in tumors lacking *p53*. Keratin 8 is only expressed in postnatal keratinocytes upon dedifferentiation to SCC. Staining for Keratin 8 across the various genotypes presented demonstrated that only mice with deletion of *p53* showed significant dedifferentiation (Fig. 2).

The skin is highly sensitive to inflammation, and numerous inflammatory cells migrate to the skin in cases of wounding, infection or tumorigenesis. Myeloid-derived suppressor cells (MDSCs) are thought to suppress proliferation and contain tumor growth (9). MDSCs are defined by immunostaining with antibodies for Gr1 and Cd11b. Attempts to identify MDSCs with these markers only reliably uncovered them in tumors formed from *K15CrePR; KrasG12D;p53fl/fl* mice (Fig. 2). To further characterize the immune response in tumors generated by loss of various tumor suppressors, we performed a complete pathological examination of immune cells present in the tumors characterized in Figure S1 (Figure S4).

Summary

While some driver mutations have been identified consistently across SCCs, it is unclear whether the heterogeneity of phenotypes is due to variability across mutations, cell of origin, immune response or variable genomic instability. Our data show that HFSCs can drive a variety of SCC phenotypes that correlate strictly with the type of tumor suppressor deleted.

Acknowledgements

This work was supported by NIH (5R01AR057409-05 and TCBT32CA09056), a CIRM Training Grant (TG2-01169), a fellowship from the Broad Center for Regenerative Medicine (UCLA, AF), MARC program (UCLA, WG).

Author contributions

AF, WG, ACW, PS and RT performed the research and analysed the data. WL wrote the manuscript.

Conflict of interests

The authors have declared no conflicting interests.

Supporting Information

Additional Supporting Information may be found online in the supporting information tab for this article:

Figure S1. Blinded pathological analysis of tumor phenotype across different genotypes.

Figure S2. Phenotypic characteristics of KrasG12D/Pten mutant backskin.

Figure S3. Phenotypic characteristics of KrasG12D/Rb mutant backskin.

Figure S4. Pathological examination of immune cells in tumor models.

Appendix S1. Materials and Methods.

References

1 Rapini R P. Practical dermatopathology. Philadelphia: Elsevier Mosby, 2005.

2 Agrawal N, Frederick M J, Pickering C R *et al.* Science 2011: **333**: 1154–1157.

3 Pickering C R, Zhou J H, Lee J J *et al.* Clin Cancer Res 2014: **20**: 6582–6592.

4 Pierceall W E, Goldberg L H, Tainsky M A *et al.* Mol Carcinog 1991: **4**: 196–202.

5 van der Schroeff J G, Evers L M, Boot A J *et al.* J Invest Dermatol 1990: **94**: 423–425.

6 White A C, Tran K, Khuu J *et al.* Proc Natl Acad Sci U S A 2011: **108**: 7425–7430.

7 Nassar D, Latil M, Boeckx B *et al.* Nat Med 2015: **21**: 946–954.

8 White A C, Khuu J K, Dang C Y *et al.* Nat Cell Biol 2014: **16**: 99–107.

9 Husain Z, Huang Y, Seth P *et al.* J Immunol 2013: **191**: 1486–1495.

Materials and Methods

Animals

Animals were housed and treated according to protocols approved by DLAM (UCLA) and IACUC. KRasG12D (Jax 008179, K15-CrePR (Jax 005249), lsl-YFP (Jax 006148), p53fl/fl (NCI 01XC2), Ptenfl/fl (Jax 006440) and Rb1fl/fl (NCI 01XC1) mice were acquired from Jackson Labs and the NCI Mouse Repository and described previously(9, 10). For tumor modeling, KrasG12D expression and deletion of p53, Rb1 or Pten were instigated by injection with Mifepristone solubilized in sunflower seed oil and delivered by intraperitoneal injection at 7 weeks of age, when the hair cycle is synchronized across the backskin in telogen.

Histology and Immunostaining

Tumorand control tissues were isolated from the indicated genotypes and embedded fresh in OCT for frozen tissue preparations, or fixed overnight in 4% formalin and embedded in paraffin. For frozen tissue, sectioning was performed on a Leica 3200 Cryostat, and fixed for 5-10 min in 4% paraformaldehyde. Paraffin embedded tissue was sectioned, de-paraffinzed, and prepared for histology. All sections prepared for staining were blocked in staining buffer containing appropriate control IgG (Goat, Rabbit etc.). Images were collected on either a Zeiss A2 upright microscope (immunofluorescence) or Olympus upright microscope (immunohistochemistry). All images presented used a 20X objective.

Genotype	sample name	High-grade SCC (*spindle cell)	Low-grade SCC and/or keratoacanthoma	Focal or diffuse sebaceous differentiation	Verrucous/ papilloma	Trichilemomma-like	Proliferative infundibular cyst	Epidermal adnexal hyperplasia
K15CrePR, KrasG12D, P53 fl/fl, Yfp +/+	553/fvb25 Dtum2 15q534 (1/29/	yes *	no	yes	no	no	no	yes
K15CrePR, KrasG12D, P53 fl/fl, Yfp +/+	553/fvb D15 15q534 (2/6/14)	no	no	yes	no	no	no	yes
K15CrePR, KrasG12D, P53 fl/fl, Yfp +/+	1292 Vtum D 07/21/14	yes *	no	no	no	no	no	no
K15CrePR, KrasG12D, P53 fl/fl, Yfp +/+	1292 D 07/21/14	no	no	no	no	no	no	yes
K15CrePR, KrasG12D, P53 fl/fl, Yfp +/+	553 Dtum 01/29/14	yes	yes	no	no	no	no	no
K15CrePR, KrasG12D, P53 fl/fl, Yfp +/+	553 D 02/6/14	no	no	no	no	no	no	yes
K15CrePR, KrasG12D, P53 fl/fl, Yfp +/+	3404 V Tum 08/12/10	yes	no	no	no	no	no	yes
K15CrePR, KrasG12D, P53 fl/fl, Yfp +/+	3404 Cgff Vtum 07/08/10	yes *	no	yes	no	no	no	yes
K15CrePR, KrasG12D, P53 fl/fl, Yfp +/+	3404/05 Ftum 07/15/10	yes	no	no	no	no	no	yes
K15CrePR, KrasG12D, P53 fl/fl, Yfp +/+	3404/05 Ftum1 08/12/10	yes	yes	yes	no	no	no	yes
K15CrePR, KrasG12D, P53 fl/fl, Yfp +/+	3388/93 V 08/06/10	no	yes	no	no	no	no	yes
K15CrePR, KrasG12D, P53 fl/fl, Yfp +/+	3393 Vtum1 5/25 (2 tumors)	yes	yes	no	no	no	no	yes
K15CrePR, KrasG12D, Pten fl/fl, Yfp +/+	6958/9 Ftum 06/09/11	no	no	no	yes	yes	no	yes
K15CrePR, KrasG12D, Pten fl/fl, Yfp +/+	6958/9 Htum 06/09/11	no	yes	no	yes	yes	no	yes
K15CrePR, KrasG12D, Pten fl/fl, Yfp +/+	6958/9 D 06/09/11	no	no	no	no	no	no	yes
K15CrePR, KrasG12D, Pten fl/fl, Yfp +/+	7321/2 Ftum 09/19/11	no	no	no	yes	yes	yes	yes
K15CrePR, KrasG12D, Pten fl/fl, Yfp +/+	7321/2 D 09/12/11	no	no	no	no	no	no	yes
K15CrePR, KrasG12D, Pten fl/fl, Yfp +/+	7321/2 D 09/12/11 (one piece w	no	yes	no	yes	yes	yes	yes
K15CrePR, KrasG12D, Pten fl/fl, Yfp +/+	8501 D cgffwy 25 5/17/12	no	yes	no	no	no	no	yes
K15CrePR, KrasG12D, Pten fl/fl, Yfp +/+	8501 V cgffwy 5 5/17/12	no	yes	no	no	no	no	yes
K15CrePR, KrasG12D, Rb fl/fl, Yfp +/+	1620/21 Dtum 01/08/10	no	no	yes	no	no	yes	yes
K15CrePR, KrasG12D, Rb fl/fl, Yfp +/+	1620/21 15gRb D 20 1/8/10	no	no	yes	no	no	no	yes
K15CrePR, KrasG12D, Rb fl/fl, Yfp +/+	1620/21 D 01/08/10	no	no	no	yes	no	yes	yes
K15CrePR, KrasG12D, Rb fl/fl, Yfp +/+	2475/79 D 01/18/10	no	no	yes	yes	no	no	yes
K15CrePR, KrasG12D, Rb fl/fl, Yfp +/+	2475/79 Vtum 01/18/10	no	no	yes	yes	no	no	yes
K15CrePR, KrasG12D, Rb fl/fl, Yfp +/+	6215/fvb15 15gRb (3/28/11)	no	no	no	no	no	no	yes

definition of pathological terminology

High-grade squamous cell carcinoma Tumors are composed of a proliferation of poorly differentiated keratinocytes with minimal evidence of keratinization, and infiltrate deeply into the dermis and subcutis. Constituent cells are pleomorphic, with a high nuclear to cytoplasmic ratio, and demonstrate numerous mitoses. In certain tumors a considerable portion of cells have attained a spindled cell morphology.

Low-grade squamous cell carcinoma Tumors are fairly-well circumscribed exo-endophytic, and in some cases crateriform, proliferations of moderately to well differentiated keratinocytes with keratin whorl formation. Tumors are minimally invasive at the edges or the base of the lesion. Constituent cells have a "glassy" cytoplasm and demonstrate minimal nuclear pleomorphism.

Sebaceous differentiation Foci within tumors display evidence of sebocytic differentiation including large amount of clear cytoplasm, and scalloped, centrally placed nuclei. In some cases, tumor cells directly infiltrate into the dermis from sebaceous glands.

Verrucous/papilloma Tumors consist of a papillomatous, exophytic growth of squamous keratinocytes with some dyskeratosis and mild koilocytosis of cells within the granular layer.

Trichilemmoma-like Tumors consist of a slightly endophytic growth of keratinocytes displaying trichilemmal differentiation. Basilar keratinocytes display peripheral palisading and suprabasilar keratinocytes display a clear cytoplasm. Tumors are not infiltrative. In some cases, tumors feature a trichilemmoma-like structure at the surface with a proliferative infundibular cyst within the dermis.

Proliferative infundibular/epidermal inclusion cyst A large cystic structure with filled with lamellated, loose infundibular type keratin is seen in the dermis. The cyst lining cells are proliferative and cyst walls are greater than 10 cells thick. There are buds of keratinocytes extending from beyond the cyst wall structure into the dermis.

Epidermal and adnexal hyperplasia Epidermis displays acanthosis, and dermis displays hyperplasia compared to normal mouse skin. There are increased hair follicle structures with hypertrophy of sebaceous glands. In some cases, the hyperplasia could be consistent with a hair follicle nevus where 15-20 disorganized hair follicle structures can be seen along with hypertrophic sebaceous glands within a 10-15υm area.

Fig S1. Blinded pathological analysis of tumor phenotype across different genotypes **Top**, the results of blinded examination of various aspects of tumor phenotype and the resulting correlation to genotype. **Bottom**, a description of the criteria used to label phenotypes.

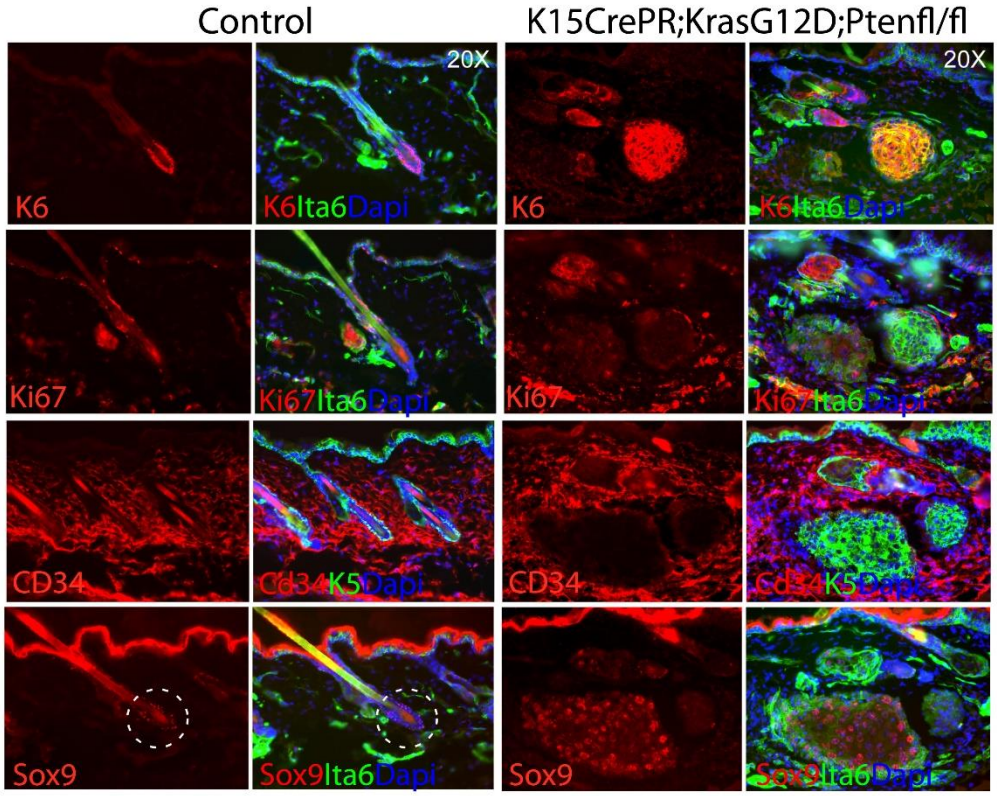

Fig S2 Phenotypic characteristics of KrasG12D/Pten mutant backskin Left, control tissue shows staining for K6 (inner root sheath and hyperplastic epidermis), Ki67 (proliferation), CD34 (HFSC and fibroblast marker), and Sox9 (HFSC marker). **Right**, In phenotypic tissue due to gain of KrasG12D and loss of Pten, immunostaining shows hyperplastic cysts (K6), cystic proliferation (Ki67), and expansion of a HFSC marker (Sox9).

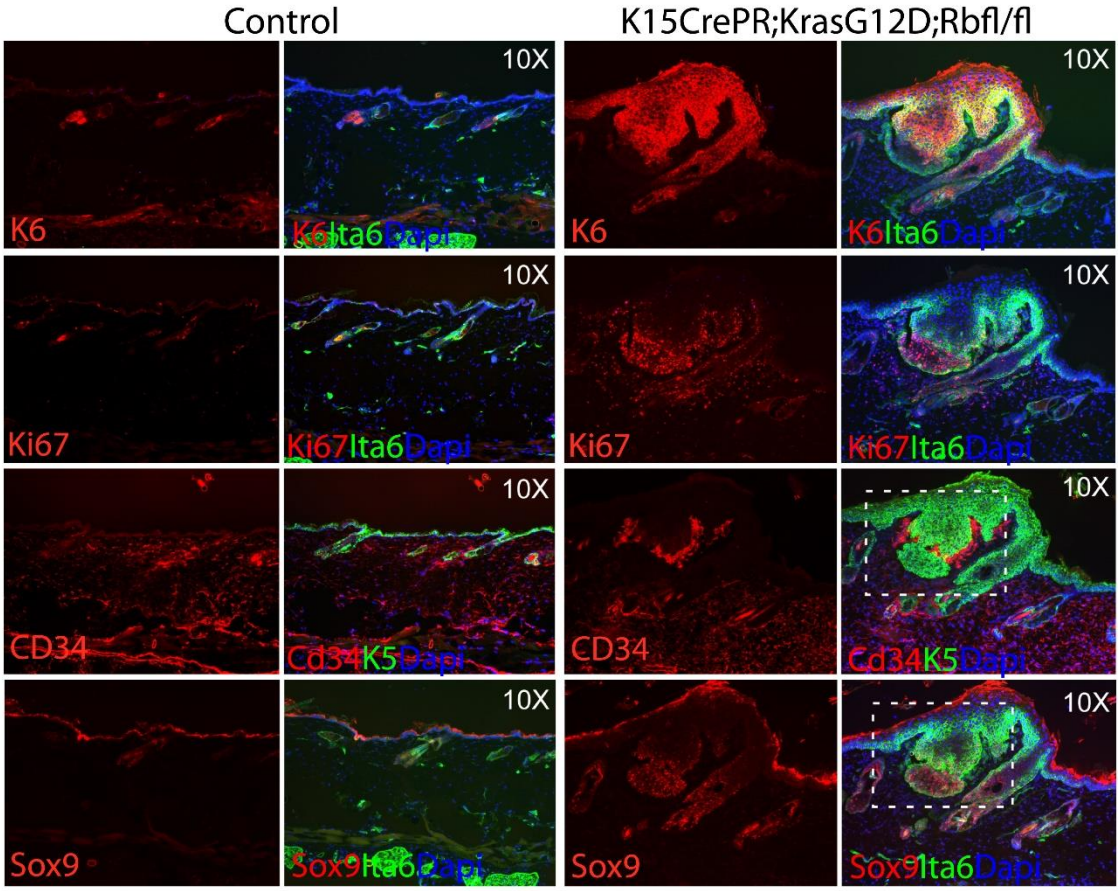

Fig S3 Phenotypic characteristics of KrasG12D/Rb mutant backskin Left, control tissue shows staining for K6 (inner root sheath and hyperplastic epidermis), Ki67 (proliferation), CD34 (HFSC and fibroblast marker), and Sox9 (HFSC marker). **Right**, In phenotypic tissue due to gain of KrasG12D and loss of Pten, immunostaining shows hyperplastic papilloma formation (K6), papilloma proliferation (Ki67), and expansion of a HFSC marker (Sox9).

Genotype	sample name	Myeloid		Myeloid/Monocytic		Lymphoid	
		Neutrophils	Histiocytes	Eosinophils	Multinucleated giant cells	Plasma Cells	Lymphocytes
K15Cre; KrasG12D; p53 fl/fl; Yfp -/-	f3393 25 cgt cww/15g53y vtum	X				X	X
K15Cre; KrasG12D; p53 fl/fl; Yfp -/-	3388/93 Ntum H&E 8/11/10		X			X	X
K15Cre; KrasG12D; p53 fl/fl; Yfp -/-	f3388/93 12 cgffwy/15g53y v H&E 8/6/10	X	X		X	X	X
K15Cre; KrasG12D; p53 fl/fl; Yfp -/-	3404/5 Ftum1 H&E 8/12/10	X	X	X	X	X	X
K15Cre; KrasG12D; p53 fl/fl; Yfp -/-	m3404/05 15 15g534 Ftum1 H&E 7/15/10	X	X		X	X	X
K15Cre; KrasG12D; p53 fl/fl; Yfp -/-	m3404 cgffwy/15g53y vtum H&E 7/8/10	X	X			X	X
K15Cre; KrasG12D; p53 fl/fl; Yfp -/-	3404/5 vtum H&E 8/12/10		X			X	X
K15Cre; KrasG12D; p53 fl/fl; Yfp +/+	553/fvb D25 2/6/14 25	X	X				X
K15Cre; KrasG12D; p53 fl/fl; Yfp +/+	553/fvb 15g53y Dtum1 H&E 1/29/14	X	X		X		X
K15Cre; KrasG12D; p53 fl/fl; Yfp +/-	1292 D 15g53yEC H&E 7/21/14		X				X
K15Cre; KrasG12D; p53 fl/fl; Yfp +/-	1292 vtum 15g53yEC H&E 7/21/14	X	X		X	X	X
K15Cre; KrasG12D; Pten fl/fl; Yfp +/-	7009/10D 15 H&E 1/25/12	X	X				X
K15Cre; KrasG12D; Pten fl/fl; Yfp +/-	7321/2 Df 15 H&E 15gpty 9/12/11		X			X	
K15Cre; KrasG12D; Pten fl/fl; Yfp +/-	7321/2 25 Ftumf H&E 9/19/11		X				X
K15Cre; KrasG12D; Pten fl/fl; Yfp -/-	f6958/9 15 15gpt H&E 6/9/11		X			X	
K15Cre; KrasG12D; Pten fl/fl; Yfp -/-	f6958/9 15 15gpt Htum H&E 6/9/11		X	X		X	X
K15Cre; KrasG12D; Pten fl/fl; Yfp -/-	f6958/9 15 15gpt Ftum1 H&E 6/9/11	X	X			X	X
K15Cre; KrasG12D; Rb fl/fl; Yfp +/-	2475/79 30 15yRby/vtum H&E-1/15/10	X	X			X	
K15Cre; KrasG12D; Rb fl/fl; Yfp +/-	2475/79 15yRby1Dskh1 H&E 1/18/10		X				X
K15Cre; KrasG12D; Rb fl/fl; Yfp +/+	1620/21 40 15gRb H&E 1/8/10	X	X	X			X
K15Cre; KrasG12D; Rb fl/fl; Yfp +/+	1620/21 18 15gRb Dtum 20uM H&E 1/8/10		X	X			

Fig S4 Pathological examination of immune cells in tumor models

Blinded pathological examination of immune cells across tumors of various genotypes indicated that several types of immune responses could be detected in all genotypes. The only distinguishing feature was the presence of multinucleated giant cells only in tumors lacking p53.

Chapter 5: Increased lactate dehydrogenase activity is dispensable in squamous carcinoma cells of origin

Increased lactate dehydrogenase activity is dispensable in squamous carcinoma cells of origin

Flores A[1,5], Sandoval-Gonzalez S,[1] Takahashi R[3], Sathe L[1], Wei L[7], Radu C[7], Jolly J[8], Graham N[8], Christofk H[6@], and Lowry WE[1,2,3,4,5@]

1, Department of Molecular Cell and Developmental Biology, UCLA
2, Jonsson Comprehensive Cancer Center, UCLA
3, Division of Dermatology, David Geffen School of Medicine, UCLA
4, Broad Center for Regenerative Medicine, UCLA
5, Molecular Biology Institute, UCLA
6, Department of Biological Chemistry, UCLA
7, Department of Pharmacology, UCLA
8, Department of Engineering, USC

@To whom correspondence should be addressed:

William Lowry
621 Charles Young Drive South
Los Angeles, CA 90095
blowry@ucla.edu
3107945175

Heather Christofk
621 Charles Young Drive South
Los Angeles, CA 90095
HChristofk@mednet.ucla.edu
3107944882

Abstract

Decades of experimentation have suggested that tumors acquire an increased ability to use the glucose utilization pathway to create lactate, even in the presence of oxygen, a process called aerobic glycolysis first discovered by Otto Warburg. This has led to significant efforts to inhibit aerobic glycolysis to inhibit tumor formation or progression, however, these efforts have not yet led to effective clinical strategies. Murine squamous cell carcinoma (SCC) can be initiated by hair follicle stem cells (HFSCs) through induction of active Kras and loss of p53. In addition, HFSCs are now known to use glucose to make more lactate than other cell types in the epidermis, and the activity of lactate dehydrogenase (Ldh) acts to promote HFSC activation. Therefore, we sought to determine whether Ldh activity in SCC tumors is a marker of the cell type from which these cells arise, or a key metabolic activity important for tumor initiation or progression. Here we show that genetic abrogation of Ldh enzyme activity in HFSC-mediated tumorigenesis had no effect on tumor number, time to tumor formation, tumor proliferation, epithelial to mesenchymal transition in tumors, gene expression in tumors, tumor pathology, or the immune response to tumors. Ldha-null tumors showed dramatically reduced levels of most glycolytic metabolites by metabolomics, and significantly reduced glucose uptake as measured by Positron Emission Tomography live animal imaging (FDG-PET). Finally, neither deletion of Ldha in existing tumors nor genetic induction of Ldh activity had an effect on tumor initiation or progression. These surprising results suggest that squamous cancer cells of origin do not require increased glycolytic activity to generate cancers.

Introduction

As tumors begin and grow, cells within them strive to grow without restraint. It is thought that to support this proliferation, cells adopt distinct modes of gene expression, signaling and metabolism. Originally described by Otto Warburg, tumors are known to increase their uptake and utilization of glucose to power the production of essential metabolites and cell products required for proliferation[1-3]. Nearly all tumors described display an increased propensity to stimulate a conversion of glucose to lactate through glycolysis ending with conversion of pyruvate to lactate by Lactate Dehydrogenase[3-6]. Lactate was once considered a waste product of glycolysis, but inhibition of lactate production by blocking Ldh activity has been shown to have some effect on the growth of tumor cells[7, 8]. Others have argued that lactate production is the purpose of the Warburg effect as Lactate plays roles in angiogenesis, immune response, acidification of the microenvironment, motility of cancer cells, and the production of NAD+ [5, 9, 10]. So despite decades of research in this area, it is still not clear whether the increased utilization of glucose to produce lactate is necessary for tumor initiation or progression, or just a by-product of altered metabolism.

In fact, while there is a mountain of data suggesting that Lactate production is important for cancer cell growth *in vitro* and in *ex vivo* models[11-14], there is much less evidence from *in vivo* models to demonstrate that lactate production is important for tumor initiation or progression. One study that used a model of lung carcinoma driven by oncogenic Ras coupled with deletion of Ldha showed a regression of tumors, suggesting a requirement of Ldh activity for maintenance of tumor cells[11]. In that model, the Ldh activity was abrogated in the entire tissue, which left uncertain the role of glycolytic activity specifically in cancer cells of origin.

Here we use a model of cutaneous SCC to model tumor formation and progression from hair follicle stem cells (HFSCs). HFSCs have been shown to be cancer cells of origin for SCC[15], and have also been demonstrated to show a high level of glycolytic activity during homeostatic conditions[16]. This model is inducible through administration of mifepristone or tamoxifen to mediate Cre recombination in HFSCs. Because increased glycolytic activity is now known to be a hallmark of even quiescent HFSCs[16], and HFSCs are cells of origin for SCCs[15], we sought to determine whether perhaps SCC tumors are glycolytic simply because they were initiated by HFSCs. If true, this hypothesis would suggest that at least in some tumors, perhaps the glycolytic nature associated with the Warburg effect is simply an expansion of the phenotype of the cell of origin and potentially not a requirement for tumorigenesis.

Results

To determine whether lactate production is a hallmark of cutaneous squamous cell carcinoma, we measured lactate production and lactate levels with an *in situ* enzymatic assay and metabolomics in a murine model of Squamous Cell Carcinoma (SCC) driven by gain of oncogenic Ras coupled with loss of p53 activity[15]. K15CrePR or Lgr5CreER can both be used to target transgene expression to HFSCs[17, 18]. We and others used these previously to show that delivery of KrasG12D coupled with loss of p53 can generate squamous cell carcinoma from HFSCs.

Here, we show that in normal skin, the HFSC niche is high in Ldh activity[16], and that this activity is also quite apparent even in very early stage tumorigenesis driven by oncogenic stimulation of HFSCs. In fact, we typically characterize squamous tumors in the following categories starting with hyperplasia, then papilloma/keratoacanthoma stage, and finally high grade undifferentiated squamous carcinoma. The activity of Ldh appeared by *in situ* activity assay to peak at the

papilloma/keratoacanthoma stage, and decreased somewhat in high grade tumors, while still remaining higher than in normal skin (Fig 1a). For a more quantitative measure, we isolated tissue at various stages and performed a plate-reader assay for Ldh activity, which confirmed our *in situ* observations (Fig 1b).

As a comprehensive measure of glycolytic activity, we also performed metabolomics on cells from tissue taken from the various stages of tumorigenesis. This analysis showed that as the skin became filled with tumorigenic cells, the levels of most glycolytic metabolites increased dramatically, particularly lactate (Fig 1c). We also performed glucose tracing experiments where animals with tumors at various stages were pulsed with $^{13}Carbon_6$-glucose to follow the conversion of glucose to various metabolites. These analyses also demonstrated that, compared to normal skin, the conversion of glucose to lactate was strongly induced as SCC initiated and progressed. Interestingly, the peak of lactate production appeared to be in the earlier stages of tumor development, and dropped off somewhat in high grade tumors (Fig 1d).

Finally, we measured gene expression changes in HFSCs as they proceed through various stages of tumorigenesis. As expected from Flores et al, Ldha expression was high in normal HFSCs, and stayed high during tumorigenesis (Supplemental Fig 1). The expression of other glycolytic enzymes, such as Pgm, HK, Pgk, Pkm2, and Eno, appeared to be further increased during tumorigenesis. Furthermore, the transcriptome data appeared to demonstrate that transporters for Lactate, Pyruvate, Glucose and Glutamine were all upregulated, as has been described for other tumors where glycolytic metabolism is induced. These data suggested that despite a relatively high glycolytic rate in HFSCs under homeostatic conditions[16], the glycolytic

rate could still be further induced in a Warburg-like manner. However, none of these measures indicated whether lactate production in HFSCs is important for their ability to generate a tumor.

Previously, we showed that inducible deletion of Ldha with either K15CrePR- or Lgr5CreER-mediated recombination effectively abrogated lactate production in HFSCs[15, 16, 19]. To determine whether the induction of lactate production is required for squamous cell carcinoma initiated by HFSCs, we coupled this system with conditional deletion of p53 and activation of constitutively active Kras (LSL-KrasG12D) to stimulate tumorigenesis in HFSCs while also deleting their ability to produce lactate from pyruvate.

Based on numerous observations linking glycolysis and lactate production to tumorigenesis, we expected that loss of Ldh activity would abrogate tumor formation. However, tumor formation resulting from expression of KRasG12D coupled with loss of p53 in HFSCs was not affected by loss of Ldha (Fig 2a). Quantification of tumorigenesis showed that neither the timing nor number of tumors formed was affected by loss of Ldha (Fig 2b). Deletion of Ldha was validated by western blotting (Fig 2c). To validate these results, we induced oncogenesis by a distinct HFSC-specific Cre (Lgr5CreER), but this also showed no difference in tumorigenesis (Fig 2d). Finally, we induced tumorigenesis in the skin through DMBA/TPA administration, a classical SCC paradigm, but in this context loss of Ldha also had no effect on tumorigenesis (Fig 2b). By stringent pathological analysis, tumors expressing Ldha showed hallmarks of spindle cell proliferation, papillomatous papulae, infiltration etc, and tumors lacking Ldha were not distinguished pathologically (Fig 2d). Because it has been suggested that lactate made by cancer cells can affect immune cells, we explored the possibility that tumors could elicit distinct immune responses

depending on their expression of Ldha (Fig 2e). Again, we were unable to detect a distinct pattern of immune response in the absence of Ldh activity.

To more deeply probe the potential effect of loss of Ldh on tumorigenesis, we measured proliferation, Epithelial to Mesenchymal transition (EMT), markers of HFSC fate, and total gene expression (Supplemental Fig 2). Staining for Ki67 to measure proliferation did not identify any significant difference between tumors that express or lack Ldha. Epithelial cells express keratins such as keratin 14, whereas mesenchymal cells express markers such as fibronectin and tenascin C. Staining for markers of EMT showed that all tumors upregulated mesenchymal markers and downregulated epithelial markers, regardless of Ldha status. HFSCs are well-established to express markers such as CD34 and Sox9 (as well as secrete Tnc)[20-22]. Immunostaining for these HFSC markers showed that tumors generated from HFSCs do indeed continue to express Sox9 and CD34, and that this is not affected by loss of Ldha. These data are consistent with the notion that perhaps high Ldh activity in SCC tumors is simply a reflection of the fact that the cells that initiate them (HFSCs) show this same activity, and is therefore a marker of the cell of origin as opposed to a driver of tumor formation.

Finally, to identify any molecular changes in tumors due to loss of Ldha, we performed RNA-seq on six tumors that express Ldha versus six that were deleted for Ldha. Following normalization, stringent analysis failed to detect significant gene expression changes associated with loss of Ldha. In particular, we examined the same genes described to be induced during SCC generation from HFSCs (Supplemental Fig 1), and found that none of these genes or pathways were distinctly different in tumors formed in the absence of Ldh activity (Supplemental Fig 2).

One explanation for the lack of effect of loss of Ldha on tumor formation could be that another Ldh isoform (Ldhb, Ldhc or Ldhd) was able to compensate for the loss. To determine whether Ldha-null tumors had indeed lost enzyme activity, we assayed for the activity with several independent methods. First, we used an *in situ* activity assay to identify tumors or areas within tumors that show Ldh activity. All tumors genotypically positive for Ldha showed robust Ldh activity (Fig 3a). Amongst the Ldha-null tumors, most had completely lost Ldh activity in this assay, while some showed mosaic activity, presumably due to the inducible method of Cre recombination employed. There was no significant difference in appearance between the tumors that had full activity, lacked activity or were mosaic for Ldh activity (Fig 3a). Second, we isolated tumor material and performed a plate reader assay for Ldh activity. This method also showed that Ldha-null tumors lacked Ldh activity (Fig 3b). Third, we used metabolomics to measure the relative level of lactate in all the tumors analyzed. This analysis showed that lactate and most of the other glycolytic metabolites were dramatically lower in Ldha-null tumors (Fig 3c). In addition, the NAD+/NADH ratio was reduced in Ldha-null tumors, consistent with decreased oxidation of NADH to NAD+ (Fig 3d). Finally, we also injected animals prior to sacrifice with U13C-labeled glucose to measure glucose utilization. Again, the level of glucose conversion to lactate was dramatically lower in Ldha-null tumors (Fig 3e). Together, these data strongly suggest that the tumors formed in genotypically null mice in fact lost Ldh activity due to the deletion of the Ldha gene, and that none of the other Ldh isoforms (b, c, d) could compensate for the loss of Ldha.

The metabolomic data suggest that during tumor formation, if Ldh activity is deleted, production of most of the glycolytic metabolites was also abrogated. To determine whether loss of Ldha led to decreased uptake of glucose in tumors, we performed glucose tracing at the organismal level. FDG is a glucose analogue that can be detected by Positron Emission Tomography (PET) imaging[5, 23, 24]. Prior to sacrifice, animals of various genotypes were injected with FDG and

imaged by PET. Tumors are known to be highly glycolytic and take up significantly more FDG than normal tissue, and this was observed in all tumors expressing Ldha (Fig 4a). On the other hand, tumors null for Ldha, showed significantly less glucose uptake. This was the case in both tumors induced by KrasG12D/loss of p53, as well as tumors generated by DMBA/TPA (Fig 4b). These data indicate that tumors unable to process the last step of glucose utilization somehow abrogate their glucose uptake in response, and can also explain why all glycolytic metabolites were decreased in Ldha null tumors (Fig 3).

The fact that loss of Ldh activity did not affect tumor initiation led to the hypothesis that perhaps lactate production is important for tumor progression as opposed to tumor initiation. To test this, we administered DMBA/TPA for several weeks until the first signs of tumorigenesis[25-27] then deleted Ldha by Cre activation with Mifepristone in transgenic animals. The experiment was allowed to continue for several more weeks, and the results were quantified. In fact, we were unable to detect an effect of loss of Ldh activity even in existing tumors (Fig 5a). Deletion of Ldha in the midst of tumor formation did not affect the timing or degree of tumorigenesis (Fig 5b). *In situ* staining for Ldh activity confirmed that the deletion of Ldha during tumorigenesis did indeed abrogate Ldh activity (Fig 5c). Furthermore, a plate reader assay on tumor material also showed decreased Ldh activity in this model.

A key interpretation of the Warburg effect is that increased glycolysis and lactate production is important for production of metabolites used for the generation of nucleotides and components necessary to increase biomass. As a further test of this hypothesis in SCC, we genetically *induced* lactate production through the deletion of the Mitochondrial Pyruvate Carrier (Mpc1). We and others previously showed that inhibiting the ability of pyruvate to enter the mitochondria leads

to increased Ldh activity. In addition, deleting Mpc1 with K15CrePR or Lgr5CreER-mediated recombination effectively increased lactate production specifically in HFSCs[16]. Here, we used a floxed Mpc1 allele in conjunction with DMBA/TPA to induce tumorigenesis in cells with enhanced Ldh activity. As in the case where Ldh activity was deleted, Ldh activation failed to affect the timing or degree of tumorigenesis (Fig 6a). To show that this genetic manipulation indeed led to increased Ldh activity, we performed a plate reader assay on isolated tissue, and this demonstrated that deletion of Mpc1 in these tumors led to a two-fold increase in Ldh activity, though there did not seem to be a consequence to this increase on tumor formation (Fig 6b).

From these data, it appeared as though glucose utilization to make lactate is not necessary for tumor initiation or progression. Surely the dividing cells in Ldha-null tumors still need to create biomass, so the question arose as to how they might do this. We hypothesized that Ldha-null cells could instead choose to take up glutamine as an alternate energy source. To test this hypothesis, we injected animals with 13C5-labeled glutamine to follow their usage of this important metabolite. Metabolomics analysis for labeled glutamine indicated that Ldha-null tumors did indeed take up more glutamine than wildtype tumors and that the Ldha-null tumors showed increased usage of glutamine to make several metabolites for TCA cycle (Fig 7). These data highlight the metabolic flexibility of tumors, and underscore the difficulty of treating cancer through pharmacological inhibition of particular metabolic pathways.

Discussion

Based on decades of research showing that nearly all tumors display increased lactate production, our null hypothesis was that deletion of Ldha would block tumor formation from HFSCs. In addition, Ldha deletion in a model of lung tumor formation caused tumors to regress[11].

Despite the fact that this lung model also used KrasG12D and floxed p53, the outcome was completely different than what was observed here in a model of cutaneous SCC. The difference could be due to performing the experiments in distinct tissues, but the lung study also used deletion of Ldha in the entire tissue, and deleted Ldha only after tumors were established[11, 16]. In addition, Ldh expression appears to be distinct between lung and skin. In the lung, it appeared from the Seth et al study that Ldhb is expressed significantly higher than Ldha, while the reverse is true in skin[11, 16] (Figure 1). It is interesting that after deletion of Ldha, tumors still formed from HFSCs without compensation by Ldhb. Furthermore, deletion of Ldha in SCC appeared to strongly abrogate Ldh activity, demonstrating that Ldha is the dominant isoform in this model.

In the current study, we found that deletion of Ldha neither before nor after tumor formation had an effect on the outcome, demonstrating that Ldh activity in cancer cells of origin is not required for tumor initiation or progression in SCC. These results are consistent with the notion that high Ldh activity in tumors could be due to the fact that at least some cancer cells of origin are high in Ldh activity. Indeed, if the Warburg nature of SCC is more a reflection of expansion of phenotype of the cell from which it arose (Figure S1), this could explain why loss of Ldh activity had no significant effect on tumorigenesis.

The longer term question is why do tumors produce so much lactate if it is not required for their initiation or maintenance? Lactate was previously considered simply a waste product of the glucose utilization pathway, which could explain why loss of lactate production in SCC does not appear to have a consequence in our model. On the other hand, recent studies have indicated that Lactate is potentially an important molecule to suppress the immune response to tumor formation, affect angiogenesis, acidify the microenvironment, and increase the motility of cancer

cells. Additionally, the conversion of pyruvate to lactate by Ldh enzyme produces NAD+, whose reducing power is important for numerous metabolic reactions (Reviewed in [25-27]). As a result, some have argued that the entire purpose of the Warburg effect is to produce Lactate for the sake of driving these events that are known to be important for tumor formation[25].

Our original hypothesis based on the expression pattern and activity of Ldha during SCC progression was that Ldh inhibition should abrogate tumor growth. However, the data demonstrate instead that while *in vivo* deletion of Ldha did affect the metabolism of the tumors formed, this did not affect cancer cell proliferation, survival, pathology, immune response etc. Perhaps *in vitro* data showing that Ldh inhibition can block tumor growth are incomplete because tumor cells *in vivo* can take up Lactate from the blood to make up for the loss of Ldh activity in the treated cells. Metabolomics data from SCCs without Ldh activity showed that whether tumors are making lactate or taking it up from the circulation, not only is the pool of lactate low in SCCs, but also lactate production is low. Furthermore, lack of Ldh activity also corresponded to a negative feedback whereby all the glycolytic metabolites were decreased, suggesting that increased glucose utilization in general is not required for tumor initiation or progression in SCC. These results could provide a simple explanation for why several efforts to exploit Ldh inhibition to treat cancer have not progressed beyond early stage clinical trials.

Recent studies have suggested that tumors are metabolically flexible, which could explain why loss of Ldh activity did not affect initiation or progression of SCCs. In this scenario, tumors lacking the ability to use glucose to produce lactate simply take up other metabolites such as glutamine to generate products necessary for increased biomass during proliferation. We used glutamine labeling to trace uptake and metabolism and did indeed find that Ldha-null tumors took up and

used more glutamine to power their metabolism. It will be of great interest going forward to understand how loss of lactate production leads to increased glutamine uptake and utilization. It is possible that dual inhibition of both Ldh activity and glutamine uptake or glutaminase could potentially starve tumors by circumventing their metabolic flexibility.

Acknowledgements

We would like to thank those running key core services at UCLA including: the Flow Cytometry Shared Resource Center (JCCC), Metabolomics Core Facility, and particularly the UCLA Division of Laboratory Animal Management (DLAM). In addition, we acknowledge Novogene, where RNA library and sequencing was performed.

Materials and Methods

Animal experiments

All animal experiments and related procedures were performed in accordance with protocols approved by the Institutional Animal Care and Use Committee (IUCUC) at UCLA in facilities run by the UCLA Department of Laboratory Animal Medicine (DLAM). Animal strains came from Jackson Labs (K15-CrePR, Lgr5-CreER), the National Cancer Institute Mouse Models of Human Cancers Consortium repository (LSL-KrasG12D and p53fl/fl), the Rutter (Mpcfl/fl) and Seth laboratories (Ldhafl/fl) and were maintained under conditions set forth by IUCUC and UCLA Animal Resource Committee. For tumor initiation experiments, K15-CrePR animals were shaved and treated by injection of mifepristone and Lgr5-CreER animals were shaved and treated with tamoxifen (200 µl of 10 mg ml−1 dissolved in filtered sunflower seed oil daily for 3 days) during telogen (7-8 weeks postnatal), and monitored for hair and tumor growth following shaving. Tumors generated in K15-CrePR animals were harvested for analysis 8-9 weeks post

mifepristone induction, and tumors generated in Lgr5-CreER animals were harvested 14-16 weeks post tamoxifen induction. For tumor progression experiments, tumors were generated in K15-CrePR and Lgr5-CreER animals floxed for either Ldha or Mpc1 by cutaneous two-stage chemical carcinogenesis as previously described (Filler et al., 2008). Briefly, transgenic animals (7-8 weeks postnatal) were shaved and treated once on the shaved dorsal skin with 200nmol of DMBA dissolved in acetone. One week later, 5nmol TPA dissolved in 100% ethanol was applied to the dorsal skin. 5nmol TPA treatment continued twice a week for the duration of the experiment. At the first visible sign of tumor formation, K15-CrePR and Lgr5-CreER mice were treated with mifepristone and tamoxifen respectively to delete Ldha or Mpc1. Mifepristone or Tamoxifen were administered by intraperitoneal injection (200 µl of 10 mg ml−1 dissolved in filtered sunflower seed oil daily for 3 days). Tumors were harvested for analysis 19-20 weeks post initial DMBA treatment. Both male and female animals were used in this study in approximately equal numbers with no apparent difference in phenotype between genders. All animals shown were maintained on a mixed C57BL6/FVB background. No statistical measure was used to determine the sample size beforehand. The results described include data from all treated animals. The investigators were not blinded to allocation during the experimental data collection, nor were the experiments randomized. The results shown are representative images from at least three independently treated animals per genotype as denoted in each experimental legend, and genotyping was performed both before and after animal treatment for confirmation.

Histology and immunostaining

Tumors were isolated from animals of indicated genotypes and embedded fresh in OCT compound for frozen tissue preparations, or fixed overnight in 4% formalin and embedded in paraffin. Formalin-fixed paraffin-embedded (FFPE) tumor sections were cut at 5 µm and fresh frozen tumors in OCT compound were cut at 10 µm for hematoxylin and eosin staining, and immunostaining. Immunohistochemistry on FFPE tissue sections was performed as previously

described (White et al., 2011). Briefly, paraffin-embedded tumor sections were de-paraffinized, rehydrated and blocked in staining buffer containing appropriate control IgG (goat, rabbit etc.). Antigen retrieval was performed on formalin-fixed paraffin-embedded tumor sections with citrate or Tris-EDTA buffers for 30 minutes at 95 degrees with the following antibodies: Ki-67 (Abcam, ab16667, 1:50), p-S6 (Cell Signaling, CST2215, 1:50), Sox9 (Abcam, ab185230, 1:1,000), CD34 (Abcam ab81289, 1:1000) , K14 (Covance, PRB-155P, 1:800), Fibronectin (Abcam, ab2413, 1:250), Tenascin C (Abcam ab108930, 1:500). The DAKO EnVision + HRP Peroxidase System (Dako K400911-2) and Dako AEC Substrate Chromogen (Dako K346430-2) was used for detection. Images were collected on an Olympus BX43 Upright Microscope.

Western blotting

Fresh tumor samples were homogenized with a tissue microgrinder followed by mechanical dissociation with a syringe and cell lysis in RIPA buffer (Pierce) with Halt protease and phosphatase inhibitors (Thermo-Fisher) on ice. After removing insoluble material by centrifugation at 8,000 g at 4°C for 5 min, total protein concentration was determined using the BCA assay kit (Pierce) per manufacturer's protocol with a microplate reader. 20 µg of protein per tumor sample was diluted in SDS-PAGE gel electrophoresis sample buffer (Bio-Rad) and boiled at 95°C for 5 min. Denatured proteins were resolved on SDS-PAGE gels (NuPAGE Novex Gels, Thermo-Fisher) and transferred onto PVDF membranes (Bio-Rad). Blocking was done with 5% milk in PBST, and then membranes were incubated with primary antibodies; β-actin (Abcam, ab8227; 1:1000), Ldha (Cell Signaling, CST2012; 1:1000), Mpc1 (Sigma HPA045119; 1:500) overnight at 4°C. After washing, membranes were incubated with peroxidase-conjugated secondary antibodies for 1 hr at room temperature. Signals were detected with Pierce ECL Western Blotting Substrate following washes.

Plate-reader Ldh assay

Ldh activity was determined in tumor cell lysates by measuring the formation of soluble XTT formazan in direct relation to production of NADH over time at 475 nm at 37 °C using a Synergy-MX plate reader (Biotek Instruments). Fresh tumor samples were homogenized with a tissue microgrinder followed by mechanical dissociation with a syringe and cell lysis in RIPA buffer (Pierce) with Halt protease and phosphatase inhibitors (Thermo-Fisher) on ice. After removing insoluble material by centrifugation at 8,000 g at 4°C for 5 min, total protein concentration was determined using the BCA assay kit (Pierce) per manufacturer's protocol with a microplate reader. 10µg of protein was used per well for each tumor. Samples were run in triplicates. The staining solution contained 50 mM Tris buffer pH 7.4, 150 µM XTT (Sigma), 750 µM NAD (Sigma), 80 µM phenazine methosulfate (Sigma) and 10 mM of substrate lactate (Sigma). Ldh activity was determined in cell lysates by measuring the change in absorbance of their common substrate or product, NADH, over time at 340 nm at 25 °C using a Synergy-MX plate reader (Biotek Instruments).

In situ Ldh assay

Ten-micron cryostat sections of fresh frozen tumors were briefly fixed (4% formalin for 5 min), washed with PBS pH 7.4 for 10 min, and then incubated with the appropriate solution for Ldh activity. Ldh staining solution contained 50 mM Tris pH 7.4, 750 µM NAD (Sigma), 80 µM phenazine methosulfate (Sigma), 600 µM nitrotetrazolium blue chloride (Sigma), 10 mM $MgCl_2$ (Sigma) and 10 mM of the substrate lactate (Sigma). Slides were incubated with staining solution at 37 °C until they reached the desired intensity, then counterstained using Nuclear Fast Red (Vector) or Braziliant! (Anatech) and mounted using VectaMount (Vector). Control reactions were performed by using staining solution that lacked the substrate mixture or NAD.

Mass spectrometry-based metabolomics analysis

The experiments were performed as previously described. To extract intracellular metabolites from tumor cells, tumor samples were briefly rinsed with cold 150 mM ammonium acetate (pH 7.3), followed by addition of 1 ml cold 80% methanol and homogenization on dry ice with a tissue microgrinder and mechanical dissociation through a syringe. Cell suspensions were transferred into Eppendorf tubes and 10 nmol D/L-norvaline was added. After rigorously mixing, the suspension was pelleted by centrifugation (18,000g, 4 °C for 5 min). The supernatant was transferred into a glass vial, metabolites dried down under vacuum, and resuspended in 70% acetonitrile. For the mass spectrometry-based analysis of the sample, 5 µl was injected onto a Luna NH2 (150 mm × 2 mm, Phenomenex) column. The samples were analyzed with an UltiMate 3000RSLC (Thermo Scientific) coupled to a Q Exactive mass spectrometer (Thermo Scientific). The Q Exactive was run with polarity switching (+3.50 kV/−3.50 kV) in full scan mode with an m/z range of 65–975. Separation was achieved using A) 5 mM NH4AcO (pH 9.9) and B) ACN. The gradient started with 15% A) going to 90% A) over 18 min, followed by an isocratic step for 9 min and reversal to the initial 15% A) for 7 min. Metabolites were quantified with TraceFinder 3.3 using accurate mass measurements (≤3 ppm) and retention times. Normalized metabolite data are available at figshare.com (https://doi.org/10.6084/m9.figshare.c.3801271).

RNaseq and bioinformatics

To compare gene expression profiles from tumors with and without Ldha, total RNA was isolated from fresh tumor samples. Fresh tumor samples were placed in Trizol LS reagent and homogenized by vortexing, microgrinding and mechanical dissociation through a syringe. Total RNA isolation was subsequently performed using an RNeasy Mini Kit (Qiagen) following the manufacturer's protocol with chloroform, isopropanol and ethanol washes.

Total RNA Sample QC All samples need to pass through the following four steps before library construction: (1) Nanodrop: tests RNA purity (OD260/OD280), (2) Agarose Gel Electrophoresis, (3) Agilent 2100 to check RNA integrity.

Library Construction After the QC procedures, mRNA from tumor samples was enriched using oligo(dT) beads. The mRNA was then fragmented randomly in fragmentation buffer, followed by cDNA synthesis using random hexamers and reverse transcriptase. After first-strand synthesis, a custom second-strand synthesis buffer (Illumina) was added with dNTPs, RNase H and Escherichia coli polymerase I to generate the second strand by nick-translation. The final cDNA library was ready after a round of purification, terminal repair, A-tailing, ligation of sequencing adapters, size selection and PCR enrichment.

Library QC Library concentration was first quantified using a Qubit 2.0 fluorometer (Life Technologies), and then diluted to 1 ng/μl before checking insert size on an Agilent 2100 and quantifying to greater accuracy by quantitative PCR (Q-PCR) (library activity >2 nM).

Sequencing Libraries were sequenced on HiSeq2500 (Illumina).

Data Filtering Raw reads were filtered to remove reads containing adapters or reads of low quality, so that downstream analyses were based on clean reads. The filtering process was as follows: (1) Discard reads with adaptor contamination, (2) Discard reads when uncertain nucleotides constitute more than 10 percent of either read (N > 10%), (3) Discard reads when low quality nucleotides (base quality less than 20) constitute more than 50 percent of the read.

RNA-seq Adapter sequences (Oligonucleotide sequences of adapters from TruSeqTM RNA and DNA Sample Prep Kits):

RNA 5' Adapter (RA5), part # 15013205:
5'-AATGATACGGCGACCACCGAGATCTACACTCTTTCCCTACACGACGCTCTTCCGATCT-3'
RNA 3' Adapter (RA3), part # 15013207:

5'-GATCGGAAGAGCACACGTCTGAACTCCAGTCAC(6-nucleotide index)ATCTCGTATGCCGTCTTCTGCTTG-3

Mapping to a Reference Genome Algorithm for mapping sequences: appropriate software was chosen according to the characteristics of the reference genome. TopHat2 was run for tumor genomes. The mismatch parameter were set to two, and other parameters were set to default. Only filtered reads are used to analyze the mapping status of RNA-seq data to the reference genome.

Expression Quantification Gene expression level was measured by transcript abundance to generate FPKM counts, short for the expected number of Fragments Per Kilobase of transcript sequence per Millions base pairs sequenced, which takes into account the effects of both sequencing depth and gene length counting of fragments(Trapnell, Cole, et al., 2010). HTSeq software was used to analyze the gene expression levels in this experiment, using the union mode. The result files present the number of genes with different expression levels and the expression level of single genes. In general, an FPKM value of 0.1 or 1 is set as the threshold for determining whether the gene is expressed or not. Fragments Per Kilobase of transcript per Million mapped reads (fkpm) values were ranked by the $\log_2$-transformed fold-change for knockout versus wild-type.

FDG-PET Imaging and Analysis

Small-animal PET/CT scans were performed using microPET/CT system Genisys 8 (Sofie Bioscience)(1). Mice were fasted for 4 h, placed on a heating pad to warm the mice for 60 minutes, and then anesthetized using 1.5% to 2% isoflurane. 20 μCi of ^{18}F-FDG probes was administrated via tail vein. Acquisition of static PET images was started 60 min after probe injection. Maximum-likelihood expectation maximization with 60 iterations was used for PET image reconstruction. All images were corrected for photon attenuation. The CT acquisition parameters were 40 kVp, 190 mA, and 720 projections with an exposure time of 55 ms at each projection. ^{86}Y-AABD PET

imaging was acquired fourteen hours after injection. For image analysis, PET/CT images were analyzed using OsiriX Imaging Software (Version 3.9.3; Pixmeo SARL, Bernex, Switzerland).

Statistics and reproducibility

Experiments were performed on male and female animals in approximately equal numbers with no apparent difference in phenotype between sexes. All phenotypes described are representative of a minimum of n = 3 littermate pairs (or a total of 6 mice) as indicated in the description of each experiment. For analysis of the hair regrowth phenotype no statistical measure was used to determine the sample size beforehand, nor were statistics used to measure effects, as the results were essentially positive or negative as represented in the figures. The results described include data from all treated animals. Investigators were not blinded to allocation during the experimental data collection. Experiments were not randomized. All results shown are representative images from at least three independently treated animals, and genotyping was performed both before and after animal treatment for confirmation. Pairwise comparisons between two groups were performed by two-tailed statistical analysis using Student's t test. Statistical significances were considered if $p < 0.05$ ($*$); $p < 0.01$ ($**$); $p < 0.001$ ($***$). Experimental data are demonstrated as the mean ± standard error of the mean (SEM). Sample size and statistical details can be found in the figure legends.

Data availability

Previously published transcriptomics data that were reanalysed here are available under accession (NIH GEO submission in progress. Normalized metabolite data are available at figshare.com (Submission in progress). All other data supporting the findings of this study are available from the corresponding author on reasonable request.

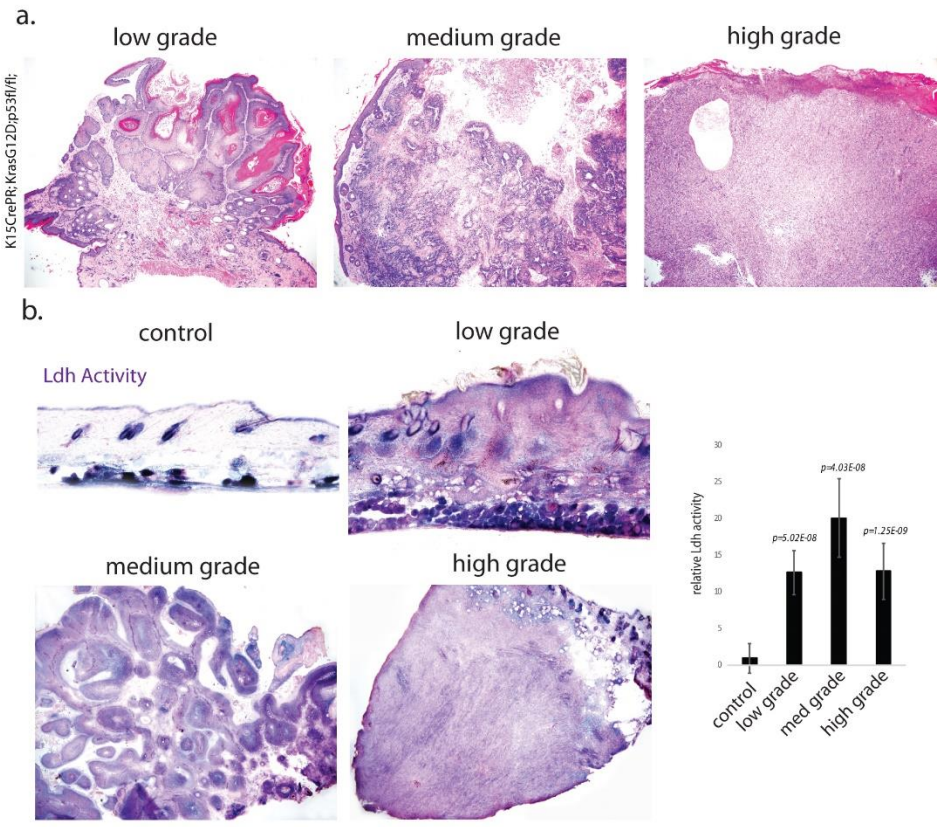

c.

	Low Grade				Medium Grade				High Grade				
	1	2	3	4	1	2	3	4	1	2	3	4	5
Glc													
G6P-F6P													
F16-BP													
DHAP													
3PG													
Lac													

d.

		Low Grade				Medium Grade				High Grade				
		1	2	3	4	1	2	3	4	1	2	3	4	5
Glc	M6	12.43	15.33	15.44	70.00	62.72	78.78	76.04	11.04	2.16	1.57	1.91	7.14	25.61
G6P-F6P	M6	1.72	5.79	1.87	2.32	3.37	3.52	2.86	3.30	4.77	1.46	1.44	2.62	3.99
F16-BP	M6	4.56	1.60	12.75	10.76	1.03	1.61	1.25	0.03	2.73	1.62	2.79	9.01	1.92
DHAP	M3	28.33	38.47	18.42	26.60	26.48	29.61	11.72	22.61	18.48	8.87	1.49	5.58	20.67
3PG	M3	8.99	11.25	5.09	2.11	3.38	12.47	3.38	3.69	2.19	1.14	2.34	3.69	1.14
Lac	M3	25.89	35.60	33.80	33.53	39.33	40.79	38.99	37.91	16.33	6.24	1.91	4.44	27.23

Figure 1. Correlation of Ldh activity and tumorigenesis of SCC

a, *in situ* Ldh activity assay highlights maximal potential Ldh activity in murine skin during KrasG12D/p53 mediated SCC formation from HFSCs. Purple stain indicate relative Ldh activity in the skin of control (top left; +mifepristone/-oncogenic stimulation) versus hyperplasia stage (top right; +mifepristone/+oncogenic stimulation), papilloma stage (lower left), and high grade SCC

(lower right). **b**, Isolation of tissue from each indicated stage of tumorigenesis was subjected to Ldh activity assay in a plate reader to provide more quantitative assessment of relative maximal Ldh activity in each stage of tumorigenesis. **c**, Metabolomic profiling of tissue taken from each stage of tumorigenesis as represented in a heat map of relative levels of pools of metabolites. **d**, following systemic injection of animals with C13-Glucose, tumors at various stages were isolated and profiled by metabolomics. The heat map depicts the relative levels of metabolites derived from the labeled glucose across different grades of tumors.

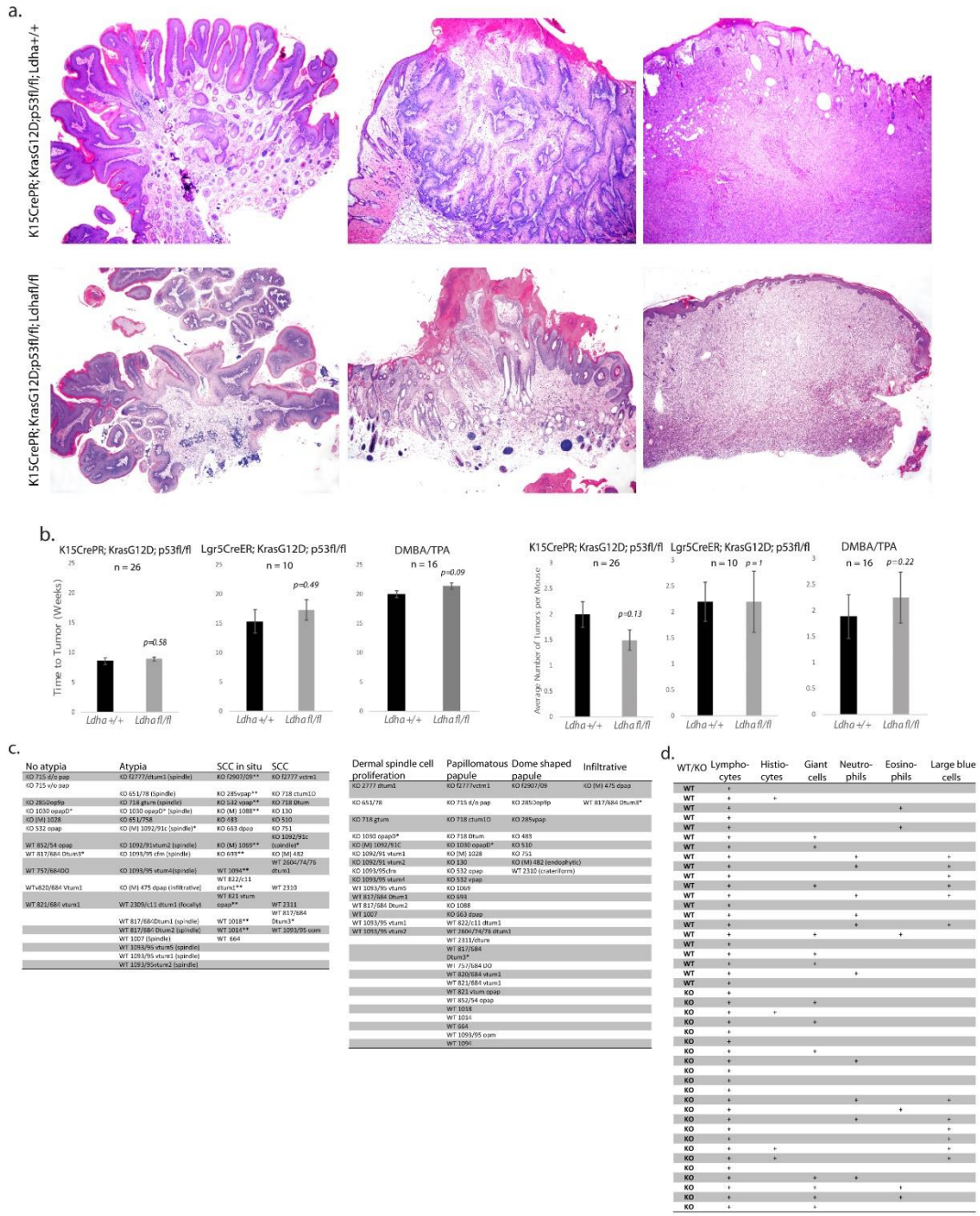

Figure 2. Loss of Ldha does not affect tumor initiation, progression or pathology

a, pathology of KrasG12D/p53 induced tumors from HFSCs with and without Ldha deletion appear indistinguishable across tumorigenesis. **b,** quantification of time to tumor formation (left) or number of tumors formed showed no significant difference between Ldha expressing vs Ldha

deleted tumors. Also shown is results from animals where KrasG12D/p53 was generated under the control of the Lgr5CreER, or in independent experiments where chemical carcinogenesis (DMBA/TPA) was carried out. **c**, Pathological examination of tumors generated with or without Ldha showed no significant differences in appearance, features, atypia etc. **d**, an examination of immune response to tumor formation showed a variety of immune features in SCC progression, but no difference based on expression of Ldha.

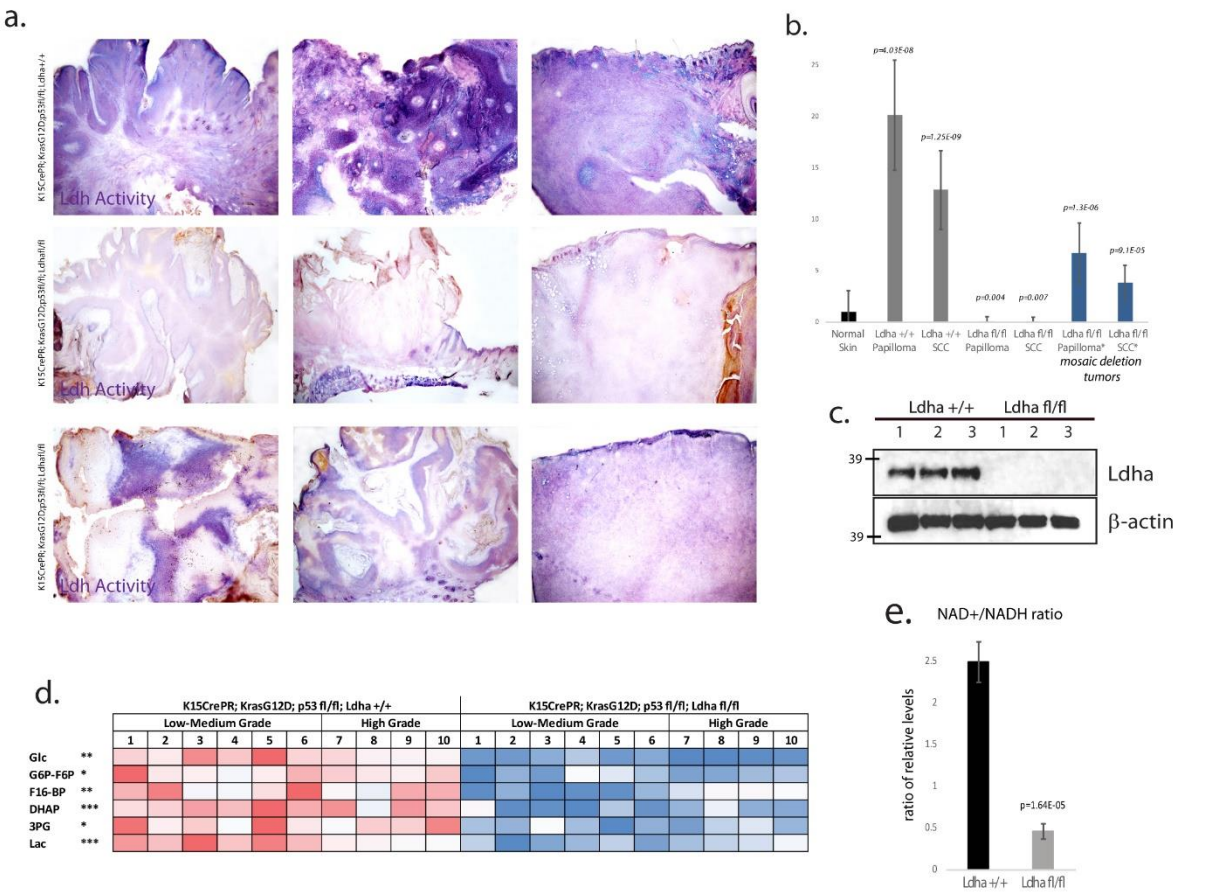

f.

		K15CrePR; KrasG12D; p53 fl/fl; Ldha +/+										K15CrePR; KrasG12D; p53 fl/fl; Ldha fl/fl									
		Low-Medium Grade						High Grade				Low-Medium Grade						High Grade			
		1	2	3	4	5	6	7	8	9	10	1	2	3	4	5	6	7	8	9	10
Glc	M6	60.81	70.00	5.44	15.33	62.72	78.78	0.20	1.11	62.06	67.49	12.14	12.43	7.03	0.73	0.57	6.71	8.93	4.83	25.61	11.04
G6P-F6P	M6	1.85	2.32	1.87	5.79	3.37	3.52	2.42	4.38	1.49	2.76	0.46	0.17	1.31	1.56	1.46	0.35	0.03	0.03	0.04	0.03
F16-BP	M6	11.67	10.76	12.75	8.68	13.31	21.83	7.37	9.59	11.16	19.29	4.78	4.56	3.82	3.88	1.62	2.51	0.45	0.32	0.92	0.48
DHAP	M3	21.28	26.60	18.42	38.47	26.48	29.61	23.91	25.90	6.82	34.63	0.76	0.03	11.34	15.26	8.87	2.00	0.52	0.03	0.03	0.03
3PG	M3	2.57	2.11	5.09	11.25	0.03	12.47	2.45	6.98	1.28	2.28	0.03	0.03	3.90	2.75	1.14	1.54	0.03	0.03	0.03	0.03
Lac	M3	38.38	33.53	33.80	35.60	40.79	38.99	20.95	24.05	31.13	39.66	7.29	5.89	14.05	13.10	6.24	8.96	0.88	1.87	2.72	4.93

Figure 3. Metabolic effects of loss of Ldha during tumorigenesis

a, *in situ* measurement of maximal Ldh activity in tumors with and without Ldha deletion shows a dramatic loss of activity in most tumors from the Ldha deletion mice (middle row). In addition, some tumors formed in deletion mice show mosaicism for Ldh activity, presumably due to mosaic deletion of Ldha mediated by CrePR induced recombination. **b**, isolation of tumor material from the indicated stages of tumorigenesis and measurement of Ldh activity by plate reader assay

provides a more quantitative view of Ldh activity. Those samples with * indicated tumors that were deemed to be mosaic for Ldha deletion by the *in situ* assay. **c**, Western blotting for Ldha protein indicated the effectiveness of the genetic deletion. **d**, Metabolomic profiling of tumor material from animals with and without Ldha expression shows a profound loss of pools of glycolytic intermediates in the absence of Ldha. **e**, Metabolomic profiling also captured data for NAD+/NADH. This analysis showed that the NAD+/NADH ratio was decreased in Ldh null tumors. **f**, Glucose tracing for glycolytic intermediates also shows a strong decrease in the absence of Ldha.

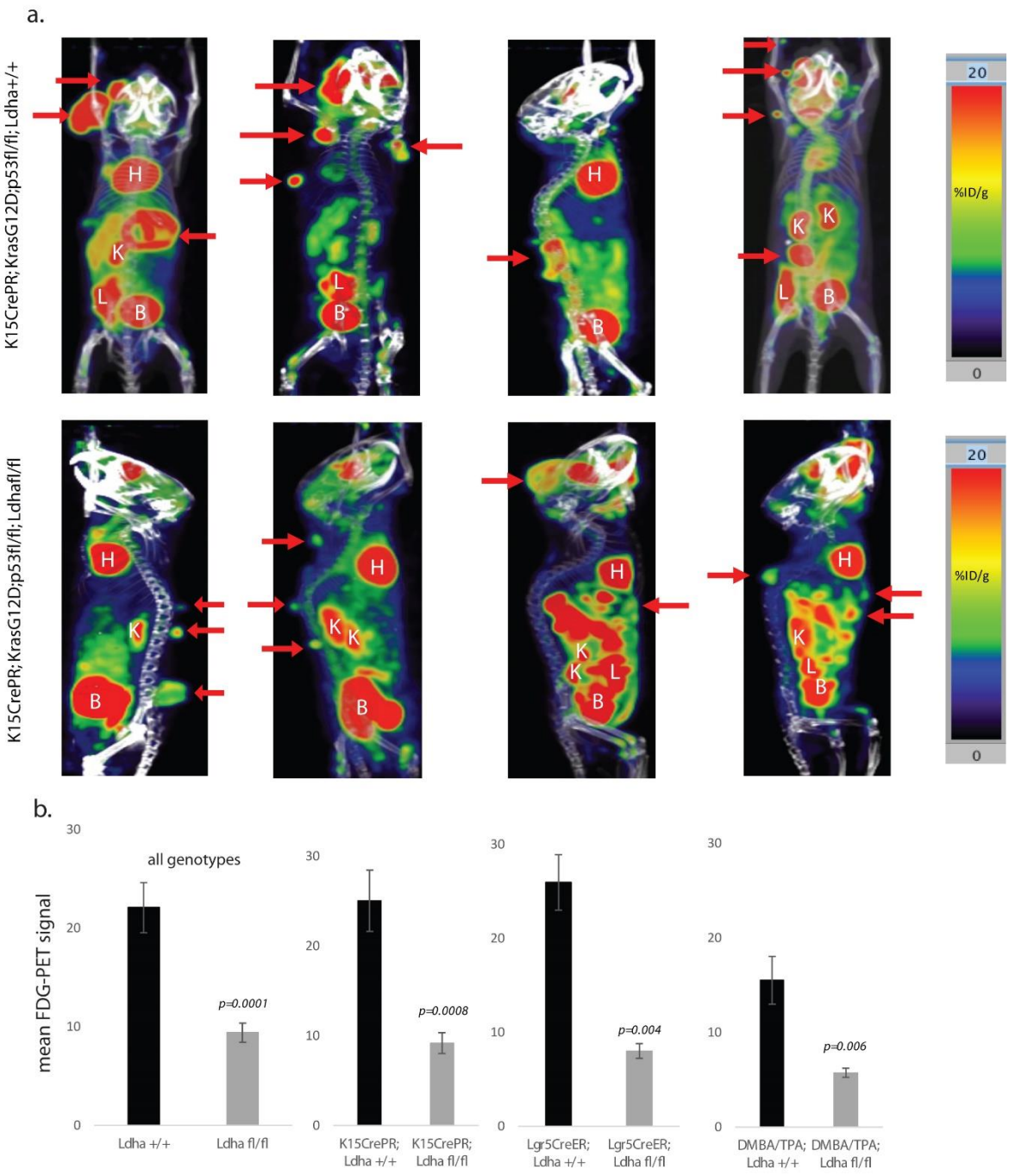

Figure 4. Absence of Ldha leads to decreased Glucose uptake in tumors

a, Positron Emission Tromography imaging after injection of FDG, a glucose analogue was used to demonstrate the relative degree of glucose uptake across tumors formed in the indicated genotypes. Red coloration indicates a high level of glucose uptake, and further demonstrates

that SCC tumors are highly glycolytic. **b**, quantification of FDG-PET signal showed that Ldha null tumors (from either K15CrePR, Lgr5CreER, or DMBA/TPA mice) consistently show lower glucose uptake.

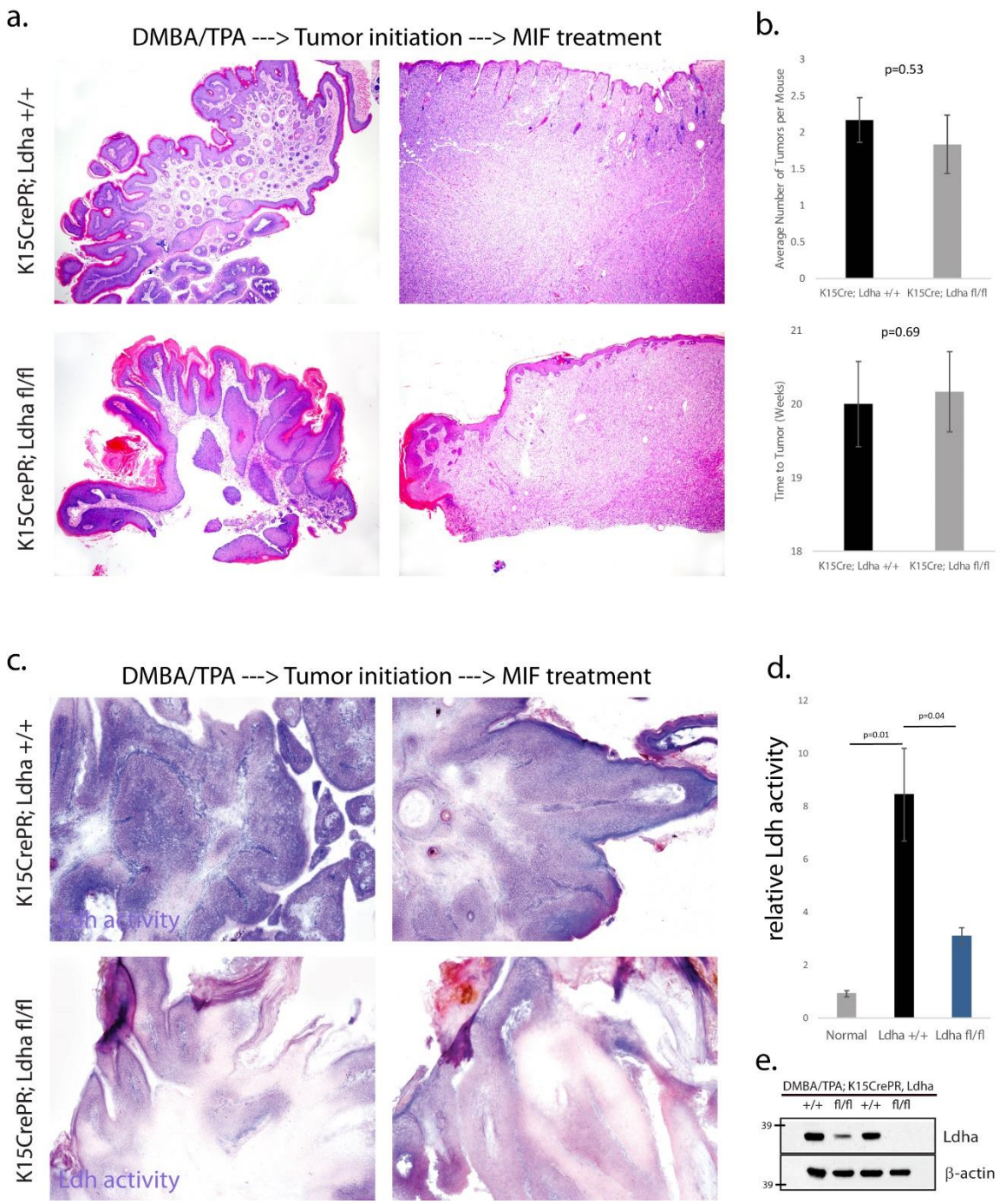

Figure 5. Deletion of Ldh activity in nascent tumors does not affect tumor progression

a, Taking advantage of chemical carcinogenesis coupled with transgenic deletion of Ldha, we allowed tumor initiation to begin and then deleted Ldha by administration of Mifepristone in

transgenic animals. **b**, Quantification of tumor formation and progression failed to uncover an effect of loss of Ldha. **c**, *in situ* Ldh activity assay confirmed that deletion of Ldha after tumorigenesis had begun was effective at abrogating Ldh activity in tumors. **d**, a platereader assay for Ldh activity also showed that the Ldha deletion was effective. **e**, western blotting for Ldha and a loading control to show the effectiveness of Ldha deletion after tumor initiation.

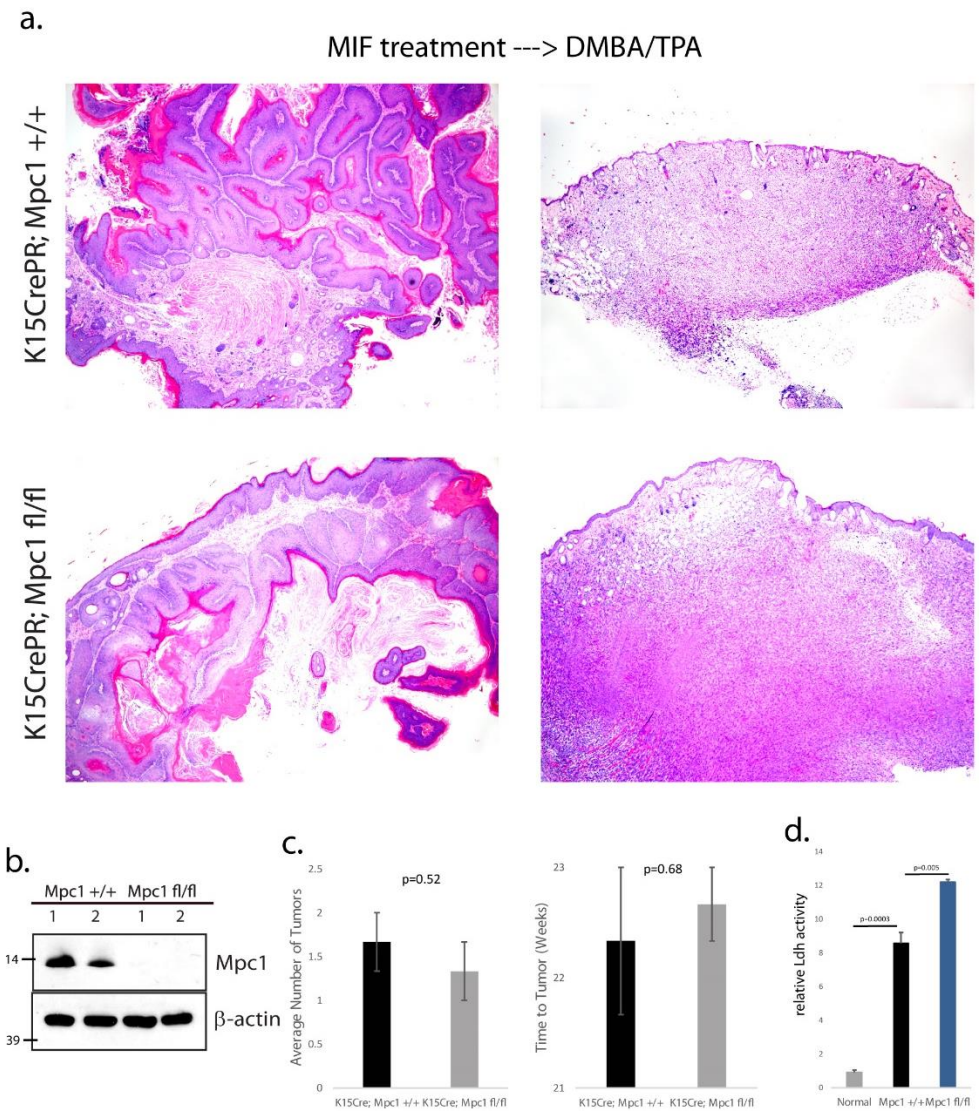

Figure 6. Induction of Ldh activity by deletion of mitochondrial pyruvate transport does not affect tumor initiation or progression in SCC.

a, coupling DMBA/TPA carcinogenesis to transgenic deletion of Mitochondrial Pyruvate Carrier function allowed for an examination of tumorigenesis following stimulation of Ldh activity. **b**, western blotting indicated that the genetic deletion of Mpc1 was effective. **c**, Quantification of time to tumor formation and number of tumors formed showed that Mpc1 deletion did not affect tumorigenesis. **d**, a plate reader assay on isolated tumor material showed that Mpc1-deleted tumors had increased Ldh activity.

		K15Cre; Ldha +/+; DMBA/TPA					K15Cre; Ldha fl/fl; DMBA/TPA								
		1	2	3	4	5	1	2	3	4	5	6	7	8	9
Gln	M5	10.3	5.6	7.3	9.4	3.2	16.1	20.3	18.4	18.1	16.8	16.5	16.6	19.2	16.7
Glu	M5	3.6	1.2	2.4	3.0	1.0	7.5	7.7	7.1	7.7	5.9	5.7	7.4	6.8	5.7
a-KG	M5	0.6	0.6	3.0	0.2	0.1	4.2	5.1	2.4	1.6	4.4	5.0	1.9	1.9	2.3
Asp	M4	1.3	0.1	0.7	0.2	0.1	0.7	1.7	1.9	2.1	1.5	1.3	1.4	1.5	1.1
Ala	M3	0.5	0.3	0.3	0.2	0.1	0.9	1.1	0.9	1.0	1.0	1.0	1.0	1.0	1.0

Figure 7. Glutamine uptake and glutaminolysis are induced in the absence of Ldha in tumors. Animals with tumors were pulsed with 13C-Glutamine prior to sacrifice. Tumors were then isolated and subjected to metabolomics profiling. Shown are the relative levels of labeled metabolites.

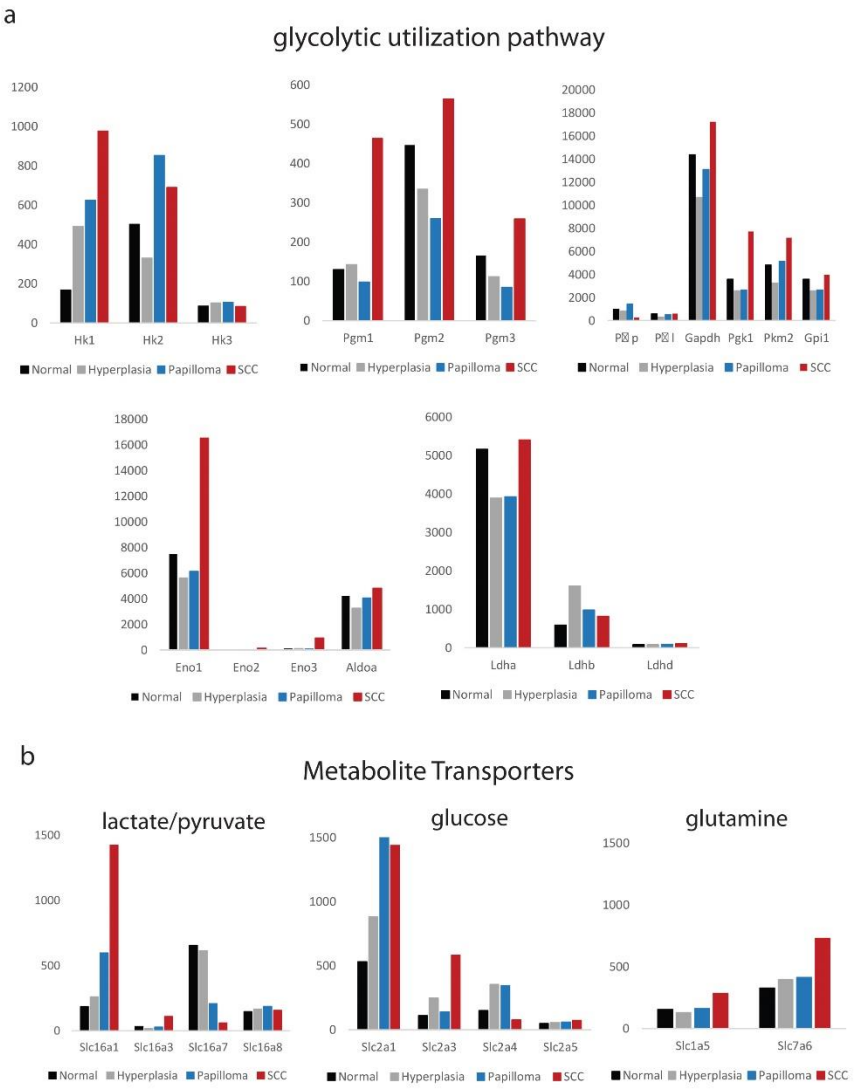

Supplemental Figure 1. Transcriptome changes during SCC initiation and progression.

Transcriptome data from a previous study on HFSC-driven SCC shows a dynamic pattern of expression of glycolytic enzymes over varying stages of tumorigenesis. The data presented are from cells labeled at the HFSC stage and then purified during the indicated stages of tumorigenesis. While *Ldha* was high in HFSCs and remained high at all stages of tumorigenesis, *Pgm, Hk, Pgk, Pkm, Eno* were all induced across tumorigenesis.

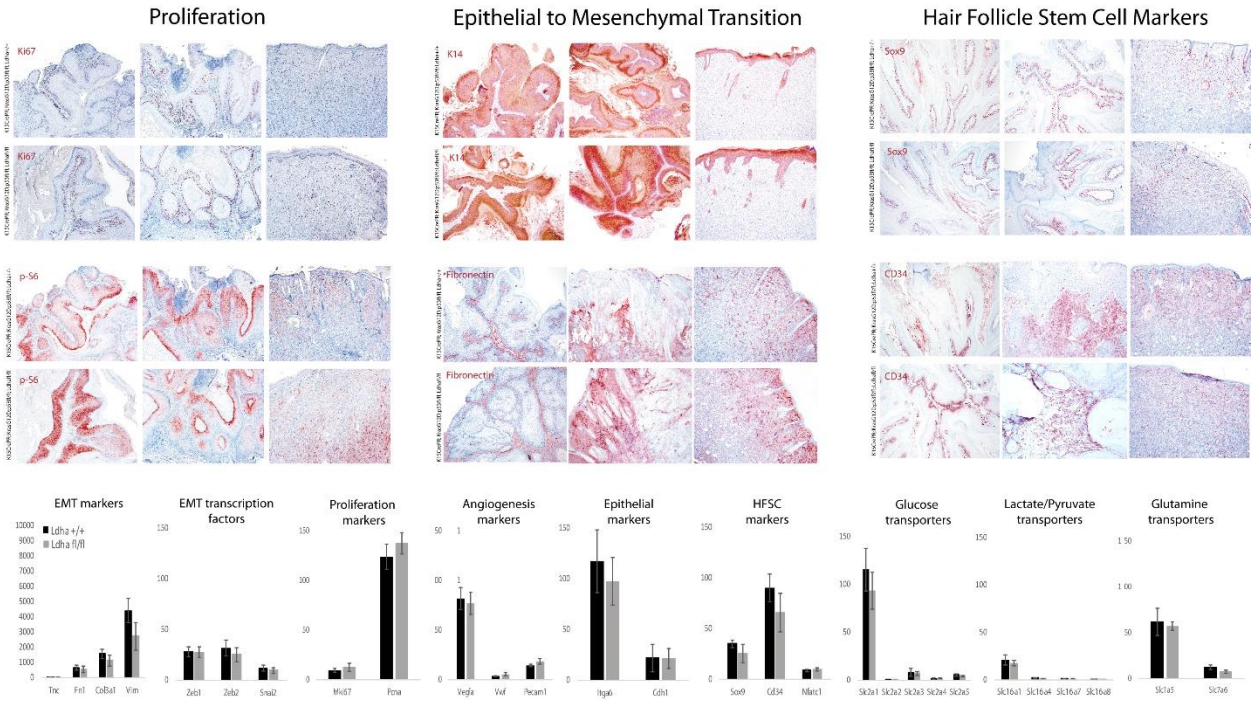

Supplemental Figure 2. Extended characterization of SCCs generated with and without Ldha

a, Proliferating cells in the tumor were highlighted by immunostaining with an antibody against Ki67. **b**, Evidence for Epithelial to Mesenchymal Transition (EMT) was assessed by immunostaining for Keratin 14, an epithelial marker and Fibronectin, a mesenchymal marker. **c**, To measure the expansion of HFSC fate in the tumors formed, we immunostained for markers Cd34 and Sox9. **d**, RNA-seq on tumors with and without Ldh activity failed to uncover significantly expressed genes (Summarized in Supplemental Table 1 and 2). Here we present RNA-seq results for the same genes presented in Supplemental Figure 1, the genes related to the Glucose utilization pathway that were induced in normal SCC tumorigenesis.

References

1. Paldino, E., Tesori, V., Casalbore, P., Gasbarrini, A. & Puglisi, M.A. Tumor Initiating Cells and Chemoresistance: Which Is the Best Strategy to Target Colon Cancer Stem Cells? *Biomed Res Int* **2014**, 859871 (2014).
2. Warburg, O. On respiratory impairment in cancer cells. *Science* **124**, 269-270 (1956).
3. Warburg, O. On the origin of cancer cells. *Science* **123**, 309-314 (1956).
4. Palsson-McDermott, E.M. & O'Neill, L.A. The Warburg effect then and now: from cancer to inflammatory diseases. *Bioessays* **35**, 965-973 (2013).
5. Bensinger, S.J. & Christofk, H.R. New aspects of the Warburg effect in cancer cell biology. *Semin Cell Dev Biol* **23**, 352-361 (2012).
6. Vander Heiden, M.G., Cantley, L.C. & Thompson, C.B. Understanding the Warburg effect: the metabolic requirements of cell proliferation. *Science* **324**, 1029-1033 (2009).
7. Seth, P. *et al.* On-target inhibition of tumor fermentative glycolysis as visualized by hyperpolarized pyruvate. *Neoplasia* **13**, 60-71 (2011).
8. Xie, H. *et al.* LDH-A inhibition, a therapeutic strategy for treatment of hereditary leiomyomatosis and renal cell cancer. *Mol Cancer Ther* **8**, 626-635 (2009).
9. Doherty, J.R. & Cleveland, J.L. Targeting lactate metabolism for cancer therapeutics. *J Clin Invest* **123**, 3685-3692 (2013).
10. Husain, Z., Huang, Y., Seth, P. & Sukhatme, V.P. Tumor-derived lactate modifies antitumor immune response: effect on myeloid-derived suppressor cells and NK cells. *J Immunol* **191**, 1486-1495 (2013).
11. Xie, H. *et al.* Targeting lactate dehydrogenase--a inhibits tumorigenesis and tumor progression in mouse models of lung cancer and impacts tumor-initiating cells. *Cell Metab* **19**, 795-809 (2014).

12. Shim, H. *et al.* c-Myc transactivation of LDH-A: implications for tumor metabolism and growth. *Proc Natl Acad Sci U S A* **94**, 6658-6663 (1997).

13. Le, A. *et al.* Inhibition of lactate dehydrogenase A induces oxidative stress and inhibits tumor progression. *Proc Natl Acad Sci U S A* **107**, 2037-2042 (2010).

14. Fantin, V.R., St-Pierre, J. & Leder, P. Attenuation of LDH-A expression uncovers a link between glycolysis, mitochondrial physiology, and tumor maintenance. *Cancer Cell* **9**, 425-434 (2006).

15. White, A.C. *et al.* Defining the origins of Ras/p53-mediated squamous cell carcinoma. *Proc Natl Acad Sci U S A* **108**, 7425-7430 (2011).

16. Flores, A. *et al.* Lactate dehydrogenase activity drives hair follicle stem cell activation. *Nat Cell Biol* **19**, 1017-1026 (2017).

17. Leushacke, M. & Barker, N. Lgr5 and Lgr6 as markers to study adult stem cell roles in self-renewal and cancer. *Oncogene* **31**, 3009-3022 (2012).

18. Jaks, V. *et al.* Lgr5 marks cycling, yet long-lived, hair follicle stem cells. *Nat Genet* **40**, 1291-1299 (2008).

19. White, A.C. *et al.* Stem cell quiescence acts as a tumour suppressor in squamous tumours. *Nat Cell Biol* **16**, 99-107 (2014).

20. Blanpain, C., Lowry, W.E., Geoghegan, A., Polak, L. & Fuchs, E. Self-renewal, multipotency, and the existence of two cell populations within an epithelial stem cell niche. *Cell* **118**, 635-648 (2004).

21. Morris, R.J. *et al.* Capturing and profiling adult hair follicle stem cells. *Nat Biotechnol* **22**, 411-417 (2004).

22. Trempus, C.S. *et al.* Enrichment for living murine keratinocytes from the hair follicle bulge with the cell surface marker CD34. *J Invest Dermatol* **120**, 501-511 (2003).

23. Wang, J. *et al.* Fast metabolic response to drug intervention through analysis on a miniaturized, highly integrated molecular imaging system. *J Nucl Med* **54**, 1820-1824 (2013).

24. Palaskas, N. *et al.* 18F-fluorodeoxy-glucose positron emission tomography marks MYC-overexpressing human basal-like breast cancers. *Cancer Res* **71**, 5164-5174 (2011).

25. San-Millan, I. & Brooks, G.A. Reexamining cancer metabolism: lactate production for carcinogenesis could be the purpose and explanation of the Warburg Effect. *Carcinogenesis* **38**, 119-133 (2017).

26. Pavlova, N.N. & Thompson, C.B. The Emerging Hallmarks of Cancer Metabolism. *Cell Metab* **23**, 27-47 (2016).

27. Vander Heiden, M.G. & DeBerardinis, R.J. Understanding the Intersections between Metabolism and Cancer Biology. *Cell* **168**, 657-669 (2017).

Chapter 6: Conclusion

The regenerative capacity for many tissues and organ systems is driven and maintained largely by resident somatic stem cell populations. Both quiescence and self-renewal through cell division are necessary to maintain adult stem cell populations in tissues and organs. Ageing and disease are often accompanied by a deregulation of stem cell function and a decline in regenerative capacity. A mechanistic understanding of stem cell quiescence, activation and transformation is crucial for elucidating its role in human diseases such as cancer and investigating the potential use of adult stem cells in transplantation therapy and regenerative medicine. The work presented in this thesis represents my efforts to understand the genetic and metabolic changes that occur in somatic stem cells during tissue homeostasis and tumorigenesis to identify strategies to better maintain stem cell function and regulation in disease.

Metabolic Regulation of Hair Follicle Stem Cell Function

Metabolic influence on the maintenance of stem cell quiescence and activation has remained mostly unexplored. Previous work showed that haematopoietic stem cells display higher glycolytic activity than their more differentiated progeny, and disruption of glycolysis in these stem cells led to activation of their cycling[1-4]. In Chapter 2 of this thesis I present data from our own lab to demonstrate that the production of lactate, through lactate dehydrogenase, is important for hair follicle stem cell activation, and that these stem cells maintain a high capacity for glycolytic metabolism at least in part through the activity of Myc. We hypothesize that increased glycolytic rate in hair follicle stem cells allows them to respond quickly to the many cues responsible for signaling the onset of a new hair cycle.

Current and future studies in our lab are focused on gaining an in-depth understanding of the mechanisms involved in maintaining the unique metabolic state we observed in hair follicle stem cells. What remains to be determined is how exactly changes in metabolic states interact with other signaling pathways to regulate stem cell activation. How do secondary pathways from various glycolytic intermediates such as the pentose phosphate pathway and one-carbon metabolism contribute to stem cell fate decisions? By entering the pentose phosphate pathway, glucose 6-phosphate can generate NADPH and ribose which drive anabolic reactions and nucleotide synthesis[5]. One-carbon metabolism produces S-adenosylmethionine which is necessary for methylation reactions, and this process can be initiated by the glycolytic intermediate 3-phosphoglycerate. 3-phosphoglycerate can also generate NADPH and necessary intermediates for redox reactions and nucleotide synthesis[6-7]. These are only a few examples of the many possible metabolic pathways involved in stem cell function and regulation. Future studies into the metabolic control of epigenetic regulation will also be important for understanding how these various metabolic pathways influence stem cell fate.

As described in Chapter 2 our data demonstrate that reducing lactate production and glycolysis in hair follicle stem cells prevents their activation. These results are different from those reported in haematopoietic stem cells in which decreasing glycolysis leads to stem cell activation[8-10]. This could be attributed to both intrinsic differences in the cycling natures of these stem cells as well as differences in experimental design. Hair follicle stem cells cycle at well-defined timepoints as the hair cycle transitions from telogen to anagen while the timing of haematopoietic stem cell activation is not as well established or synchronized. Deleting genes specifically in haematopoietic stem cells is also considerably more challenging as there are currently no conditional inducible Cre transgenic lines line those used in our hair follicle stem cell model (K15CrePR or Lgr5CreER). Somatic stem cells behave differently from one tissue to the next and we and other groups are actively investigating how metabolism influences stem cell fate

across these various populations. An in-depth understanding of the metabolic regulation of stem cells across tissues and during wounding could serve to identify new and effective strategies to preserve the regenerative capacity of many organs.

The fact that small molecules could be used to promote hair follicle stem cell activation suggests that they could be useful for regenerative medicine, and this is not only the case for hair growth, but potentially for wound healing as well. While hair follicle stem cells do not normally contribute to the interfollicular epidermis, in a wound setting, they can migrate towards the wound site to assist in healing[11]. Whether activation of hair follicle stem cells by Mpc1 inhibition (UK-5099) or Myc activation (RCGD423) can promote wound healing is the subject of intense studies going forward.

Hair Follicle Stem Cells in Squamous Cell Carcinoma

Recently developed techniques have allowed for the delivery of cancer-causing mutations to specific cell types in an inducible fashion[12-17]. These techniques have allowed for sophisticated exploration on the cellular and molecular origins of squamous cell carcinoma and have highlighted the ability of specific genetic hits to serve as tumor initiators or promoters. While some driver mutations have been identified consistently across squamous cell carcinomas, it is unclear whether the heterogeneity of phenotypes is due to variability across mutations, cell of origin, immune response, or variable genomic instability. In Chapters 3 and 4 of this thesis, I provided evidence that demonstrate the ability of hair follicle stem cells to serve as cancer cells of origin, and the ability of various molecular players to drive heterogeneity of tumor cell types. These studies provide unique insights into the process by squamous cell carcinoma initiates and propagates.

For over two decades, HMGA2 was implicated as a player in human cancer; however, the question of whether HMGA2 is required for tumor initiation or progression had not been addressed[18-19]. Numerous studies have tested whether Hmga2 plays a role in epithelial-to-mesenchymal transition (EMT) or cancer progression through gain of function studies, but it remained unclear whether Hgma2 is necessary for EMT, tumor formation or tumor progression[20-21]. In Chapter 3 I described experiments from our lab in which we deleted Hmga2 in two mouse models of squamous cell carcinoma and found this gene to be dispensable. The lack of substantial phenotypic effect in the absence of Hmga2 raises many questions as to the role of this gene in cancer, and whether its role as observed here is typical of other cancers as well. It will be interesting going forward to determine if the loss of Hmga2 could be compensated for by Hmga1. Hmga1 shares significant homology with Hmga2 but has typically been ascribed to different roles in the cell. According to our RNA profiling, Hmga1 is expressed throughout the epidermis at a significant level and does not change over the course of tumorigenesis, or in the absence of Hmga2, but we cannot rule out the possibility that the loss of Hmga2 was compensated for by Hmga1 in our experiments.

In Chapter 4 of this manuscript I described additional experiments to investigate tumor initiation and progression by hair follicle stem cells. In this study we showed that hair follicle stem cells can drive a variety of squamous cell carcinoma phenotypes that correlate strictly with the type of tumor suppressor deleted, and tumor suppressor deletion correlates with distinct phenotypes in proliferation, dedifferentiation and immune response. These data suggested that the identity of the tumor suppressor can affect the diversity of cellular phenotypes that arise in the tumor; a previously unappreciated source of tumor diversity. In light of this data, we believe that the future coupling genotypic and phenotypic analyses of human squamous cell carcinoma samples will be informative as it has been for many other

types of human cancers. Many of the phenotypes and processes observed in our tumor model are like other epithelial cancers both in mouse and human, and we propose that murine transgenic models of squamous cell carcinoma are useful for enabling the development of novel treatment strategies going forward.

Cellular Metabolism in Cancer

Transformed cells undergo metabolic reprogramming to support tumor initiation and progression. Metabolic pathways and their intermediates can participate directly in the process of transformation or support the many biological processes that permit tumor growth. Exploiting cancer cell metabolism for clinical benefit requires defining the pathways that are limiting for cancer progression and understanding the metabolic flexibilities these cancer cells utilize for survival.

In Chapter 5 of this thesis, I described my own efforts to target glycolytic metabolism in a squamous cell carcinoma tumor model. I sought to determine whether lactate dehydrogenase activity in squamous cell carcinoma tumors is a marker of the cell type from which these cells arise, namely the hair follicle stem cells, or a key metabolic pathway important for tumor initiation or progression. Deletion of lactate dehydrogenase enzyme activity in hair follicle stem cell-mediated tumorigenesis showed no effect on tumor number, time to tumor formation, tumor proliferation, epithelial to mesenchymal transition in tumors, gene expression in tumors, or the immune response to tumors. Tumors null for lactate dehydrogenase showed dramatically reduced levels of most glycolytic metabolites by metabolomics, and significantly reduced glucose uptake as shown by FDG-PET live animal imaging. Finally, deletion of lactate dehydrogenase in existing tumors or genetic induction of its activity also had no effect on tumor initiation

or progression. These surprising results suggested that squamous cancer cells of origin do not require lactate dehydrogenase activity to generate cancers.

Cancer cells adapt their metabolism to maintain proliferation, withstand oxygen and nutrient limitations, and disrupt the surrounding microenvironment to facilitate tumor growth and metastasis[22-24]. Research continues to uncover novel connections between nutrient utilization and tumorigenesis. While most tumor studies including our own have been focused on alterations in the metabolism of glucose, we are only beginning to understand the extent to which cancer cells can utilize a great variety of other nutrients including glutamine, lactate, amino acids, essential fatty acids, trace metals, and vitamins[25-29]. Additional studies have suggested that even metabolites produced by the body's microbiota can contribute to tumorigenesis[30]. This metabolic flexibility is one possible explanation for why loss of lactate dehydrogenase activity did not affect the initiation or progression of squamous cell carcinomas in our model. It is possible that tumors lacking the ability to use glucose to produce lactate simply take up other metabolites such as glutamine to generate the products necessary for increased biomass during proliferation. In fact, we used glutamine labeling to trace uptake and metabolism and did indeed find that lactate dehydrogenase-null tumors took up and used more glutamine to power their metabolism. Current and future studies in our lab are therefore focused on understanding how loss of lactate production leads to increased glutamine uptake and utilization. We are also exploring the possibility that a combination inhibition of lactate dehydrogenase activity, lactate uptake, glutamine uptake and glutaminase activity could in fact starve tumors by blocking access to any alternative nutrient sources.

Another challenge to consider when studying cancer metabolism is the variability between *in vitro* and *in vivo* tumor modeling. Most of the studies that inform our experimental design are performed primarily

in cancer cell lines rather than in intact tumors. And while these have been highly informative regarding the molecular mechanisms of metabolic reprogramming, it is challenging to model a true tumor microenvironment *in vitro*. *In vitro* data showing that lactate dehydrogenase inhibition can block tumor growth, for example, fail to account for the fact that tumor cells *in vivo* can still take up lactate from the blood to make up for the loss in treated cells. In our tumor model we did not block lactate uptake and as such cannot rule out the possibility that lactate dehydrogenase-null tumors continued to take up lactate from the surrounding environment to fuel its metabolism. From our data and others, metabolic flux analysis of tumors *in vivo* is essential for determining metabolic inhibitors most likely to be successful in both preclinical and clinical models of tumorigenesis.

Although we now know a lot about the metabolic pathways that support cancer cell survival, we still have many questions about how the many intrinsic and extrinsic signals integrate to create exploitable metabolic phenotypes in cancer. It is necessary for us to investigate not only the metabolism of the tumor-initiating cells, but those found in the tumor microenvironment as well. To uncover improved therapeutic strategies for targeting cancer metabolism it is important for us to consider the metabolic influences set forth the by tissue of origin, interactions between cells within the microenvironment, and influences of the diet and microbiome on the host.

References

1. Yu, W. M. et al. Metabolic regulation by the mitochondrial phosphatase PTPMT1 is required for hematopoietic stem cell differentiation. Cell Stem Cell 12, 62–74 (2013).
2. Maryanovich, M. et al. An MTCH2 pathway repressing mitochondria metabolism regulates haematopoietic stem cell fate. Nat. Commun. 6, 7901 (2015).
3. Takubo, K. et al. Regulation of the HIF-1alpha level is essential for hematopoietic stem cells. Cell Stem Cell 7, 391–402 (2010).
4. Maltepe, E. et al. Abnormal angiogenesis and responses to glucose and oxygen deprivation in mice lacking the protein ARNT. Nature 386, 403–407 (1997).
5. Chandel, N. Navigating Metabolism (Cold Spring Harbor Laboratory, 2015).
6. Boroughs, L. K. & DeBerardinis, R. J. Metabolic pathways promoting cancer cell survival and growth. Nat. Cell Biol. 17, 351–359 (2015).
7. Locasale, J. W. Serine, glycine and one-carbon units: cancer metabolism in full circle. Nat. Rev. Cancer 13, 572–583 (2013).
8. Pietras, E. M., Warr, M. & Passegué, E. Cell cycle regulation in hematopoietic stem cells. J. Cell Biol. 195, 709–720 (2011).
9. Simsek, T. et al. The distinct metabolic profile of hematopoietic stem cells reflects their location in a hypoxic niche. Cell Stem Cell 7, 380–390 (2010).
10. Takubo, K. et al. Regulation of glycolysis by Pdk functions as a metabolic checkpoint for cell cycle quiescence in hematopoietic stem cells. Cell Stem Cell 12, 49–61 (2013).
11. Ito, M. et al. Stem cells in the hair follicle bulge contribute to wound repair but not to homeostasis of the epidermis. Nat. Med. 11, 1351–1354 (2005).
12. Bailleul, B., Surani, M.A., White, S., Barton, S.C., Brown, K., Blessing, M. et al. Skin hyperkeratosis and papilloma formation in transgenic mice expressing a ras oncogene from a suprabasal keratin

promoter. Cell. 1990; 62: 697–708

13. Brown, K., Strathdee, D., Bryson, S., Lambie, W., and Balmain, A. The malignant capacity of skin tumours induced by expression of a mutant H-ras transgene depends on the cell type targeted. Curr Biol. 1998; 8: 516–524
14. French, J.E., Libbus, B.L., Hansen, L., Spalding, J., Tice, R.R., Mahler, J. et al. Cytogenetic analysis ofmalignant skin tumors induced in chemically treated TG-AC transgenic mice. Mol Carcinog. 1994; 11: 215–226
15. Greenhalgh, D.A., Rothnagel, J.A., Quintanilla, M.I., Orengo, C.C., Gagne, T.A., Bundman, D.S. et al. Induction of epidermal hyperplasia, hyperkeratosis, and papillomas in transgenic mice by a targeted v-Ha-ras oncogene. Mol Carcinog. 1993; 7: 99–110
16. Guo, L., Yu, Q.C., and Fuchs, E. Targeting expression of keratinocyte growth factor to keratinocytes elicits striking changes in epithelial differentiation in transgenic mice. EMBO J. 1993; 12: 973–986
17. Vitale-Cross, L., Amornphimoltham, P., Fisher, G., Molinolo, A.A., and Gutkind, J.S. Conditional expression of K-ras in an epithelial compartment that includes the stem cells is sufficient to promote squamous cell carcinogenesis. Cancer Res. 2004; 64: 8804–8807
18. Staats B, Bonk U, Wanschura S et al. A fibroadenoma with a t(4;12) (q27;q15) affecting the HMGIC gene, a member of the high mobility group protein gene family. Breast Cancer Res Treat 1996: 38: 299–303.
19. Hebert C, Norris K, Scheper M A et al. High mobility group A2 is a target for miRNA-98 in head and neck squamous cell carcinoma. Mol Cancer 2007: 6: 5.
20. Thuault S, Valcourt U, Petersen M et al. Transforming growth factor-beta employs HMGA2 to elicit epithelial-mesenchymal transition. J Cell Biol 2006: 174: 175–183.
21. Morishita A, Zaidi M R, Mitoro A et al. HMGA2 is a driver of tumor metastasis. Cancer Res 2013: 73: 4289–4299.

22. Pavlova N and Thompson C. The Emerging Hallmarks of Cancer Metabolism. Cell Metab. 2016 Jan 12; 23(1): 27–47. doi: 10.1016/j.cmet.2015.12.006
23. Altman, B.J., Stine, Z.E., and Dang, C.V. From Krebs to clinic: glutamine metabolism to cancer therapy. Nat. Rev. Cancer. 2016; 16: 619–634
24. DeBerardinis, R.J. and Chandel, N.S. Fundamentals of cancer metabolism. Sci. Adv. 2016; 2: e1600200
25. White, E. Exploiting the bad eating habits of Ras-driven cancers. Genes Dev. 2013; 27: 2065–2071
26. Vander Heiden, M.G., Cantley, L.C., and Thompson, C.B. Understanding the Warburg effect: the metabolic requirements of cell proliferation. Science. 2009; 324: 1029–1033
27. Commisso, C., Davidson, S.M., Soydaner-Azeloglu, R.G., Parker, S.J., Kamphorst, J.J., Hackett, S., Grabocka, E., Nofal, M., Drebin, J.A., Thompson, C.B. et al. Macropinocytosis of protein is an amino acid supply route in Ras-transformed cells. Nature. 2013; 497: 633–637
28. Guo, J.Y., Teng, X., Laddha, S.V., Ma, S., Van Nostrand, S.C., Yang, Y., Khor, S., Chan, C.S., Rabinowitz, J.D., and White, E. Autophagy provides metabolic substrates to maintain energy charge and nucleotide pools in Ras-driven lung cancer cells. Genes Dev. 2016; 30: 1704–1717
29. Palm, W., Park, Y., Wright, K., Pavlova, N.N., Tuveson, D.A., and Thompson, C.B. The utilization of extracellular proteins as nutrients is suppressed by mTORC1. Cell. 2015; 162: 259–270
30. Garrett, W.S. Cancer and the microbiota. Science. 2015. 348, 80-86